



University  
of Glasgow

<https://theses.gla.ac.uk/>

Theses Digitisation:

<https://www.gla.ac.uk/myglasgow/research/enlighten/theses/digitisation/>

This is a digitised version of the original print thesis.

Copyright and moral rights for this work are retained by the author

A copy can be downloaded for personal non-commercial research or study,  
without prior permission or charge

This work cannot be reproduced or quoted extensively from without first  
obtaining permission in writing from the author

The content must not be changed in any way or sold commercially in any  
format or medium without the formal permission of the author

When referring to this work, full bibliographic details including the author,  
title, awarding institution and date of the thesis must be given

Enlighten: Theses

<https://theses.gla.ac.uk/>  
[research-enlighten@glasgow.ac.uk](mailto:research-enlighten@glasgow.ac.uk)

HYDROCARBON BUBBLE CHAMBERS.

by

Ian R. Birss.

Department of Natural Philosophy,  
University of Glasgow.

Presented to the University of Glasgow, January 1959,  
as a Thesis for the Degree of Doctor of Philosophy.



ProQuest Number: 10646824

All rights reserved

INFORMATION TO ALL USERS

The quality of this reproduction is dependent upon the quality of the copy submitted.

In the unlikely event that the author did not send a complete manuscript and there are missing pages, these will be noted. Also, if material had to be removed, a note will indicate the deletion.



ProQuest 10646824

Published by ProQuest LLC (2017). Copyright of the Dissertation is held by the Author.

All rights reserved.

This work is protected against unauthorized copying under Title 17, United States Code  
Microform Edition © ProQuest LLC.

ProQuest LLC.  
789 East Eisenhower Parkway  
P.O. Box 1346  
Ann Arbor, MI 48106 – 1346

## Preface.

The work of this thesis was performed in the Department of Natural Philosophy of Glasgow University from October, 1954 to July, 1958.

A short introduction reviews the need for a higher density detector of the cloud chamber type, and outlines the early experiments of Dr. D.A. Glaser, performed before this work started.

Very little technical information was available at this time, and the author was allotted the task of building a small bubble chamber similar to that of Glaser's in order to find out what the operating conditions were. Chapter 2, shows how the first chamber to be built in this laboratory was made to work. The author worked alone for the first year, and then was joined by Mr. A.F. McFarlane in October, 1955. The first tracks were photographed soon after, in November, 1955, and these were the first in Europe.

The next chapter explains how this chamber was developed as a joint project, and described several experiments conducted in it in order to gain a better understanding of how the bubble chamber worked. In particular, measurements were made on the effect of chamber conditions on bubble "density" - the number of bubbles per centimetre of track

length. The author then performed measurements on rate of bubble growth, and magnitude of temperature gradients set up during the cycle of operations.

It was soon clear, however, that this all glass chamber was too small for nuclear physics experiments. Chapter 4 describes the experiments performed on the first metal and glass chamber. This chamber was assembled by Mr. McFarlane, but design, operation and experimental measurements were done in collaboration. These investigations again included a study, in collaboration, of bubble density and one of the rate of bubble growth performed independently by the author.

In Chapter 5, all the bubble density results described in Chapters 3 and 4 are considered, together with the various theories on how bubbles are formed in superheated liquids. This work and all work described subsequently in the thesis was performed independently by the author.

The thesis then proceeds to discuss how particles which stop in the chamber can be recognised and how bubble counting might be used to aid particle identification. A larger chamber was built for this work, and a fast cycling expansion system was developed with this chamber, described in Chapter 7.

Chapter 8, describes how bubble counting was in fact used to aid particle identification, and in Chapter 9 experiments on the relation between particle energy and bubble density are explained.

The thesis is concluded with a brief review of the advantages of bubble chambers, and suggestions of further experiments which might usefully be performed in the bubble density field.

The author is indebted to Professor P.I. Dee for the interest he has shown in this work. He also wishes to acknowledge the services of Mr. J.T. Lloyd, Mr. R. Irvine and their technical staffs for making the equipment, and Dr. W. McFarlane and the synchrotron crew for operating the machine. He would also like to record his grateful thanks to his colleague Mr. A.F. McFarlane and his supervisor Mr. J.R. Atkinson.

Finally, he wishes to acknowledge the award of a St. Andrews University Post-Graduate Scholarship and Sir James Caird Travelling Scholarship.

## CONTENTS.

Page.

### Preface.

### Chapter I. Introduction.

Advantages and shortcoming of existing visual techniques.	1.
Glaser's experiments with liquids.	3.
Chamber conditions.	4.

### Chapter II. The First Chamber.

Preliminary Considerations.	7.
Apparatus and First Tracks.	8.

### Chapter III. Further development of Clean Chambers.

Shortcomings of the first chamber and the improvements introduced.	14.
Bubble Chamber Operation.	16.
Bubble Density Measurements.	16.
Rate of Bubble Growth.	18.
Compression Measurements.	21.
Temperature gradients.	22.
P-V diagram.	25.

### Chapter IV. The First Dirty Chamber.

Need for a larger chamber.	27.
Apparatus and Operation.	28.

	Page.
Chamber Operation.	30.
Bubble Density.	31.
Rate of Bubble Growth.	32.
 <u>Chapter V. Bubble Density and Chamber Conditions.</u>	
Experimental Results.	35.
Early theories.	36.
$\gamma$ -ray theories.	39.
Energy for Bubble Formation.	41.
Thermal Spike theory.	43.
Revised Viscosity Calculation.	45.
Bubble density and Volmer energy.	47.
Conclusions.	47.
Further Experiments.	48.
 <u>Chapter VI. Particles stopping in the Bubble Chamber.</u>	
Identification by Inspection.	50.
Doubtful Cases.	53.
Experiment.	53.
 <u>Chapter VII. The New Chamber.</u>	
Apparatus.	55.
Chamber Conditions.	58.
Fast Cycling.	59.
Experiments on Chamber Sensitivity.	61.

	Page.
<u>Chapter VIII. Bubble Counting and Particle Identification.</u>	
Counting Rate.	63.
Experiment.	66.
Bubble Counting.	67.
Comparison of numbers seen and expected.	69.
<u>Chapter IX. Bubble Density and Particle Energy.</u>	
Bubble Density : $\frac{1}{\beta^2}$	71.
Bubble Density : $\frac{dE}{dx}$	74.
Other Measurements.	74.
Mass Effect.	75.
Empirical formula for Bubble Density.	77.
Conclusion.	80.
<u>Chapter X. General Conclusion.</u>	81.
References.	85.
Appendix.	87.
Photographs of apparatus.	

Advantages and Shortcomings of existing visual Techniques.

Visual techniques have many advantages over counter methods of detecting sub-atomic particles. For example, a permanent record of the event is obtained, and several different measurements can be made from the same set of pictures.

All the charged particles associated with an event are visible, the identification of these particles is much easier, especially when aided by magnetic fields, and the chance of errors being made is greatly reduced. Visual methods are also much more reliable for measuring differential cross-sections and other relative measurements.

Multiple events can only be studied fully by these techniques. By using stereoscopic photography with cloud and diffusion chambers the complete mechanism of a reaction can be deduced, and with accelerators which produce beams of photons, the energy of the particular photon which caused the event can be calculated.

However, with the advent of machines capable of producing large currents of increasingly energetic particles, the density of the gaseous medium in cloud and diffusion chambers was so low that the products of



a high energy disintegration were not contained within the chamber. Also, events such as meson production have a very low cross-section and there were therefore very few of these interesting events to be seen in a medium of as low a density as gas at atmospheric pressure.

This defect had been overcome in part by increasing the pressure in these chambers to about 100 atmospheres, but the technique of operating these devices is very difficult and their cycling rate is very slow - about once per 15 minutes.

Nuclear plates have overcome the problem of low density. Further, the tracks in them are very thin, hence very high resolution can be obtained for angular and scattering measurements. Plates are continuously sensitive, which makes them ideal for cosmic ray work and detecting rare events, and emulsions have been developed which are sensitive to minimum ionizing particles.

However, scanning of nuclear plates is a long and laborious process. The complicated variety of light and heavy nuclei is unavoidable, and plates are susceptible to distortion due to processing, atmospheric conditions and temperature and pressure fluctuations.

The images tend to fade in time and an error in range measurements may occur if the moisture content is not known.

### Glaser's Experiments with Liquids.

Initial experiments to investigate the possibility of using a liquid medium were performed by Dr. D. A. Glaser in Michigan in 1952. Dr. Glaser (Ref. 1.) performed his early experiments with ether and showed that a liquid in a highly superheated state could be made to boil by bringing a radioactive source near the vessel containing the liquid. He then developed a chamber consisting of a small glass bulb of capacity 4 ccs., with a mechanism attached, by means of which the pressure in the chamber could be altered rapidly.

The base of the chamber was filled with glycol and the ether above it. The bulb was heated to  $140^{\circ}\text{C}$ , at which temperature the saturated vapour pressure of ether is 13 atmospheres.

On expansion it was found that the liquid could be maintained at a pressure of 1 atmosphere, that is, in a highly superheated state, for as long as a second before <sup>violent</sup>boiling took place. With suitable counter arrangements, tracks were successfully photographed of

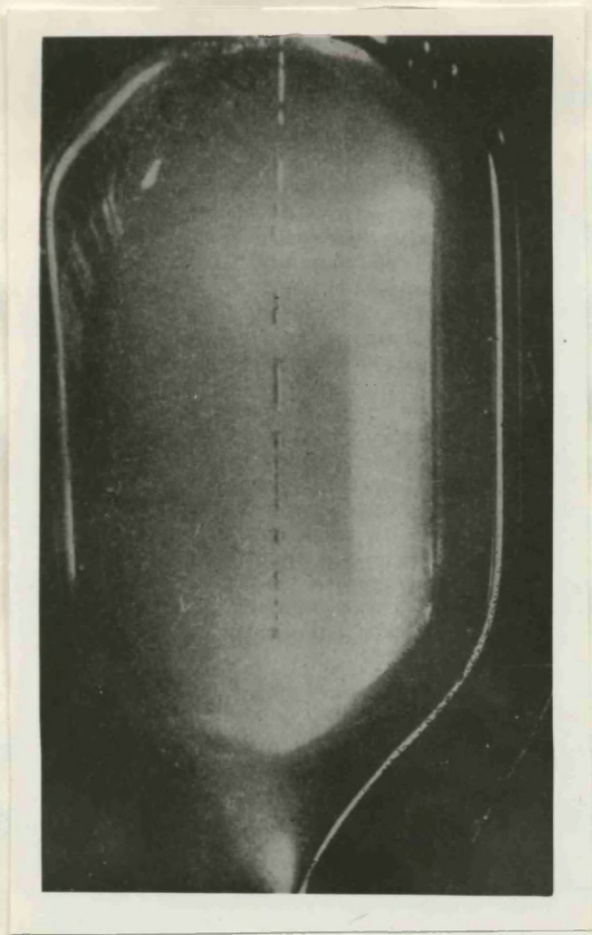


Plate 1.

cosmic rays which had passed into the chamber while it was in the sensitive condition. (Plate 1.) The track consists of a line of bubbles, photographed a few microseconds after the passage of the particle.

### Chamber Conditions.

Glaser also, at this stage, produced a formula which gave a value of the conditions required before a bubble containing a number of charges  $n$ , will grow to microscopic size.

He considered that in a superheated liquid, that is, one in which the pressure  $P_0$  is considerably lower than the saturated vapour pressure  $P_{\infty}(T)$  at the temperature  $T$ , tiny spherical bubbles a few molecules across are continually forming and collapsing because of thermal fluctuations in the liquid. It can be shown - as indeed it was by Bertanza et al (Ref. 2.) that a bubble containing no ions or one ion will tend to collapse, but if there are several ions of like charge present they can be considered to smear themselves on the surface of the bubble and their electrostatic forces of repulsion tending to make the bubble grow, will overcome the surface tension and pressure forces which are tending to make the bubble collapse. This is so if:-

$$P_{\infty}(T) - P_0 > P_n(T) = \frac{3}{2} \left( \frac{4\pi}{n^2 e^2} \right)^{\frac{1}{3}} \left( \sigma(T) \right)^{\frac{4}{3}} \left( \epsilon(T) \right)^{\frac{1}{3}}$$

- $n$     -    number of charges
- $e$      =    electronic charge
- $\sigma(T)$  =    surface tension
- $\epsilon(T)$  =    dielectric constant

To find the temperature at which a bubble chamber operates, values of  $P_n(T)$  are calculated for various temperatures and values of  $n$ , and a plot of these values and  $P_\infty(T)$  against  $T$  made on the same curve. Glaser found that for ether at about  $140^\circ\text{C}$  it appeared that values of between 2 and 10 were obtained for  $n$ .

Developments which followed were an increase in the size of the chamber, and the possibility of making a chamber made of metal with glass windows. However, it was anticipated that a chamber of this kind would not work. The early chambers, or clean chambers, were made of smooth glass with no discontinuities in the operating region. The metal chambers would have a sharp discontinuity between the metal wall and glass window, and boiling would start as soon as the liquid became superheated, this effect being similar to that produced by the presence of dirt in glass chambers, the metal ones were called dirty chambers.

The possibility of using liquid hydrogen was

6.

also being considered. This would be a most useful material since the bubble chamber would serve the dual role of target and detector.

From this work it was clear that a liquid medium detector was feasible.

At this time there was very little collaboration between ourselves and the few existing bubble chamber operators. The author was allotted the task of building a bubble chamber, with very little information to go on, and the thesis therefore develops as an investigation of bubble chamber physics.

CHAPTER II.THE FIRST CHAMBER.Preliminary Considerations.

Since so little information was available about how to build bubble chambers, it was decided to attempt to construct the type of chamber with which Glaser had first been successful so that the technical difficulties could be discovered. This was especially necessary since the photon beam of the electron synchrotron introduced difficulties not experienced in particle machines, the most notable being the production of electron pairs to a much greater degree than any other event.

From the information that was available, to construct a bubble chamber it was necessary first to choose a suitable liquid.

Pentanes whose boiling points are a little above room temperature seemed to be ideal. They are highly volatile, stable, transparent liquids and in addition have very simple chemistry - saturated hydrocarbons - and it was therefore decided to use isopentane, which boils normally at  $28^{\circ}\text{C}$ .

Values of surface tension, dielectric constant and saturated vapour pressure for this liquid were obtained from International Critical tables. Surface tension was

Constants used when evaluating Glaser's  
equation for isopentane.

$$\sigma = A \left( 1 - \frac{T}{T_c} \right)^n$$

For isopentane :-

$$A = 58.6$$

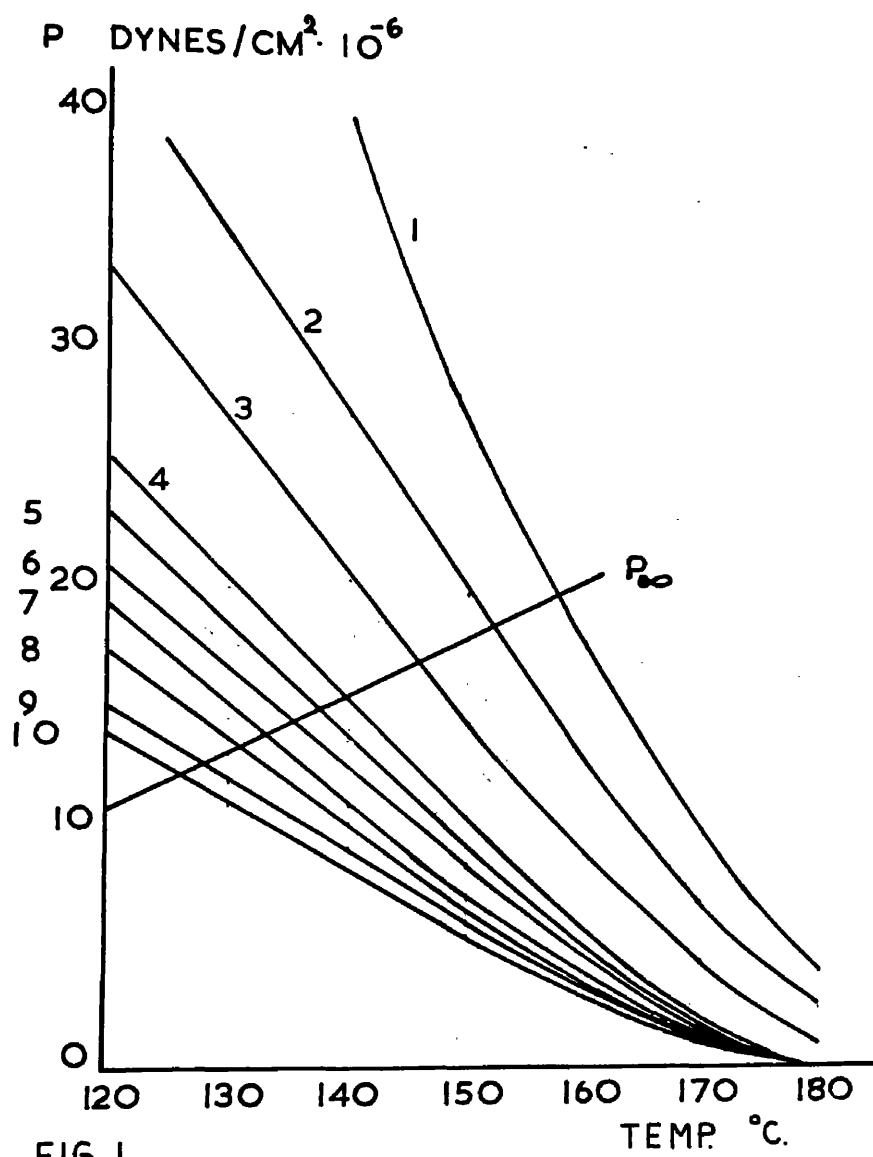
$$n = 1.23$$

$$T_c = \text{critical temperature} = 188^\circ \text{C} \\ = 461^\circ \text{K}$$

$$T = ^\circ \text{K}$$

$$\epsilon = 1.9 \text{ e.s.u.}$$





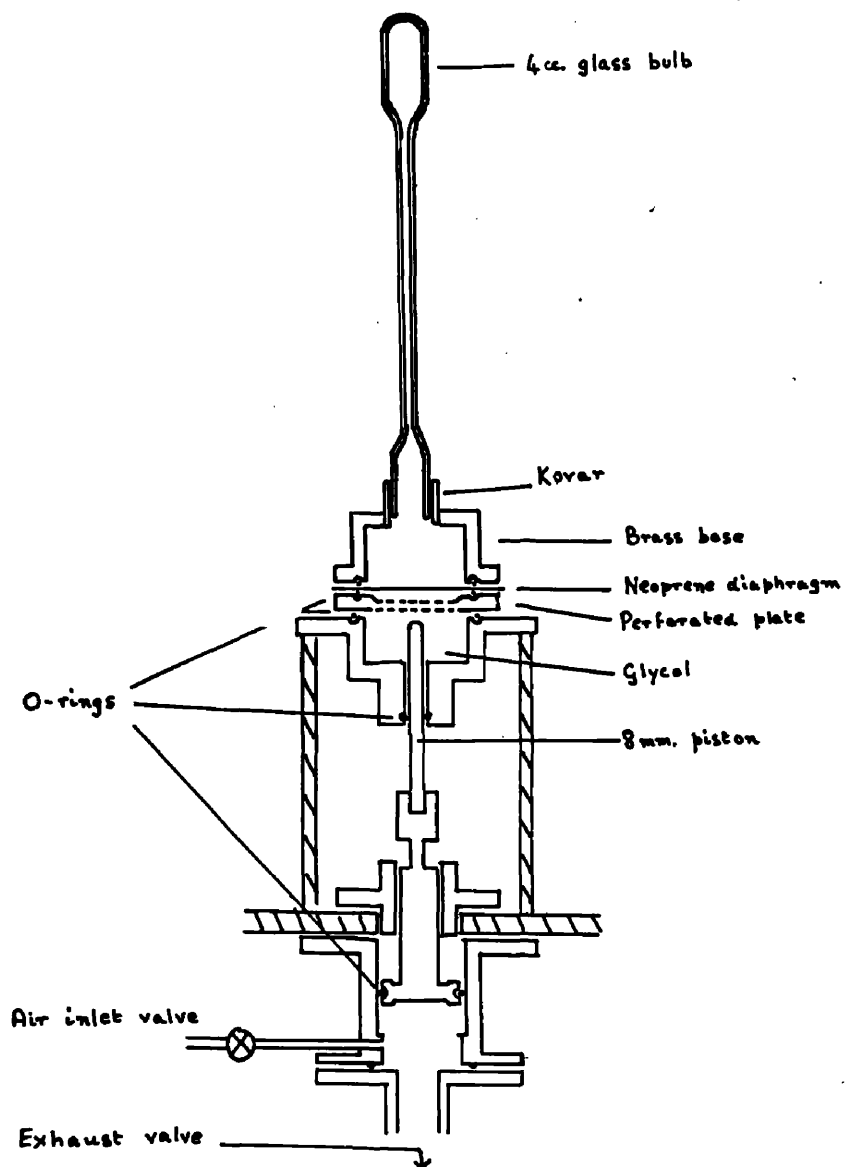


FIG 2.

not given over a wide range of temperatures, but from the empirical formula for surface tension

$$\sigma(T) = A \left( 1 + \frac{T}{T_c} \right)^n$$

a table of values was calculated. Substitution was made in Glaser's equation and the graphs shown in Fig. 1 illustrate the order of magnitude of temperature required.

This temperature is the one at which the  $P_n(T) \propto T$  curves for values of  $n$  between about 6 and 12 intersect the  $P_\infty(T) \propto T$  curve, and is in the region of 130°C with a saturated vapour pressure of 12 atmospheres.

The apparatus therefore had to consist of a cylindrical smooth-walled glass bulb of capacity 4 ccs. which could withstand pressures up to about 15 atmospheres and which could be heated to about 130°C - 140°C. This bulb must be attached to equipment by means of which the liquid can be compressed until all the vapour is removed, say to 15 atmospheres, and this pressure quickly reduced to achieve the necessary superheat.

#### Apparatus and First Tracks.

Fig. 2 shows the set-up which evolved. The chamber was attached to a glass capillary tube which widened at the base and was connected to the compression system by gluing the glass to a Kovar collar with "orgaldite" resin glue. Direct brass to glass union was not satisfact-

ory because the glass cracked while curing the or~~g~~aldite.

The diaphragm in the brass cylinder was introduced to separate working liquid and glycol. It was found necessary to allow the moving piston to move in glycol because pentane dissolved away lubricating grease. It was also convenient to separate the unit at this point since the piston could be examined without emptying the chamber.

To achieve compression and release of the piston, compressed air at 20 p.s.i. was allowed to act on a secondary piston directly connected to the stainless steel piston in the glycol well. Appropriate choice of the ratio of the areas of the pistons gave a step-up ratio in pressure to 15 atmospheres. A standard cloud chamber magnetic valve was used to give a sudden reduction of the pressure below the driving piston. Pressure was measured with a Bourdon tube pressure guage filled with glycol and directly connedted to the glycol well.

The chamber was heated by enclosing in a brass heating jacket with two circular glass windows on opposite sides through which the glass bulb was viewed. A heat-resistant silicon rubber was used as gasket material for the windows and the hole in the base through which the capillary tube passed. The jacket was filled with

glycerine as a heating fluid, and two 65 watt soldering iron elements were clamped to the outside. One heater was kept on all the time, and this maintained the glycerine at about  $110^{\circ}\text{C}$ , while the second was continually switched on and off by a "Simmerstat" control. The ratio of time on to time off could be smoothly varied by a dial control. The temperature was kept stable to within  $1^{\circ}\text{C}$  by continuously stirring the glycerine. It was measured with a mercury thermometer.

Early reports emphasised the need to clean the chamber very thoroughly and outgas the working liquid. The chamber was therefore cleaned first with soap solution then with a solution of hot nitric and chromic acid. It was carefully rinsed, first with filtered distilled water, then with alcohol, and dried off. The isopentane was outgassed by cooling in a bath of solid carbon dioxide and alcohol, and agitated under vacuum. The isopentane was introduced to the chamber by distillation.

The apparatus was mounted on a square of tufnol and built on a trolley for ease of transportation. Appropriate power supplies were led in and the chamber operated from a panel on the trolley.

The chamber was heated to  $125^{\circ}\text{C}$ , compressed then expanded, and delays varying from milliseconds to a

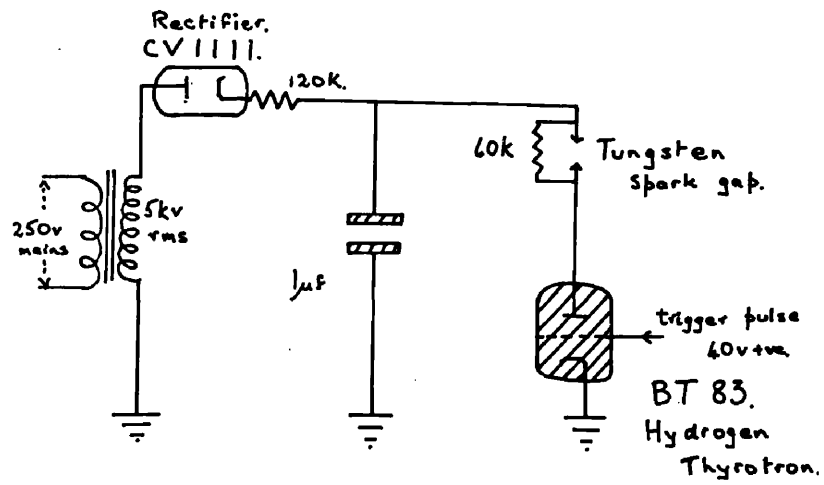


FIG.3.

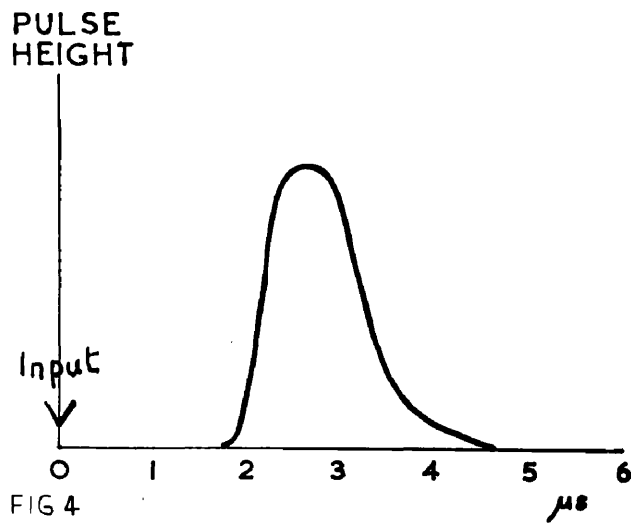


FIG 4

few seconds observed. The presence of a radioactive source ( $\text{Co}^{60}$ ) caused immediated boiling instead of exhibiting a delay on expansion, and the chamber was also made to boil by irradiating it with a pulse of 100 kv Xrays while the liquid was in the superheated condition.

It was known that bubbles, once nucleated, grew very rapidly and were big enough to be seen in a few microseconds. To illuminate the chamber, therefore, a spark discharge across a gap in the anode circuit of a B.T.83 hydrogen thyatron was used. The circuit is shown in Fig. 3. The spark was triggered by applying a 40 volt positive pulse to the grid of the thyatron and a graph of the time scale between input pulse and flash is shown in Fig. 4.

The camera used was a 35mm. Shackman Automatic, with shutter and winding-on mechanism which could be operated electrically. An extension piece was fitted to the lens holder to enable the camera to be placed close to the heating jacket and thus gave a full frame sized image of the chamber. HP3 film developed in Microphen fine grain developer was found to give the most satisfactory results.

Bright field photography was used, the light

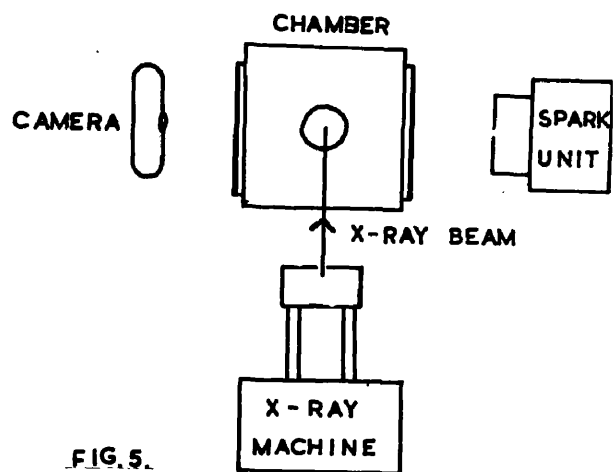


FIG. 5.

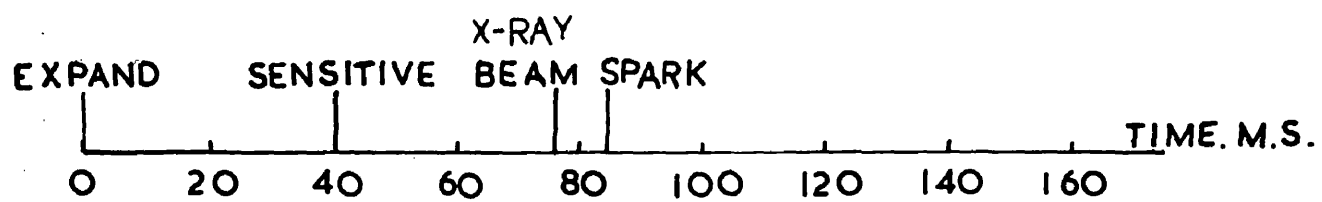


FIG 6



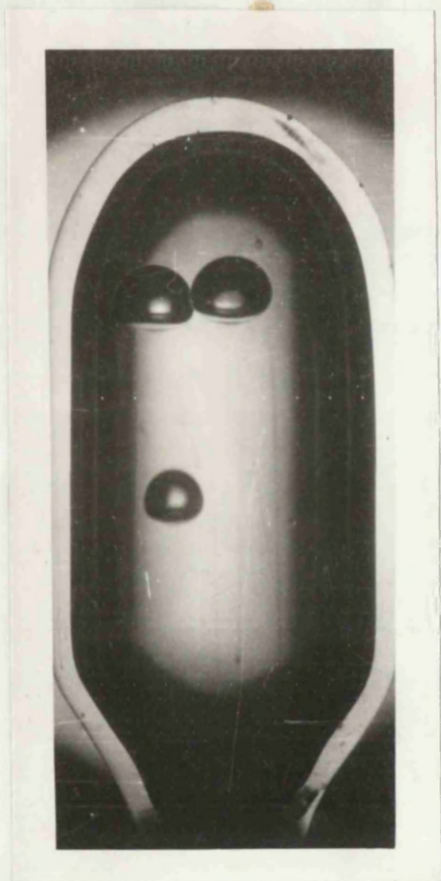


Plate 2.

from the spark being diffused by a ground glass screen. The relative positions of camera, chamber and spark gap can be seen in Fig.5.

First photographs were taken of bubbles produced by irradiating the chamber while it was in a superheated condition with the X ray beam. The set-up is shown in Fig.5, the sequence of events is shown in Fig.6, and Plate 2 shows the result.

These photographs showed that large bubbles could be seen clearly, and since the source experiment had shown the chamber to be radiation sensitive, the bubble chamber was then taken to the electron synchrotron in order to attempt to photograph tracks of ionising particles.

The electron synchrotron (Ref.3) in this department produces a Bremsstrahlung spectrum up to 350 M.e.v. The beam is collimated (Ref.4) as it leaves the doughnut, and appears in the beam room 1" in diameter. This beam occurs in pulses of from 10  $\mu$ s. to 200 ms. duration, five times per second.

To produce particles to be photographed in the bubble chamber, the beam was fired through a solid target and the chamber was placed below this target, so that some of the particles produced by a reaction in the target

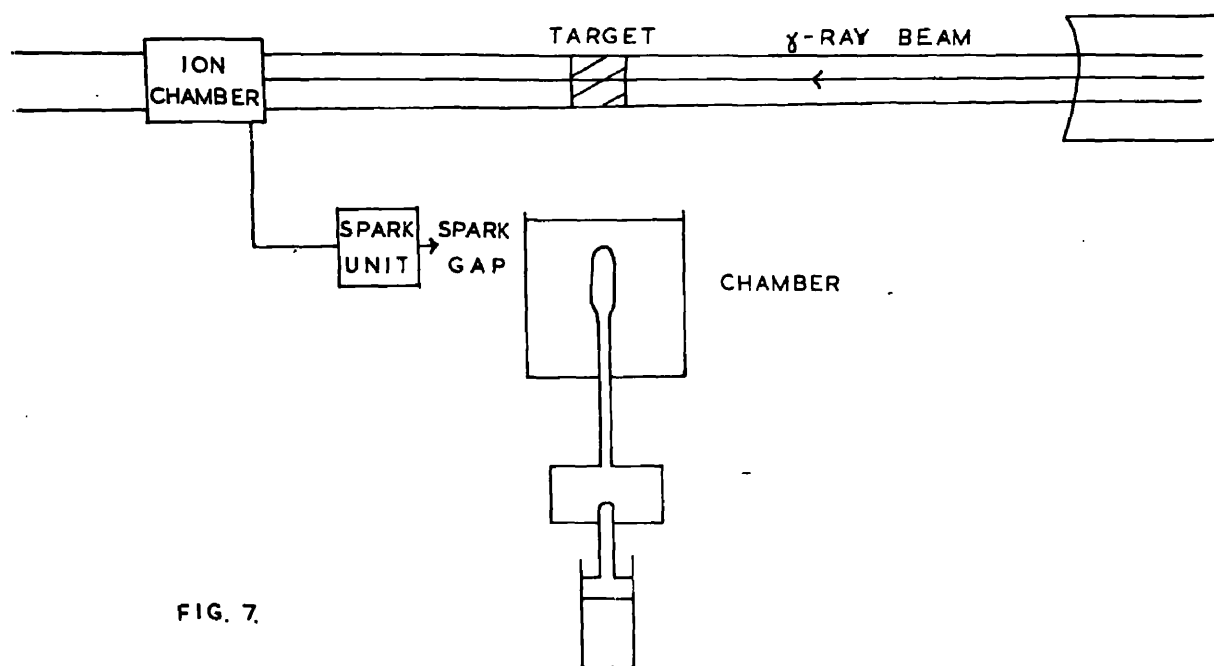


FIG. 7.

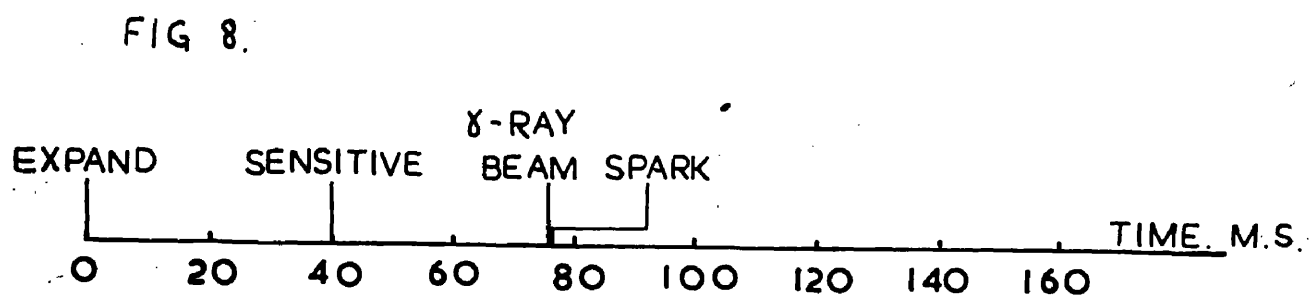


FIG 8.



Plate 3.

would pass into the chamber.

The bubble chamber could not be cycled five times per second, therefore the magnet of the synchrotron was allowed to pulse at its normal rate, while a bias was applied to the electron gun. This bias was removed by the bubble chamber operator with a manual switch when the chamber had been expanded and was in a sensitive condition.

The timing of the spark with respect to the beam was effected by taking a pulse from the ion chamber at the end of the beam room through which the photons passed, and applying it to the thyatron. The layout is shown in Fig. 7.

The sequence of events which led to the photographing of the first tracks is illustrated in Fig. 8, and Plate 3 shows these tracks.

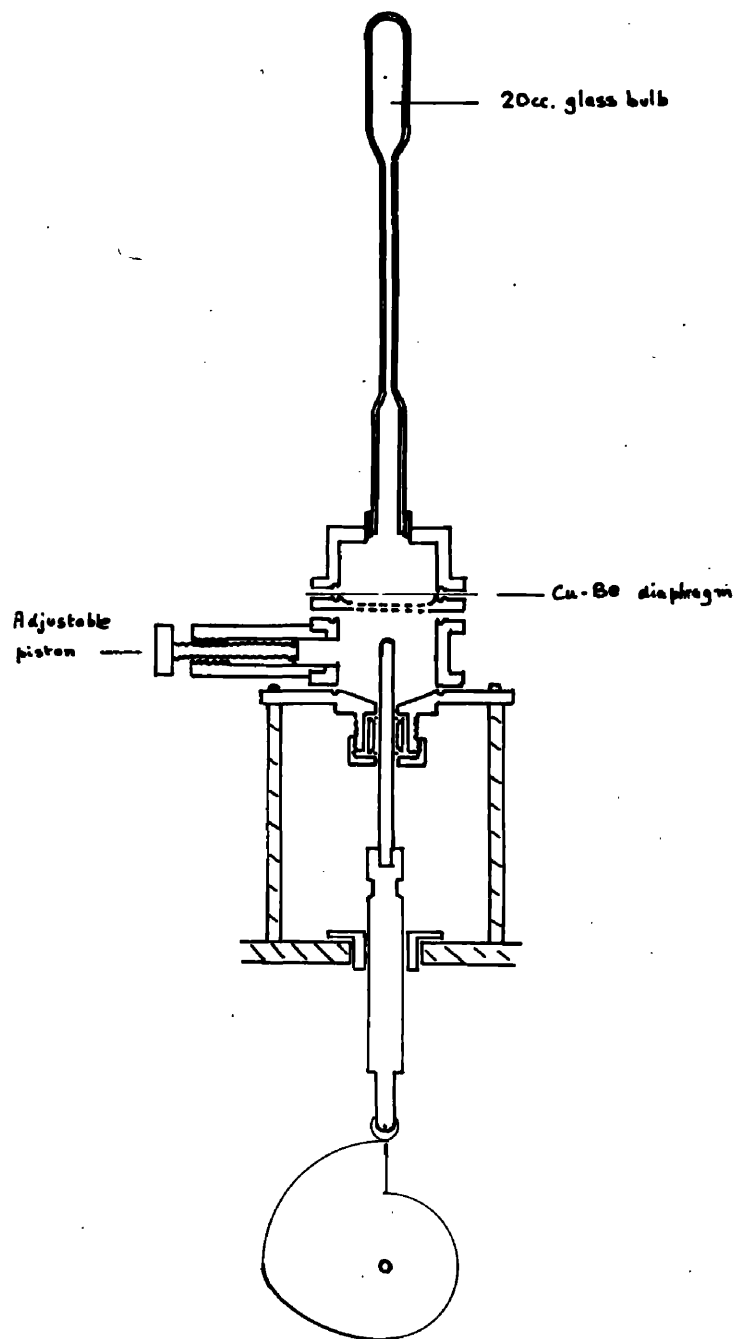


FIG 8a.


### CHAPTER III.      FURTHER DEVELOPMENT OF CLEAN CHAMBERS.

#### Shortcomings of the First Chamber and the Improvements Introduced.

Although tracks had been successfully photographed, it was clear that their quality left much to be desired.

The chamber was so small that it presented a very small solid angle to the target from which particles were being ejected. Also, because of its shape it acted as a very strong converging lens and the distribution of light was not uniform. Finally, there was very little control over the sequence of events - expansion, beam and flash.

A larger chamber was therefore built - a glass cylinder 2 cm. inside diameter, of capacity 20 ccs.

The method of applying pressure was altered, the piston now being moved by a cam wheel which was caused to rotate by an electric motor . The piston was held up by a magnetic valve connected to the other end of a lever. Releasing the current on the valve caused the piston to drop.

Although photography was immediately improved by increasing the size of the chamber, a further improve-

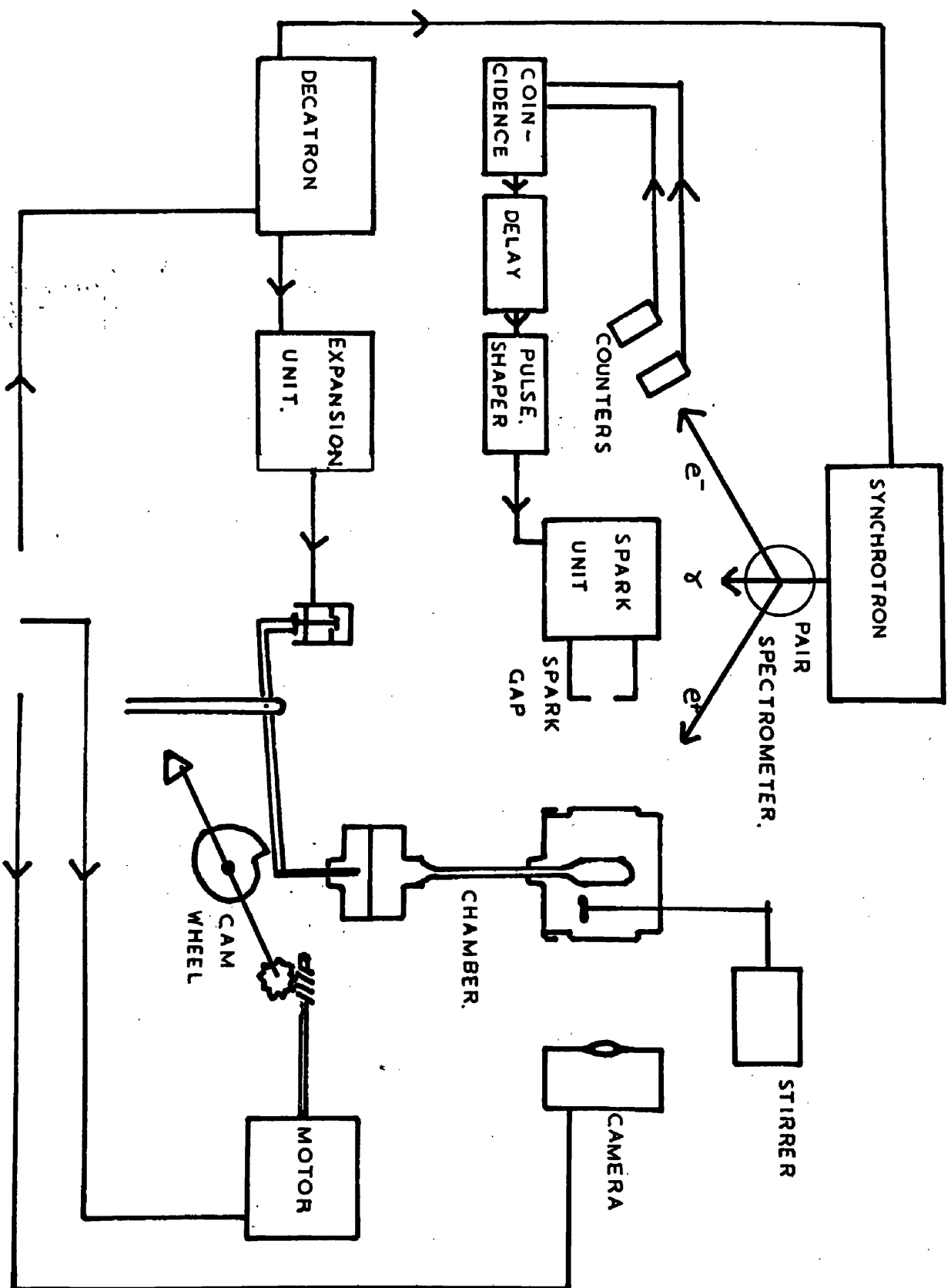


FIG 9.

CONTROL PANEL.



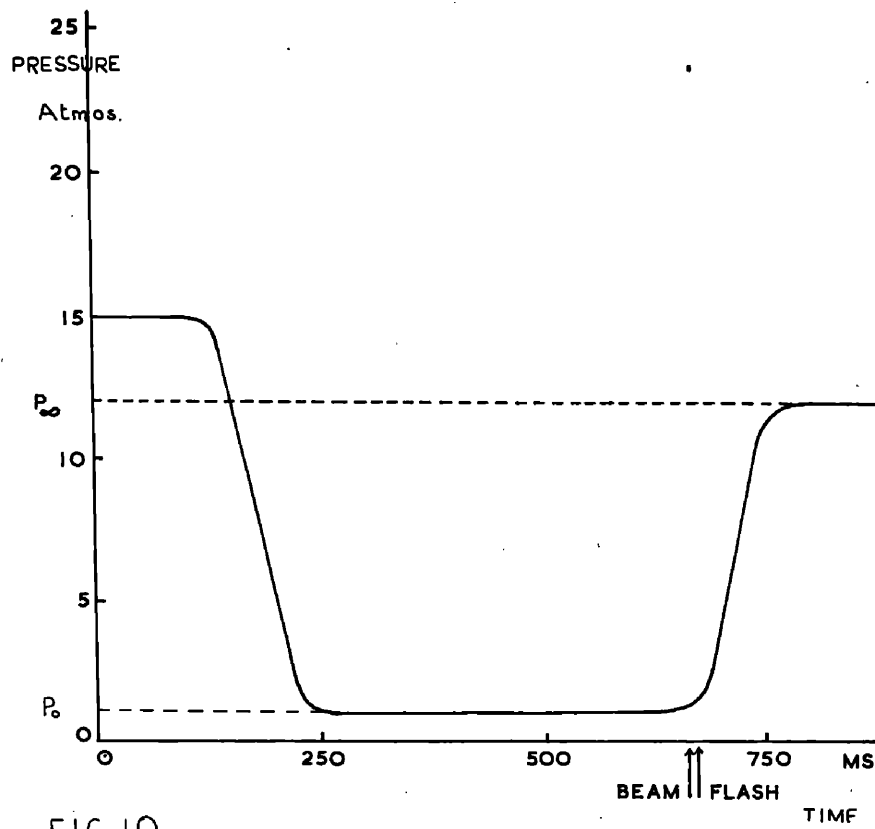


FIG 10

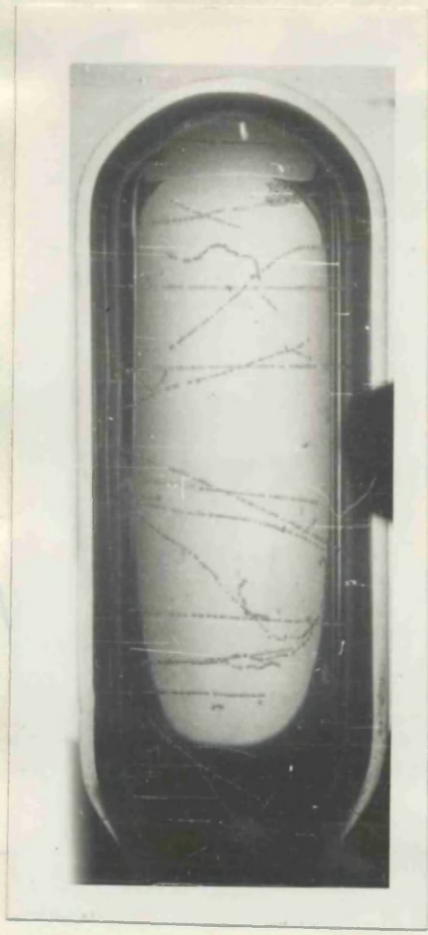
48  
Pressure  
Atmos  
50

10

5

0

FIG 10



350 145  
FLASH TIME

Plate 4

ment was achieved by placing the spark at the focal point of a large converging lens so that a parallel beam of light went through the chamber.

The method of producing particles was not very satisfactory for initial experiments to determine good operating conditions. The beam of high energy electrons from a pair spectrometer in the beam room was therefore utilised.

To control the time between expansion of the chamber and the arrival of the particles a different method of firing the synchrotron was used. A decatron unit used with cloud chamber experiments is linked to the synchrotron and both are in phase with the A.C. mains supply. With this device, it is possible to have a beam of photons only when required. In addition, pulses at 20 ms intervals before and after this beam can be taken from the unit. Ref. 4. The operator started the sequence of events with a push button control, then a pulse from the decatron was fed to a delay unit of variable amount thence to the chamber valve. The chamber then expanded about 200 ms before the beam came.

Fig. 9 is a block diagram showing the control units and Fig. 10 shows the variation of pressure with time in the chamber, and the time sequence of expansion, particles and flash. The cycling rate possible with this system was about one cycle per minute. Plate 4

shows the vastly improved quality of pictures achieved.

#### Bubble Chamber Operation.

It was decided at this stage that experiments be performed in order to study how the bubble chamber worked. Further, by counting droplets on the photographs of tracks of particles in cloud chambers, or grains in emulsion photographs, an estimation can be made of the mass and energy of the particle causing the track. Therefore, if an understanding of this bubble-forming process could be obtained, perhaps bubble counting might be used in a similar fashion in this type of device.

#### Bubble Density Measurement.

If the expansion process is studied on Fig. 10 it can be seen that a quantity of  $P_{\text{sat}} - P_0$  known as the superheat - the difference between saturated vapour pressure and pressure to which the chamber is expanded - can be readily varied by altering the temperature and ensuring that the chamber expands to 1 atmosphere.

The beam of high energy electrons is ideal for experiments of this nature since, although the particles lose energy in the dense  $\text{CH}_2$  medium, if they enter the chamber with about 100 M.e.v. of kinetic energy they lose so little energy ( a few M.e.v.) that they are still uniformly ionizing particles. Therefore any change in

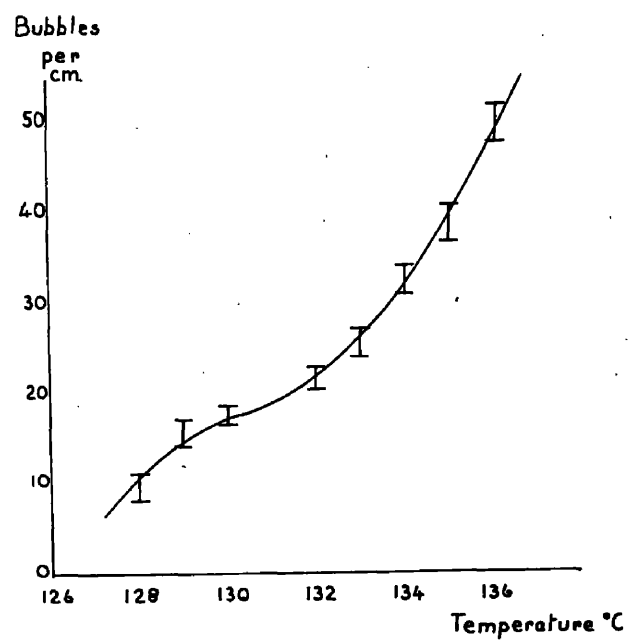


FIG II.

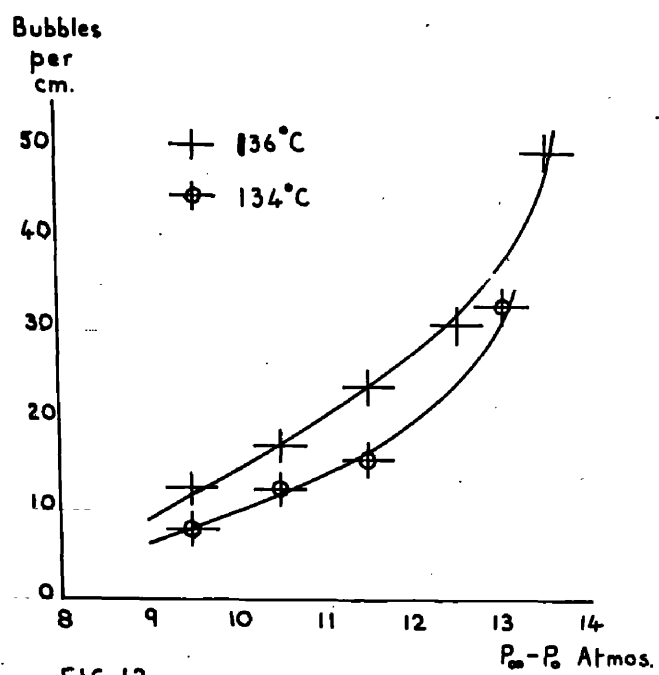


FIG 12.

bubble density - bubbles per centimetre of track length - is caused by change in chamber conditions.

Photographs were taken of these 100 M.e.v. electron tracks in the temperature range  $128^{\circ}\text{C}$  -  $136^{\circ}\text{C}$ . Photographs were also taken of tracks of similar particles at temperatures of  $134^{\circ}\text{C}$  and  $136^{\circ}\text{C}$  but in this case the pressure  $P_0$  to which the chamber expanded was varied. This was done by increasing the top pressure and since the piston movement was always the same,  $P_0$  was increased.  $P_0$  was measured from the static pressure guage.

To count the number of bubbles per centimetre of track, the film was projected on to a white sheet giving about 10 fold magnification. Only bubbles on straight tracks were counted, to ensure that the particles were uniformly ionizing.

The inside diameter of the chamber had been measured accurately, therefore a calibration of the length of a particular track could be made. The number of bubbles on one centimetre length of track was measured on about twenty tracks for each point on the graphs.

The results of these experiments are shown in Figs. 11 and 12. There have been no other measurements of this kind in a clean isopentane-filled chamber.

Since further experiments of this type were

performed in a different chamber, a discussion of the results will be left until Chapter 5.

#### Rate of Bubble Growth.

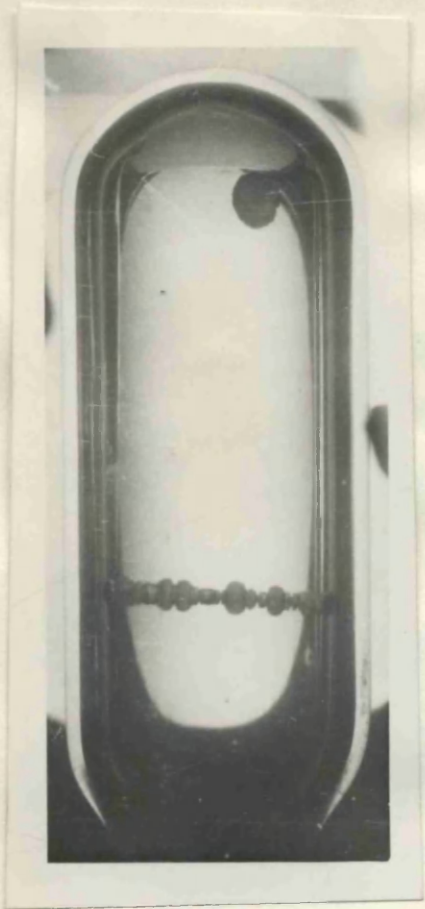
The second effect studied was the rate at which bubbles grew in the chamber. To obtain measurements of this kind, the delay between the entry of the particles and triggering the spark gap was varied from 2  $\mu$ s. to several ~~hundred~~ milliseconds, several photographs being taken at each stage.

Bubble diameters were measured with a low power microscope. The scale in the eyepiece of the microscope was calibrated by measuring the thickness of a wire whose diameter had previously been measured with a micrometer screw guage. A correction had to be made for actual bubble size from the size of the bubble on the film negative. Other measurements made were of the number of tracks in a particular frame. From this, and knowing the temperature of operation and hence the bubble density, an estimate of the number of bubbles in a frame could be made, thus giving an estimate of the total volume of vapour which existed in the chamber at a given instant.

The two main factors which determined the size of a bubble were time, and the number of other bubbles



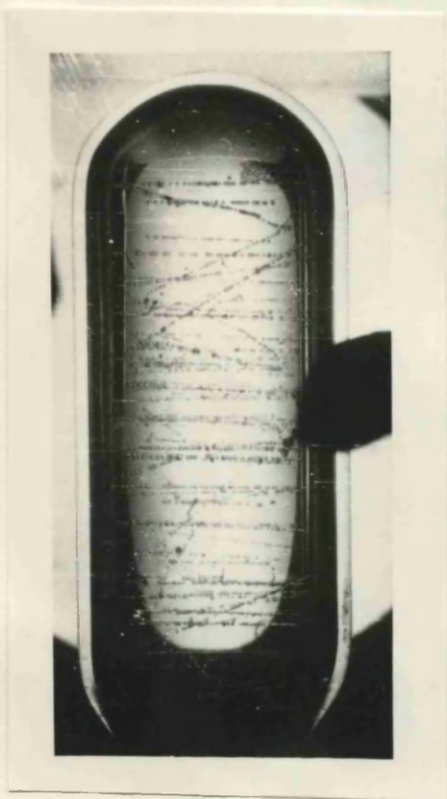
Plate 5



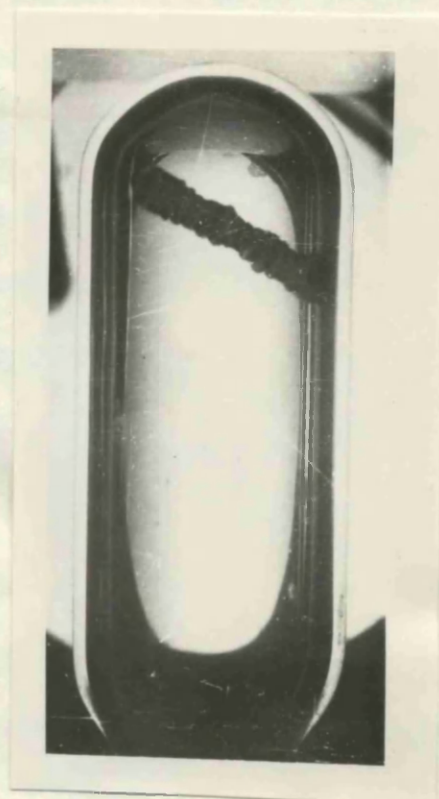
a. 60  $\mu$ s.



b. 2 ms.



c. 60  $\mu$ s.



d. 2 ms.



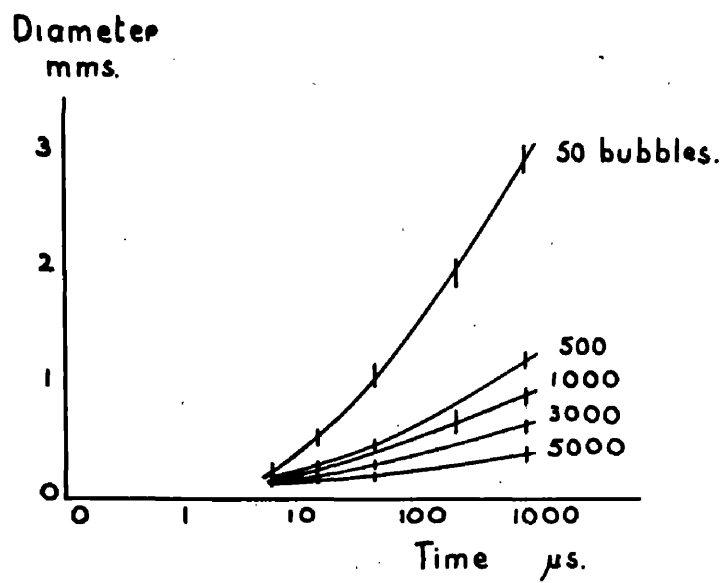


FIG 13

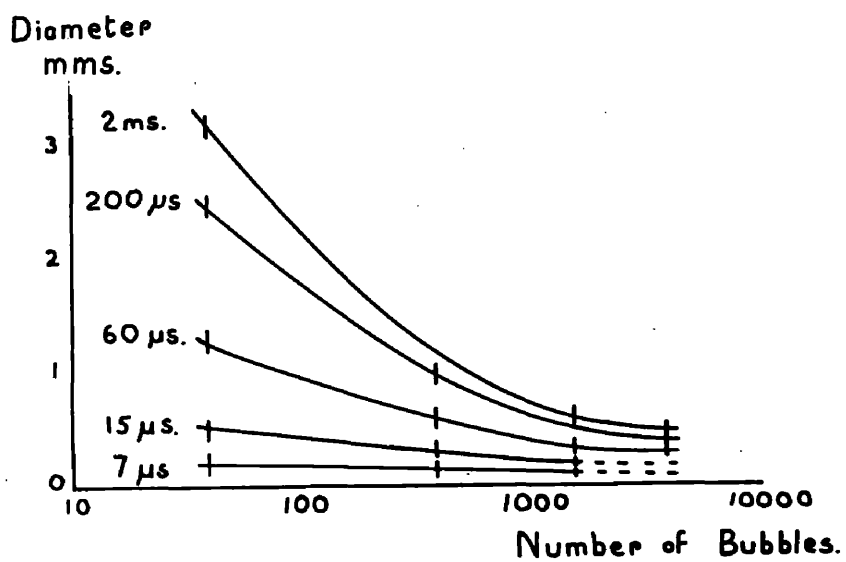


FIG 14

present. Plate 5 gives a variety of photographs of bubbles taken under different conditions. Although the diameters of the bubbles in b and c are almost identical, b was taken 2 ms after the particles entered the chamber, and c only  $60\mu s$  after.

Fig. 13 is a graph of bubble diameter drawn against time with a parameter of the number of bubbles. This shows that at short delay times between the bubble being formed and photographed, all bubbles are about the same size. As this delay is increased, the number of bubbles has a large effect. Fig. 14, a graph of diameter against number of bubbles, illustrates this effect more clearly.

At times of the order of  $10\mu s$  or less the effect of a bubble at a particular point in the chamber cannot be transmitted throughout the chamber. Assuming that the pressure wave travels at the velocity of sound, hence in  $5\mu s$  it will have travelled  $\sim 1$  cm. In a chamber of 2 cm inside diameter by about 5 cm long, this will not be effective throughout the chamber until after about  $15\mu s - 25\mu s$ .

Thus in a clean chamber two regions of time can be considered, i.e., longer and shorter than about  $20\mu s$ .

Measurements have been made of the bubble dia-

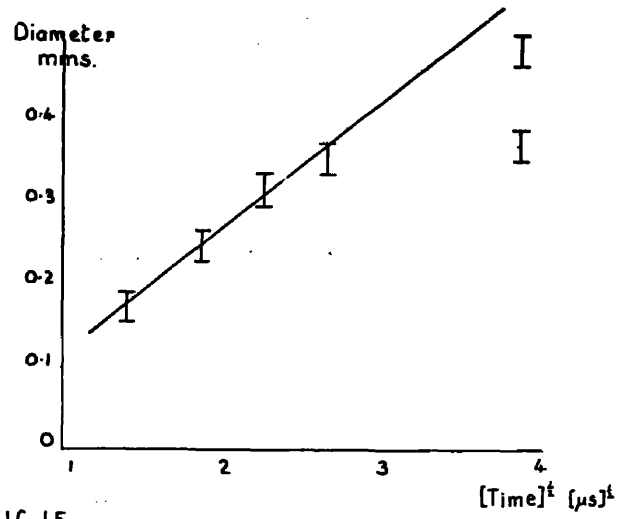


FIG 15.

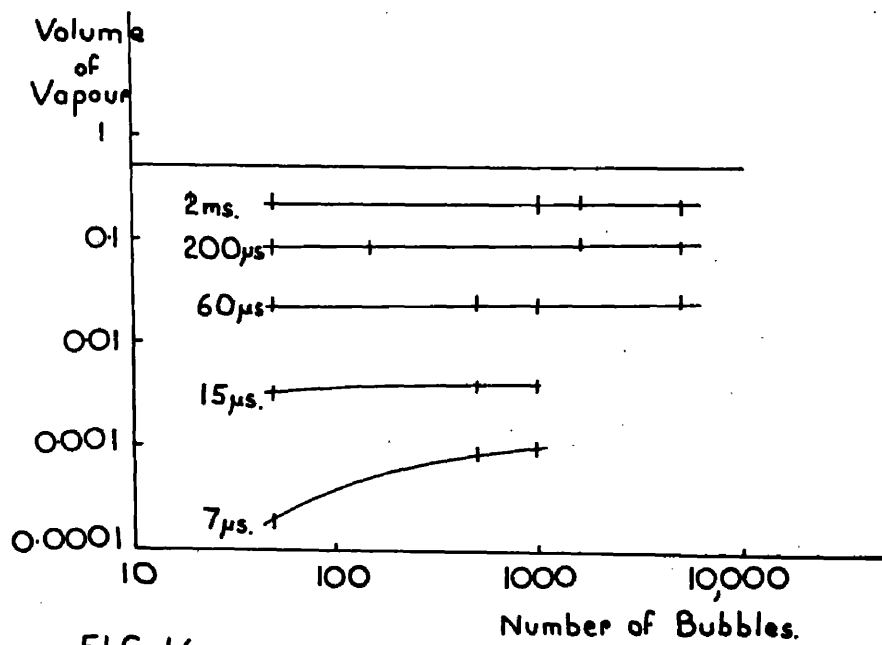


FIG 16

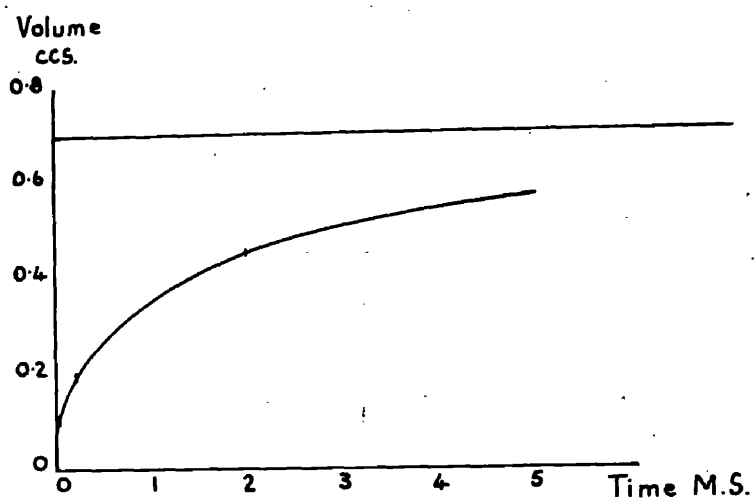


FIG 17

meters for times as short as 2  $\mu$ s. and although these results are not accurate, the graph of bubble diameter against  $(\text{time})^{\frac{1}{2}}$  is a straight line up to about 10  $\mu$ s., (Fig. 15) agreeing with a formula on rate of growth of bubbles in superheated liquids. (Ref. 5)

$$d = \left\{ \frac{3}{\pi} \right\}^{\frac{1}{2}} (\theta - \theta^1) \left\{ \frac{K}{\sqrt{D}} \right\}_{\theta} \left\{ \frac{1}{C_p} \right\}_{\theta^1} t^{\frac{1}{2}}$$

where  $\theta$  = temperature of liquid

$\theta^1$  = temperature at which the pressure of the saturated vapour = hydrostatic pressure

$K$  = thermal conductivity

$D$  = diffusivity

$C$  = latent heat of evaporation

$p$  = vapour density

In this expression  $\theta^1$  is the pressure term, in effect and at times  $< 10 \mu$ s. the pressure change is negligible because the bubbles are so small.

To investigate the region above 20  $\mu$ s., graphs were drawn of volume of vapour against number of bubbles, (Fig. 16) with a time parameter. It can be seen clearly that in this time region the volume of vapour is constant for a given time, that is, it increases at a fixed rate, independent of the number of bubbles in the chamber, hence the curve in Fig. 17 is a single line.

TABLE 1.

Isopentane ( densities given at pressures of  
1, and 13 atmos. respectively.)

Chamber	Volume of Isopentane	T °C	Density <sub>1</sub>	Density <sub>13</sub>	$\Delta V$ . ccs.
4cc.	4ccs.	130	0.4826	0.4842	0.011
	36	15	0.6247	0.6259	0.070
20cc.	18	130	0.4826	0.4842	0.060
	7	15	0.6247	0.6259	0.014

## Glycol

Chamber	Volume of Glycol	T °C	$\beta$	$\Delta V$ . ccs.
4cc.	20ccs.	15	34	0.0094
20cc.	50	15	34	0.0238

## Total

Chamber	Piston diameter	Distance moved	$\Delta V$ experiment	$\Delta V$ calculation
4cc.	0.8cm.	1cm.	0.76ccs.	0.0904ccs.
20cc.	0.25in.	1in.	0.766ccs.	0.1078ccs.

The rate of increase of volume of vapour is also that of increase of pressure in the chamber.

No other measurements on the effect of chamber conditions on the rate at which bubbles grow have been reported.

#### Compression Measurements.

When the piston was being designed for the compression system, values of the compressibility of isopentane and glycol were obtained from International Critical Tables in order that the distance which the piston would have to move could be calculated. However, when this was related to the distance which the piston moved in practice for a particular pressure change there appeared to be a large discrepancy.

A careful measurement was therefore made of top and bottom pressures, temperature, and piston movement for this chamber, and the result is shown in Table 1.

The rough calculation made for the early 4 cc. chamber is also shown, and the difference in actual and expected volume change is about the same.

The volume change of isopentane was calculated from the densities of isopentane under different conditions of temperature and pressure given in International Critical Tables. The volume change of glycol was calculated from

the formula

$$\beta = \frac{10^6}{V} \left\{ \frac{V_1 - V_2}{P_2 - P_1} \right\} T$$

where the value of  $\beta$  was obtained from International Critical Tables.

A possible explanation of this effect is that under such very high pressures the apparatus stretches elastically. When at 15 atmospheres, there is a <sup>pressure</sup> ~~force~~ of 5 atmospheres on each of the eight 4B.A. bolts holding the brass cylinders together. Since the compressibility of the liquids is so small, a very small change in the capacity of the system could account for this effect.

This effect proved to be important when designing compression systems for larger chambers.

#### Temperature Gradients.

A further measurement gave an estimate of the temperature gradients which might be set up in this chamber during the cycle of operations.

To calculate this quantity the Latent Heat of vaporisation and the mass of vapour involved are required.

The Latent Heat of vaporisation can be calculated from the Clausius Clapeyron Equation.

$$L = T(V_2 - V_1) \frac{dP}{dT}$$

$V_2$  = molar volume of vapour at N.T.P.

$V_1$  = molar volume of liquid



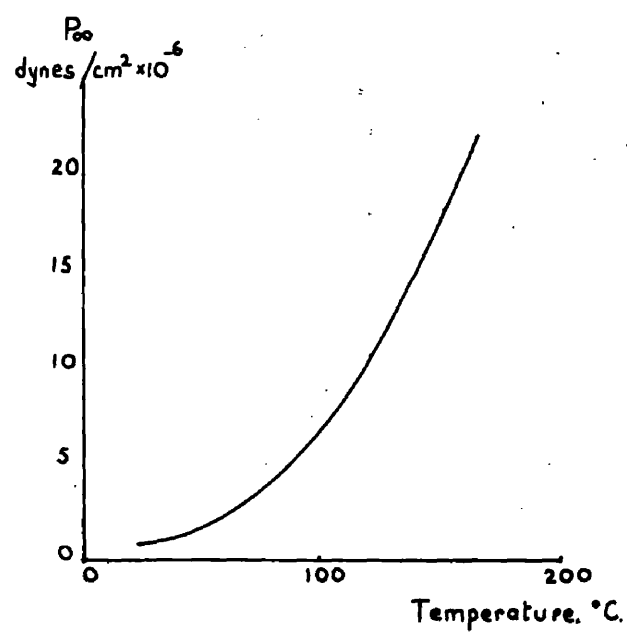


FIG 18.

To a good enough approximation  $V_2 \gg V_1$  and assuming an ideal gas  $V_2 = \frac{RT}{P}$  if  $T < T_c$ .

Hence 
$$L = \frac{RT^2}{P} \frac{dP}{dT}$$

The latent heat will be calculated at  $130^\circ\text{C}$ .  $\frac{dP}{dT}$  is obtained from the Saturated Vapour Pressure curve (Fig. 18) and at this temperature is  $18.5 \text{ cm.}/^\circ\text{C}$ . ( $0.21 \times 10^6 \text{ dynes/cm}^2/^\circ\text{C}$ )

$$\therefore L = 6510 \text{ cal/mole.}$$

$= 90.5 \text{ cal/gm. for } \text{C}_5\text{H}_{12}$  where the gram molecular weight is 72 gms.

To estimate the temperature to which the top of the chamber will rise it is first necessary to know the mass of vapour which forms after boiling takes place.

First the volume of vapour was calculated from the distance moved by the piston. The change in capacity of the system due to the removal of the piston on expansion is equal to the volume of piston extracted, which could be measured. The three different conditions of pressure were known - top, bottom, and saturated vapour pressure.

Further, since the top pressure and the saturated vapour pressure are not very different, it was reasonable to assume little change in the capacity of the system due to stretching of the apparatus. Hence the actual volume of liquid in both these cases was about the same, and the volume of vapour when the piston was down, was, to a suff-

iciently good approximation, equal to that volume of piston removed, that is about 0.7 ccs.

The density of vapour was calculated as follows  
72 gms. at <sup>S</sup>N.T.P. occupies 22.4 litres

∴ From Boyle's Law

Vol. of gm. molecular wt. at 13 atmos. = 1.77 litres

Density of vapour = 0.0405 gm/cc.

∴ Mass of vapour in chamber M = 0.028 gms.

Therefore amount of heat released  $H = ML = 2.5$  cals.

Now, when boiling due to ionization occurs, bubbles form throughout the chamber, and this heat is taken from all parts and will cause a slight uniform fall in temperature. However, when the chamber is recompressed, the heat is returned at the top of the chamber.

The specific heat  $S$  of isopentane is about 0.3 cals/gm/°C

The mass of liquid in the chamber  $m \div 20p = 9.5$  gms.

Hence temperature drop throughout chamber  $t \div \frac{H}{mS} \div 1.0^\circ\text{C}$

If heat given, say, to top third of liquid, i.e. ~ 3 gms.

Temperature rise  $\div 3.0^\circ\text{C}$ .

∴ it is possible for the bottom of the chamber to be  $1^\circ\text{C}$  below the heater temperature and the top about  $2^\circ\text{C}$  above.

In practice, a difference in bubble density on horizontal electron tracks at the top and bottom of the chamber was not observed. However, the slow cycling rate

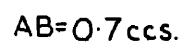


FIG. 19.

probably gave adequate time for gradients to disappear.

### P - V Diagram.

Finally the PV diagram was constructed, where it can be seen that the work done on the liquid is represented by the area FABE Fig. 19.

A rough estimate of this area gave

$$\begin{aligned}\text{Work} &\doteq 4.5 \times 10^6 \text{ ergs.} \\ &= 0.1 \text{ cal.}\end{aligned}$$

causing a temperature rise of  $< 0.1^\circ\text{C}$  in 20 ccs. of isopentane.

Although in a chamber of this size, the effect is negligible, it is clear that it must be considered in larger chambers.

If the PV diagram is investigated in more detail, starting from A, the expansion is an adiabatic process, causing slight cooling, and as the chamber sits in a superheated state the liquid temperature and therefore pressure will rise slightly to C since volume is fixed.

The boiling process is from C  $\rightarrow$  D since energy removed in the form of latent heat was removed from the liquid. The resulting lower temperature gives a lower saturated vapour pressure. In time the liquid temperature again rises to  $130^\circ\text{C}$  - E on the curve.

The recompression process is adiabatic, causing

a temperature rise, and in time the liquid again settles to 130°C at A.

BC and DE were observed on the static pressure gauge, but they were too small to be measured accurately being about 3 pounds per square inch and 6 or 7 pounds per square inch respectively. The step FA was not observed. They have all been exaggerated in the diagram for purposes of illustration.

All these measurements and studies gave a great insight into the workings of the device, proved to be extremely useful when larger chambers were built, and were used when calculations on bubble formation theories were being considered.

CHAPTER IV.THE FIRST DIRTY CHAMBERS.Need for a Larger Chamber.

While the clean chamber was being developed, it became clear that it was not of much practical value for nuclear physics experiments. This was due in part to its size and partly because of its shape. A cylinder is the strongest shape, besides, all sharp corners must be avoided, and the optical defect on a track is therefore large, making angle measurement, for example, almost impossible. Another consideration was that in this laboratory it was desirable to have a detector through which the photon beam of the synchrotron could be fired. This involves introducing a thin entrance window to the chamber for the beam, and having a chamber of dimensions which could contain tracks of particles from a high energy disintegration.

The experiments on the rate at which bubbles grow showed that vapour was still forming a few milliseconds after the bubbles were initiated. That is, the saturated vapour pressure had not been reached. If an expansion mechanism was devised which could reduce the pressure on the liquid at a faster rate than the pressure could rise from boiling, a superheated condition could be

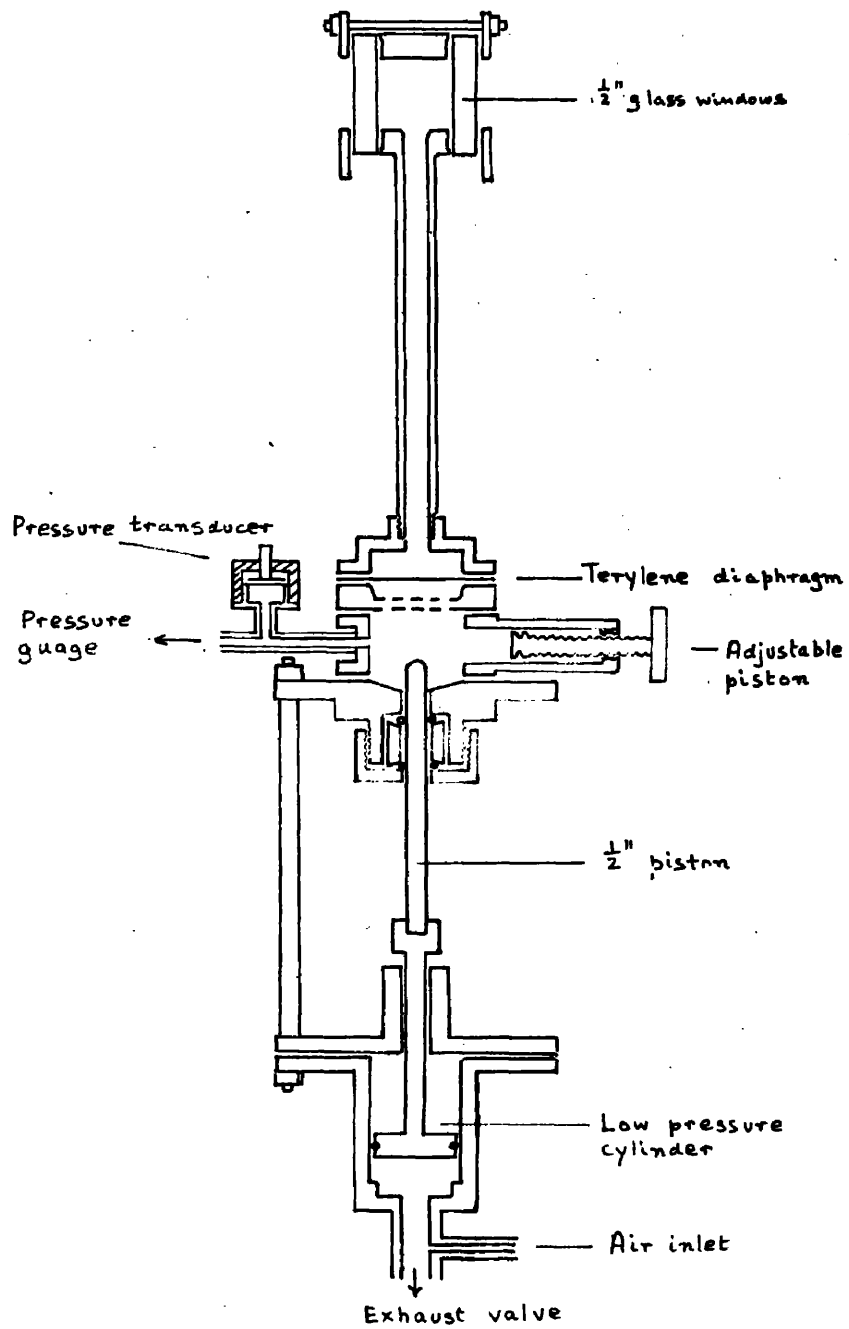


FIG. 20.



achieved for a short time and might perhaps be radiation-sensitive.

### Apparatus and Operation.

A chamber was therefore built which consisted of a brass cylinder, with flat plate glass windows clamped to the ends, separated from the brass by a fluon gasket. The principle of the expansion system was similar to the first method used with glass chambers.

Although calculations from compressibility indicated that a smaller piston should be sufficient, a  $\frac{1}{2}$ " diameter piston which could move up to 1.5" was used, giving a total volume change of  $2\frac{1}{2}\%$ . The apparatus is shown in Fig. 20.

Heating was done by the same process as before and the rest of the equipment was identical to that of the clean chamber.

When the chamber was expanded violent boiling was immediately observed, starting from the discontinuity between the glass window and the brass wall. It was not possible to observe the pressure change on the guage, since it happened so quickly. Therefore a pressure transducer was built, which operated on the principle of changing capacity in a condenser, one plate of which was directly connected to the chamber. This condenser was

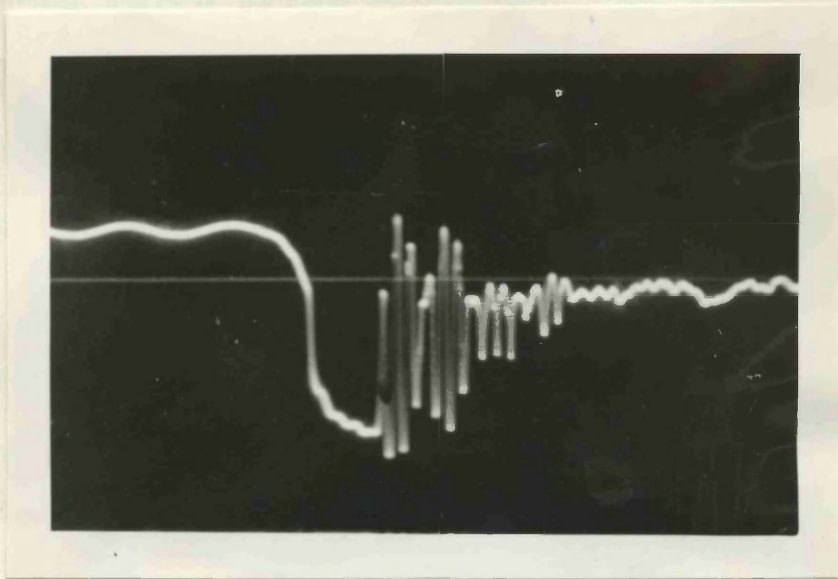
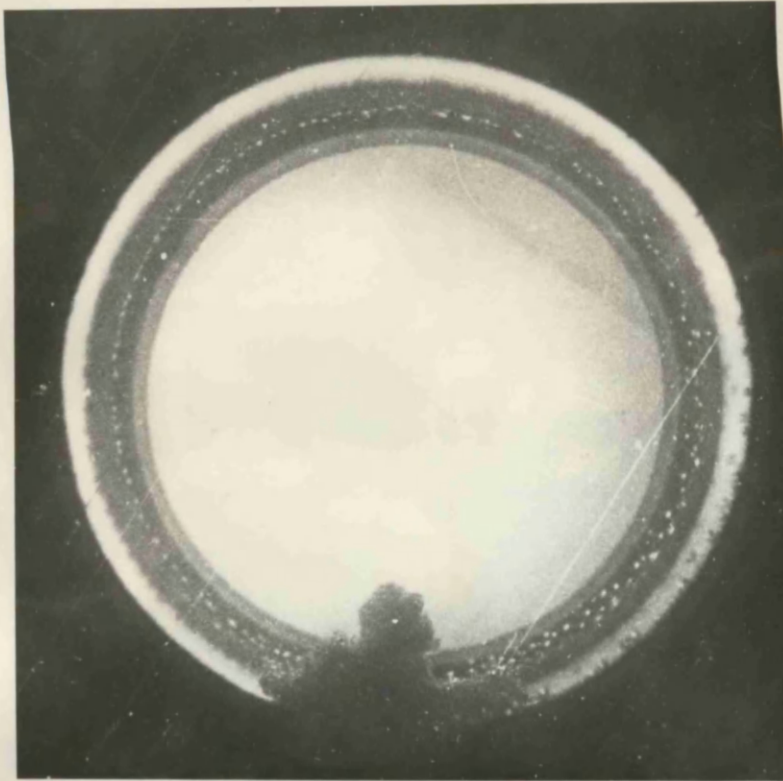
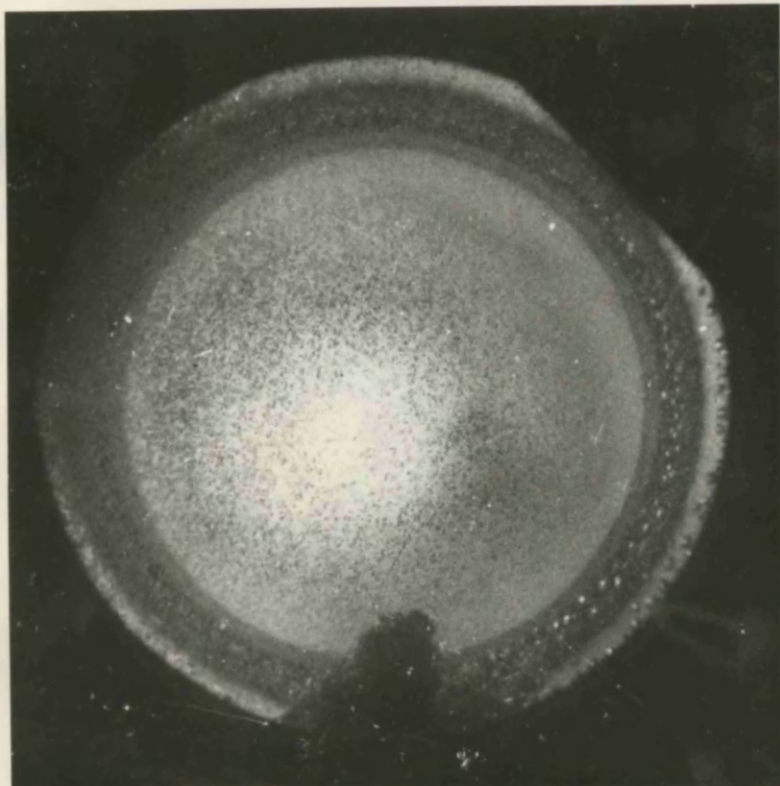


Fig 21.



a.

Fig 21



b.

then made part of a tuned circuit, the frequency changing as the capacity of the condenser changed, and this was detected by a frequency-modulated detector, and the trace shown on an oscilloscope.

Because of the non-linearity of the circuit, it was not possible to calibrate the trace with respect to pressure, but the trace proved to give a very accurate indication of change of pressure with time. Fig. 21 is a typical trace.

The presence of a radioactive source could not indicate whether this chamber was radiation-sensitive similar to the method used with the glass chamber. However, if the chamber was expanded and a photograph taken any time after the minimum on the transducer trace, bubbles due to ionization produced from the source could be seen if the temperature was raised by about  $20^{\circ}\text{C}$  to  $150^{\circ}\text{C}$ .

Plate 6a shows a photograph with no source, where the boiling at the walls can be clearly seen, and Plate 6b a photograph when a  $\text{Co}^{60}$  source was present.

To photograph tracks of high energy particles, the chamber was taken to the synchrotron and set up opposite the electron beam. The technique was similar to the last method used with the clean chamber, only the



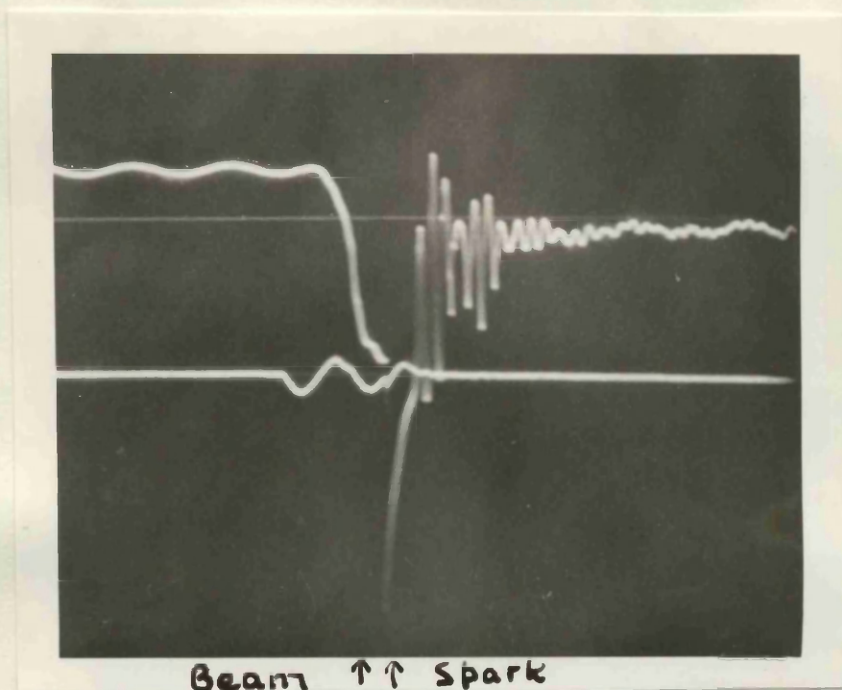


Fig 22a.

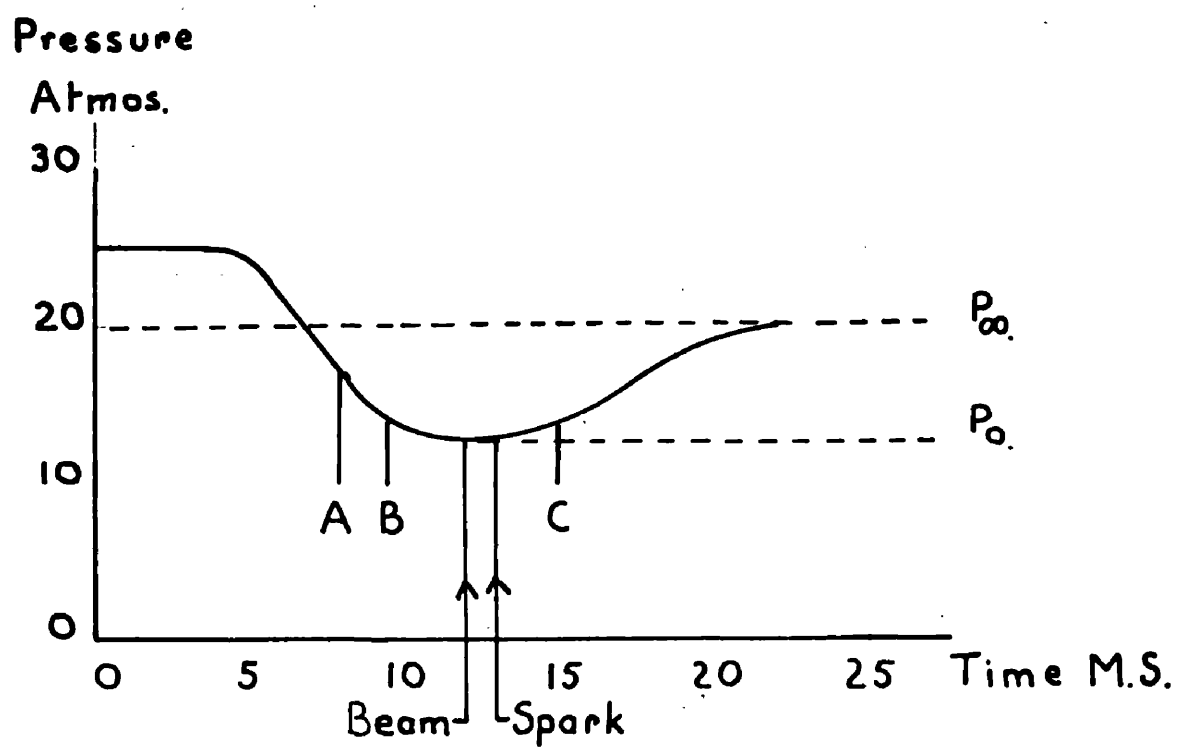


FIG 22.

timing of the chamber expansion had to be done much more accurately with respect to the beam.

It was found that if the particles entered the chamber before A(Fig.22), there were no bubbles. From A to B the bubble density gradually increased with apparently otherwise identical conditions. From B to C, a period of about 5 ms, the bubble density was uniform, while from C onwards, it gradually decreased. The delay time between the entry of particles and taking the photographs had to be greater than 0.5 ms. Fig. 22a shows, superimposed on the transducer trace, a pulse indicating beam time. Accurate beam to spark timing was done using an oscilloscope with faster time base, the time base being triggered by the beam pulse.

#### Chamber Operation.

Because there were several features in the operation of this chamber which differed from the glass chamber, they were examined in turn.

Although the limited sensitive region was expected, it is significant that bubble density is reduced if the particles enter before B on the transducer trace, and bubbles do not exist before A. This implies that the energy which goes to form a bubble is dissipated through the liquid before the conditions are such that this energy is sufficient to cause a bubble to form.

The method employed in cloud chambers to photograph tracks of cosmic rays by triggering the /

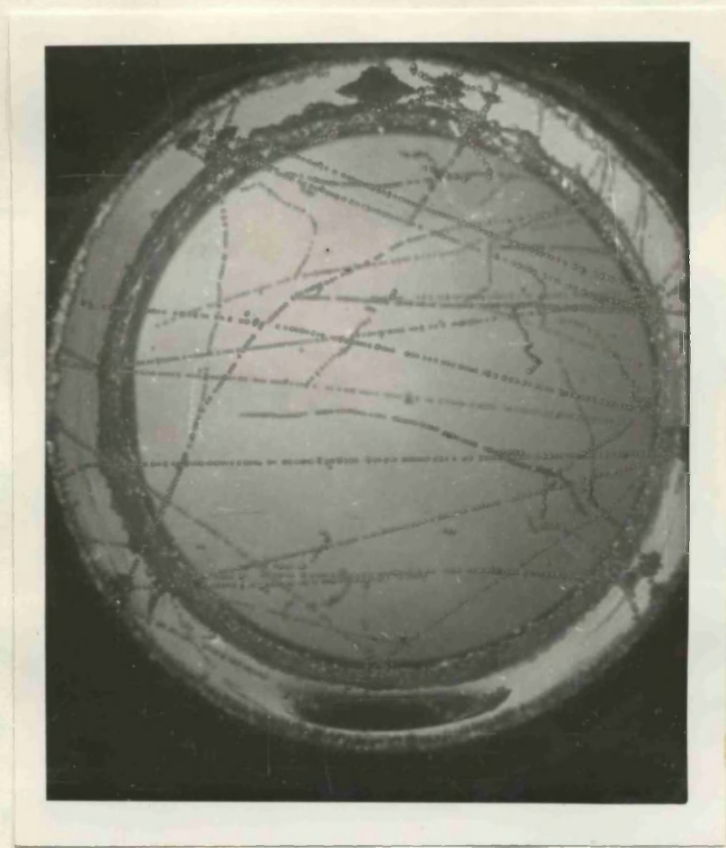


Plate 7.



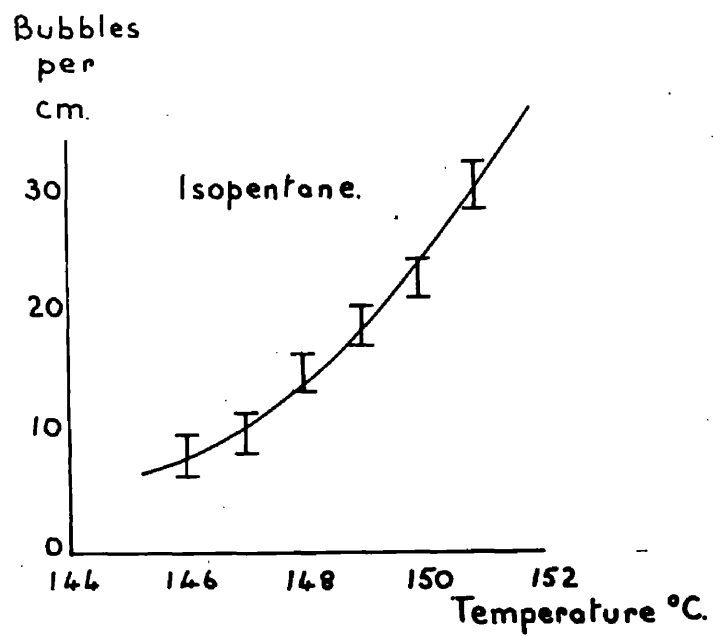


FIG 23 a.

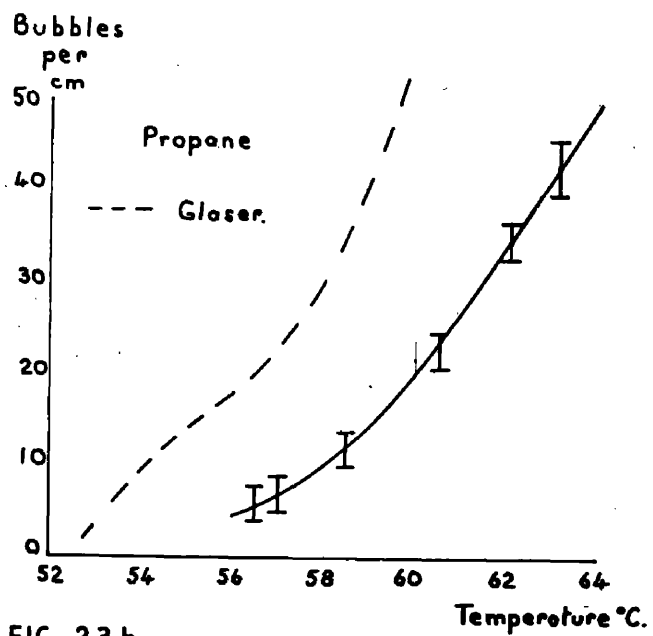


FIG 23 b.

expansion system of the chamber after the particle has passed through a counter system on its way to the chamber, is therefore not possible with bubble chambers.

#### Bubble Density.

It has been stated that the temperature of operation increased considerably. Measurements were therefore made of the change of bubble density with temperature. Unfortunately it was not possible to assess accurately the bottom pressure achieved.

A new liquid was also used in this chamber - propane  $C_3H_8$  which had the advantage that with a normal boiling point of  $-40^{\circ}C$  it was radiation-sensitive at  $60^{\circ}C$  and therefore water could be used as the heating fluid. Otherwise operation was identical.

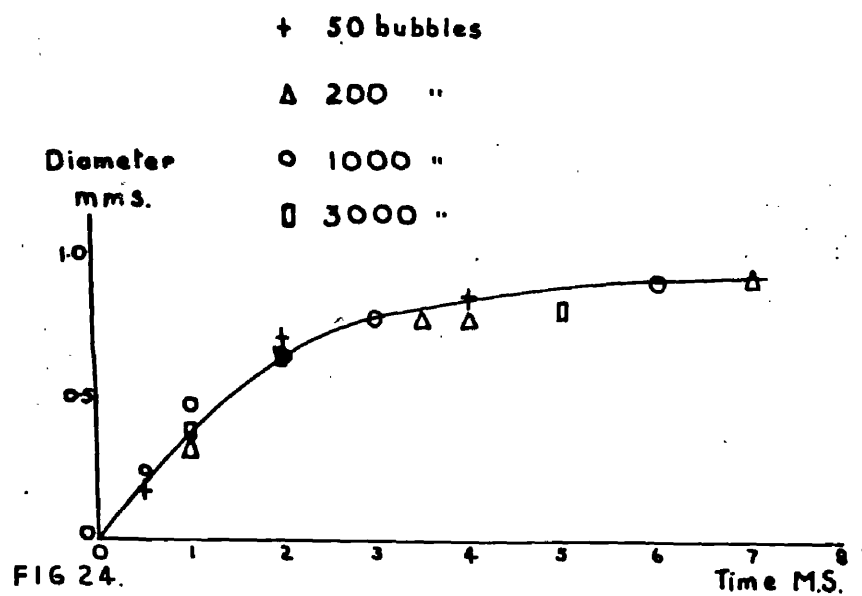
Measurements were made of the variation of bubble density with temperature for both isopentane and propane in this chamber. Measurement was by the same process as before but an error was introduced unless care was taken to ensure that the track was perpendicular to the camera. This could be seen by noting where the particle entered and left the chamber.

Fig. 23 shows the result. No comparable result is available for isopentane, but Glaser has made a similar measurement for minimum ionizing  $\pi$  mesons in

TABLE 2.

Temperature (Propane)	Straight track	Stopping electron	% Difference
63°C	41	31±3	25±7
61	25	20±2	20±5
60	22	18±2	19±5
59	15	12±1	20±5

Mean ~20 %.



propane  $C_3H_8$ .

It was observed that bubble density on tracks of electrons which showed a large degree of scattering was different from that on straight tracks in these photographs.

The bubble density was very high for the last 0.4 cm. of these tracks, but was lower even than the straight tracks, farther back than this. This result is summarised in Table 2.

These results, together with those of this kind described in Chapter III are discussed in the next chapter.

#### Rate of Bubble Growth.

The rate at which bubbles due to ionization grew was also studied in this chamber. It has already been pointed out that the minimum delay time in order that bubbles can be seen is considerably longer in this type of chamber. It was also found that the number of bubbles from ionization had no effect on their rate of growth and they grew to an optimum size of about 1 mm. - sometimes less - and no farther, then floated up to the surface of the liquid.

This is shown in Fig. 24. The time taken for the bubbles to grow to maximum size - (about 10 m.s.,) is

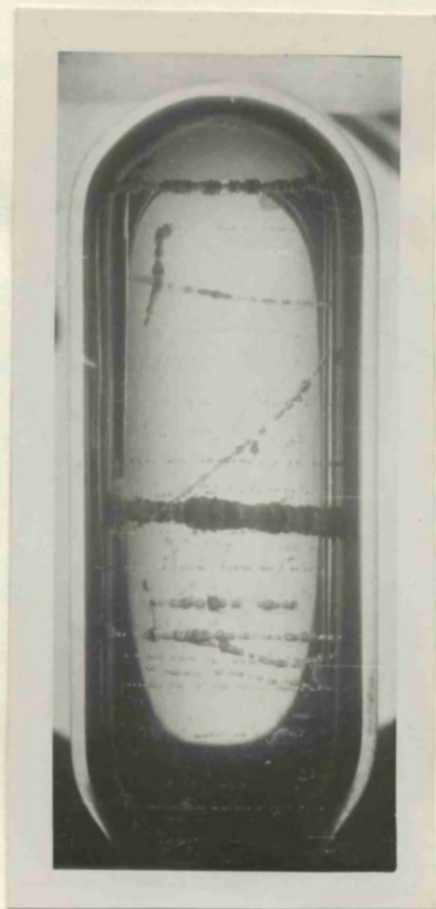


Plate 8

the same as the time taken by the chamber to reach saturated vapour pressure as shown on the transducer trace.

Although no quantitative theory is available for bubbles growing under these conditions, it is clear that the changed pressure conditions cause these differences. In the dirty chamber, the pressure is considerably higher when the bubbles start growing, and therefore their rate of growth is retarded.

Also the principal contribution to vapour is from wall boiling. This controls the rate of increase of pressure and therefore the rate of growth of ionization bubbles is substantially independent of the number of tracks in the chamber.

An interesting photograph, Plate 8, shows the effect of firing a beam of long duration - 200  $\mu$ s. - into the clean chamber and photographing the tracks 2 m.s. later. The very thick tracks are due to early particles and the thin ones to particles which occurred later in the beam. This behaviour in a clean chamber can be compared with the characteristics of a dirty chamber. The tracks of early particles compare with the wall boiling in a dirty chamber, and those of later particles with normal tracks in such a chamber. The

diameter of the bubbles on the small tracks is about the same as that of bubbles in a dirty chamber after a 2 m.s. delay. Also the bubble density on these tracks is lower than that expected for the same temperature in a clean chamber, but it is known that dirty chambers must be operated at a higher temperature than clean chambers to obtain the same bubble density for particles of the same kinetic energy.

It is also possible from this photograph to see immediately at which point in the beam pulse a particle entered the chamber.

Since the rate of growth is slower in the dirty chamber, resolution of this kind can not be done so accurately in the dirty chamber. However, from Fig. 24 it is clear that if the photograph is taken not more than about 3 m.s. after the first particle has entered, it should be possible to resolve events with respect to time if they are greater than about 0.5 m.s. apart.

Finally, it has been implied by workers in this field that there is some inherent difference between clean and dirty bubble chambers. These measurements show that the difference is due entirely to the different pressure conditions experienced by the bubbles.

## CHAPTER V.      BUBBLE DENSITY AND CHAMBER CONDITIONS.

### Experimental Results.

The experimental results which have been obtained so far on the variation of bubble density with chamber conditions will now be considered. These results are, variation of bubble density with temperature (Fig.11) and superheat (Fig.12) in the clean isopentane-filled chamber, and variation of bubble density with temperature (Fig.23) in the dirty chamber filled in turn with isopentane and propane. Glaser's result is also shown on Fig.23.

Before considering them, however, the result obtained when comparing bubble density for low energy electrons with high energy electrons will be considered. (Table 2).

Measurements of grain density in nuclear plates have shown a 15% increase for electrons of  $\beta = 0.99$  ( $\beta = \frac{v}{c}$ ) compared with electrons of  $\beta = 0.96$  and similar measurements in cloud chambers have shown an even greater increase in drop count.

The range of an 0.5 M.e.v. electron in isopentane is about 0.3 cm. and a 1 M.e.v. electron about 0.9 cm. Therefore, by taking the last 1.5 - 0.5 cm. of a track this is a region where  $\beta = 0.96$ , while  $\beta = 0.99$  for the particles traversing the chamber.



Thus from this result it is clear that about a 20% increase in bubble density is experienced in bubble chambers. Blinov has reported 12.5% for this value.

### Early Theories.

The formula derived by Glaser and shown in the introduction gave the chamber conditions necessary for a bubble to form if a known number of charges  $n$  were available.

This formula gave a good indication of the temperature of operation found in practice, and therefore Bertanza (ref.6), using the charge principle as a basis, developed an elaborate formula to give the number of bubbles which might be expected for given chamber conditions and given particle energy.

Bertanza pointed out that ion density was higher on the tracks of  $\delta$ -rays or secondary electrons produced by the initial particle, and further, that this ion density was a maximum at the end of a  $\delta$ -ray track. He said that a maximum of one bubble could be created by any single  $\delta$ -ray because the diameter of a bubble on a photograph was much larger than the range of most  $\delta$ -rays. However, there was a finite probability that a  $\delta$ -ray would not produce even one bubble, and the so called  $\delta$ -ray contribution was given by

$$n_s = \sum_0^K \int_{E_K}^{E_{K+1}} \left( \sum_0^K i \pi_i - 2 \sum_0^K i h \pi_i \pi_h + 3 \sum_0^K i h l \pi_i \pi_h \pi_l - \dots \right) \frac{C}{E^2} dE$$

where (i) the average number of  $\delta$ -rays having energies between  $E$  and  $E + dE$  is given by:

$$dN = \frac{C}{E^2} dE$$

$$C = \text{const.}$$

(ii) the probability that a  $\delta$ -ray will produce a sufficiently high ion density is given by:

$$\pi_K = \frac{e^{-N_K} N_K^{(N_0+K)}}{(N_0 + K)!}$$

$N_0$  = minimum number of ions required,

$N_K$  = number of ions obtained.

As the chamber became more sensitive and therefore the number of charges required for a successful bubble became less, there was a finite probability that bubbles could form on the path of the initial particle - a core contribution given by:

$$n_c = \frac{1}{R_K \sqrt{\pi}} \int_{T_K/\bar{\epsilon}}^{\infty} e^{-t^2} dt$$

$R_K$  = radius of critical bubble

$T_K$  = energy for critical bubble

$\bar{\epsilon}$  = average energy loss of primary particle.

Hence the total number of bubbles formed was given by:

$$n_t = n_s + n_c$$

Bertanza calculated  $n_t$  for the conditions in Glaser's

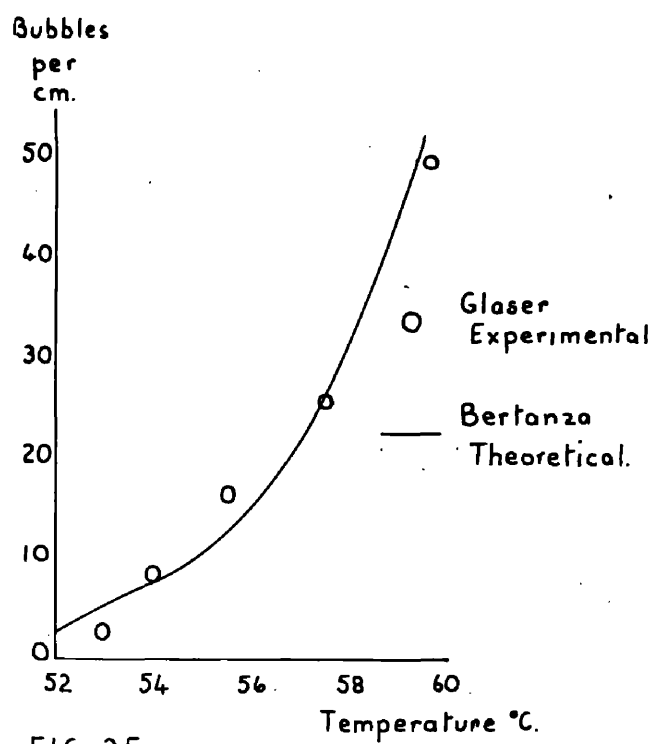


FIG. 25.

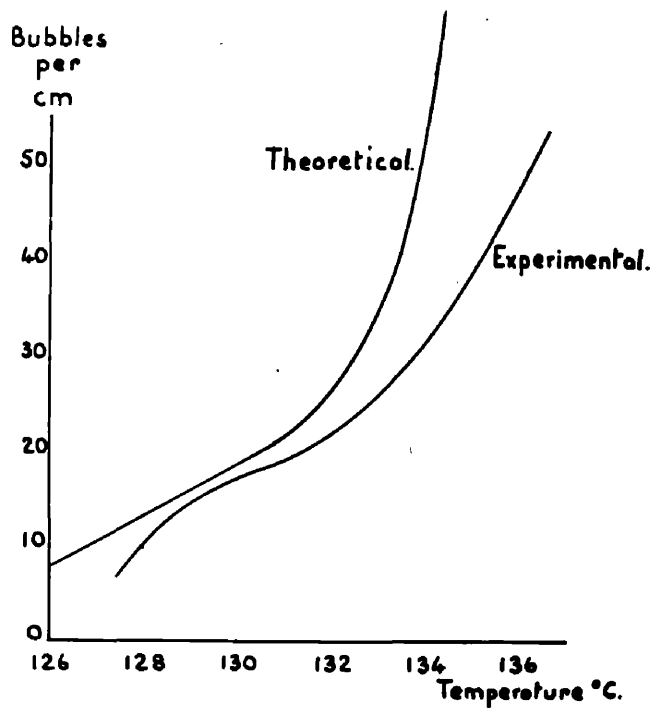


FIG 26

chamber and claimed to get a good fit to the experimental curve. (Fig. 25).

After correspondence with Bertanza to determine the exact method of calculation of  $n_g$ , the author and Mr. McFarlane, independently, calculated  $n_t$  for the conditions which existed in the clean chamber during the experiment on the variation of bubble density with temperature.

It can be seen on Fig. 26 that a very poor fit was found to the experimental curve. The  $n_c$  contribution in particular rose very sharply and indicated about 1000 bubbles/cm at  $136^\circ\text{C}$ .

The error here lies either in the formula or in the initial premise that bubbles form by the accumulation of like charges.

Although Glaser first proposed the charge theory, all he in fact showed was that if  $n$  like charges exist, then under certain conditions of temperature and pressure a bubble will form. Glaser was later able to show that an  $\alpha$ -particle could cause a bubble to form when the chamber conditions were such that 900 charges of the same sign must exist in a region  $2 \times 10^{-6}\text{cm}$  in diameter. This is greater than the maximum ionization attained by a slowing  $\alpha$ -particle (Ref. 7)

### $\delta$ -ray Theories.

Experiments performed by Glaser (Ref. 8) and Blinov (Ref. 9) on the variation of bubble density with particle energy showed that bubble density was proportional to  $\frac{1}{\beta^2}$

Now, the number of  $\delta$  -rays produced by a particle of velocity  $\beta$  is given by :

$$n_{\delta} = \frac{1.53 Z \times 10^5}{\beta^2 A} \left( \frac{1}{E_1} - \frac{1}{E_2} \right) \quad 5$$

$Z$  = atomic number of absorber

$P$  = density of absorber

$A$  = atomic weight of absorber

$E_1$  = minimum  $\delta$  -ray energy

$E_2$  = maximum  $\delta$  -ray energy

TABLE 3.

$$n_{\delta} = \frac{4.1 \times 10^4}{E} \quad \text{for } \beta = 1 \text{ in isopentane}$$

T °C	Bubbles per cm.	$\delta$ -rays producing bubbles	E <sub>min.</sub> of $\delta$ -ray.
128	10	10	3950
130	18	18	2250
132	22	22	1900
134	33	33	1250
136	50	50	820

TABLE 4.

T °C	P <sub>∞</sub> dynes/cm <sup>2</sup>	$\Delta P$ dynes/cm <sup>2</sup>	$\sigma$ dynes/cm	2R <sub>c</sub> cm.	E <sub>δ</sub> e.v.	Range E <sub>δ</sub> cm.
128	12.5 10 <sup>6</sup>	11.5 10 <sup>6</sup>	4.8	1.32 10 <sup>-6</sup>	3950	30.0 10 <sup>-6</sup>
130	13.0	12.0	4.6	1.28	2250	11.0
132	13.5	12.5	4.4	1.20	1900	8.4
134	14.0	13.0	4.2	1.13	1250	3.0
136	14.5	13.5	4.0	1.09	820	1.4

That is for fixed chamber conditions  $d \propto \frac{1}{\beta^2}$  implying that  $\delta$  -rays are in some way responsible for the creation of bubbles.

If all  $\delta$  -rays which have in themselves enough energy to form a bubble, in fact do, then it is possible to deduce this energy from equation 5. The result is shown in Table 3.

A bubble will grow spontaneously if it has reached a diameter  $2R_c$  given by

$$2R_c = \frac{4\sigma}{P_\infty - P_0} \quad 7.$$

Also, the range of an electron in a dense medium is given by

$$R = 0.58 E^2 \frac{PZ}{A} \quad \text{for Electron } < 1 \text{ MeV.}$$

$$R = \text{gm/cm}^2$$

$$E = \text{MeV.} \quad (\text{Ref. 9a.})$$

Table 4, therefore, compares the range of  $\delta$  -rays

of energy  $E$  shown in Table 3, with values of  $2R_c$  calculated for the prevailing chamber conditions.

It can be seen that the  $\delta$  -ray deposits its energy over a much longer range than the critical bubble diameter  $2R_c$ . While it is possible that some  $\delta$  -rays do deposit all their energy in this region, they will not all do so, and therefore it is clear that this simple analysis does not explain the process.

#### Energy for Bubble Formation.

It is possible, however, from a formula due to Volmer (Ref. 10) to calculate the energy required to create a stable bubble in a liquid under known conditions of temperature and pressure, a stable bubble being one which has reached a diameter  $2R_c$ .

The energy  $E_v$  required is

$$E_v = \frac{32}{3} \frac{H\pi}{KT} \frac{P_\infty \sigma^3}{(P_\infty - P_0)^3} + \frac{16\pi \sigma^3}{(P_\infty - P_0)^2} + \frac{32}{3} \frac{P_0 \sigma^3}{(P_\infty - P_0)^3} \quad 8.$$



TABLE 5.

$$\left(\frac{dP}{dT}\right) = 0.26 \cdot 10^6 \text{ dynes/cm.} / \text{K.}$$

T°C	$\frac{H}{K}$	E.mols. e.v.	E.surface e.v.	E.work e.v.	E <sub>v</sub> . e.v.
128	3345	158	26	1.5	186 ± 10
130	3274	115	22	1.5	140 ± 8
132	3161	94	17	1	112 ± 6
134	3063	75	14	1	90 ± 6
136	2978	51	11	1	63 ± 4

TABLE 6

T°C	$\Delta P$ atmos.	$\frac{H}{K}$	E <sub>v</sub> e.v.
134	9.5	3063	193 ± 22
	10.5	3063	162 ± 18
	11.5	3063	126 ± 16
136	9.5	2978	185 ± 20
	10.5	2978	140 ± 15
	11.5	2978	115 ± 12
	12.5	2978	87 ± 8

where  $H$  = heat of vaporization per molecule

$K$  = Boltzman constant

$T$  = Temperature  $^{\circ}K$

The first term is the energy required to convert molecules that were in the liquid state to molecules in the vapour state. The second is the energy to create the surface of a bubble of radius  $R_0$  and the third is the  $P dv.$  work the bubble must do against the hydrostatic pressure growing from  $R = 0$  to  $R = R_0$ .

The values of this energy have been calculated for various chamber conditions in isopentane and the results are shown in Tables 5 and 6. The heat of vaporization  $H$ , is deduced from the latent heat  $L$  calculated in Chapter III.

$$L = \frac{RT^2}{P} \frac{dP}{dT}$$

$$\therefore H = \frac{RT^2}{NP} \frac{dP}{dT}$$

$$\therefore H/K = \frac{T^2 dP}{P dT}$$

Although a measurement has been made of change of bubble density with temperature for fast electrons in the dirty chamber filled with isopentane and propane, it is not possible to calculate  $E_v$  from these results because the superheat  $P_{\infty} - P_0$  could not be measured. A guess of about 8 ± 3 atmospheres for this quantity at  $\sim 150^{\circ}C$  for

Table 7.

-----

$E_v$ .	$\delta$ rays	bubbles/cm.	corrected	$\frac{n_\delta}{n_B}$
e.v.	energy $E_v$	d.	$n_\delta = (d - 20\%)$	
186	210	10	8	26
140	290	18	14.5	20
112	360	22	18	20
90	450	33	27	18
63	640	50	40	15
193	200	8	7	26
166	230	12.5	10.5	22
140	290	17	14	21
185	215	12.5	10.5	21
140	290	17.5	14	20
115	355	24	19	19
87	460	31	25	18.5

isopentane and  $60^{\circ}\text{C}$  for propane gives a value of  $E_v$  in the region expected - that is about 150 e.v. but since  $E_v$  is so strongly dependent on  $P_0$ , this result is not of much quantitative value.

The Volmer energy for Glaser's experiment for minimum ionizing  $\pi$  mesons in propane has, however, been calculated and is 131 e.v. with associated  $n_s = 305$  where bubble density for these particles was 15 bubbles per centimetre.

The number of  $\delta$  -rays of energy  $E_v$  or greater was calculated from equation 5. To compare this with the number of bubbles per centimetre,  $d$ , it is first necessary to correct  $d$  for minimum ionising particles since  $n_s$  was calculated assuming minimum ionization.

The ratio  $\frac{n_s}{n_b}$  shown in Table 7 shows a fairly constant value except at the two extremes - very high and very low bubble density. However, there is clearly a very high casualty rate of these  $\delta$  -rays, if they do form bubbles.

Thermal Spike Theory.

So far, although the charge cluster model has been rejected, no substitute has been put forward to replace it. It is now clear that any alternative theory must also explain the high casualty rate of  $\delta$  -rays.

Several workers, notably Glaser and Seitz, have proposed that bubbles form due to the creation of thermal

spikes in the liquid, that is, small regions where the temperature is higher than that of the surroundings.

Seitz has gone into this in some detail and his paper will now be considered. (Ref. 11) The basis of the theory is that a  $\delta$ -ray of energy  $E_v$  or greater, deposits this energy initially in a region  $V_0 = \pi a^2 R$

where  $R$  = range of  $\delta$ -ray

$a$  = mean molecular radius of medium.

Now  $V_0 < V_c$  where  $V_c = \frac{4}{3}\pi R_c^3$ . This small bubble will grow, and since there is available enough energy  $E_v$  to create a bubble of size  $V_c$ , will reach a size at which it becomes stable and can therefore continue to grow without the aid of additional energy.

However, Seitz pointed out that this growing period from initial bubble  $V_0$  to bubble of volume  $V_c$  must be considered, since it is possible for heat to be lost by conduction through the liquid at a faster rate than the bubble can grow.

He calculated the rate of growth of bubbles from  $V_0$  to  $V_c$  and compared it with the rate of dissipation of heat from a region  $V_0$ . Since this calculation was largely speculative, it will not be described in detail, but the result for propane is given. For propane at  $55^\circ\text{C}$  where bubble density is about 15 bubbles/cm

and  $P_{\infty} - P_0 = 10$  atmospheres, additional energy required is  $\sim 30$  e.v., since this is the amount lost by radiation.

However, Seitz then pointed out that in this calculation viscosity effects must be taken into account since the effect of the viscosity of the liquid is to retard the growth of the microscopic bubble and hence allow more time for the loss of heat.

Although accurate values of the viscosity of propane under the conditions which exist in a bubble chamber are not known, Seitz took a value of  $\eta = 1$  centi-poise and recalculated the value of the additional energy required to be about 4750 e.v.

This implies that the energy required for a bubble is about 5000 e.v. in all, but it has been shown first that fewer  $\delta$ -rays of this energy are formed by a particle of  $\beta = 1$  than bubbles observed, <sup>Table 3</sup> and second, that a  $\delta$ -ray of energy 5000 e.v. has a range  $\sim 40 \times 2R_c$ , whereas the basis of this calculation rests with the energy starting in a localised region  $V_0 < V_c$ .

#### Revised Viscosity Calculation.

The formula Seitz used to calculate heat lost was

$$E = \frac{20}{\gamma} \frac{\eta}{\tau_c} \left( \frac{R_c}{R_0} \right)^{3\gamma-1} V_c \quad 9.$$

TABLE 8.

$$\lambda = 4 \times 10^{-4} \text{ cal/gm.}^\circ\text{C} \quad \rho = 0.47 \text{ gm/cm}^3 \quad c = 0.3 \text{ cal/gm.}$$

$T^\circ\text{C}$	$\Delta P$ $10^{-6}$	$\eta$ poise $10^{-4}$	$R_c$ $10^{+6}$	$E_\eta$ e.v.	$E_\eta + E_v$	$n_s$	$n_B$	$\frac{n_s}{n_B}$
128	12.5	9.6	0.835	571	757	54	8	6.7
130	13.0	9.5	0.765	658	658	62	14.5	4.2
132	13.5	9.3	0.705	471	585	70	18	3.9
134	14.0	9.2	0.645	424	516	80	27	3.0
136	14.5	9.1	0.590	383	453	88	40	2.2
134	9.5	9.2	0.61	570	763	52	7	7.4
	10.5		0.66	524	690	60	10.5	5.7
	11.5		0.725	474	614	65	14	4.6
136	9.5	9.1	0.715	502	687	10	10	6.0
	10.5		0.78	471	611	67	14	4.7
	11.5		0.86	428	543	75	19	3.9
	12.5		0.93	396	483	83	25	3.2

where  $\gamma$  = Ratio of specific heats 1 for hydrocarbons

$\eta$  = viscosity

$\tau$  = relaxation time for dissipation of heat in  
bubble radius  $R_c$

$$\tau = \frac{R_c^2}{4D} \quad D = \frac{\lambda}{pc}$$

$\lambda$  = thermal conductivity

$p$  = density

$c$  = specific heat

$R_c$   $R_0$   $V_c$  as already defined.

A value for viscosity for isopentane was obtained from International Critical Tables. This is  $1.98 \times 10^{-3}$  poise at  $30^\circ\text{C}$ . Also, an empirical formula relating viscosity with temperature was given thus

$$\eta = \frac{A}{(B + t)^n} \quad 10.$$

$$A = 391.1$$

$$B = 208.6$$

$$n = 2.2186$$

$$t = ^\circ\text{C}.$$

whence values of viscosity for isopentane under the conditions which applied in the clean chamber experiments are a factor of about 10 less than the value used by Seitz.

The heat lost by a bubble growing from  $R_0$  to  $R_c$  was then recalculated, the result is shown in Table 8, ~~and~~



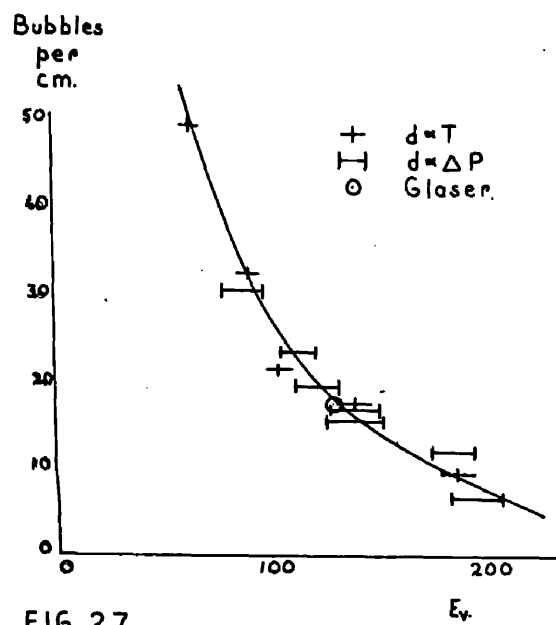


FIG. 27.

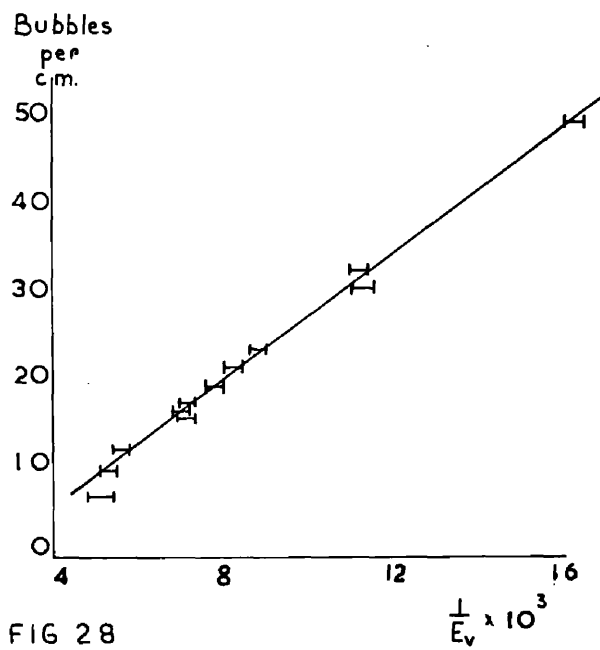


FIG 28

While there are sufficient  $\delta$ -rays available with the necessary energy, there is no obvious relation between the number of those  $\delta$ -rays and the number of bubbles found by experiment.

#### Bubble Density and Volmer Energy.

The results in Tables 5 and 6 were then reconsidered, ignoring the  $\delta$ -ray stage, and a graph drawn of bubble density against Volmer energy. It can be seen that despite the variety of conditions there appears to be a correlation between  $d$  and  $E_v$ . (Fig.27) A graph of  $d$  and  $\frac{1}{E_v}$  was then drawn and a straight line obtained. (Fig.28.)

#### Conclusions.

Although the viscosity effect suggested by Seitz does not seem to fit the overall pattern, it is possible that even the amended calculation shown in Table 8 requires further modification.

It is significant, however, that a good correlation is found between bubble density and Volmer energy. All particles of the same mass and energy will lose energy at the same rate, therefore the amount of energy available for bubbles is the same. The graph shown in Fig.28 implies that the ratio of this energy to the energy required for a bubble is proportional to the number of bubbles found - a reasonable deduction.

It would also appear that apart from the

extremes of chamber sensitivity, this energy is deposited by the  $\delta$ -rays, that is, some of the  $\delta$ -rays lose energy by creating little hot spots in the liquid, ~~that is,~~ causing molecular excitation, and the proportion of  $\delta$ -rays which do this is about one in twenty.

At high chamber sensitivity, where  $E_V$  is small, bubble density is higher than might be expected from  $\delta$ -ray processes. It is possible that Bertanza's conception of a core contribution may explain this - the primary particle, in addition to creating  $\delta$ -rays, may itself create local hot spots in the liquid.

This theory, however, does not explain the odd shape of the  $d : T$  curve observed in the clean chamber, and by Glaser. The results are not sufficiently refined to show a significant trend in the  $d : E_V$  curve. It may be that rather more energy is required for bubble formation than given by the Volmer equation in this region. Since this effect was noted in Glaser's results it is unlikely that it is a viscosity effect which is a function of temperature. The result was not observed in the dirty chamber, probably because of the mode of the expansion system.

#### Further Experiments.

Although the precise bubble-forming process

has not yet been fully explained, it would be useful to see to what extent bubble counting can be used to aid particle identification - in particular the identification of particles which stop in the chamber.

It would also be of interest to measure the effect of particle energy on bubble density, especially at low values of  $\beta$  which can be obtained from these stopping particles. The next sections describe the experiments which were performed in this field.

## CHAPTER VI.      PARTICLES STOPPING IN THE BUBBLE CHAMBER.

### Identification by Inspection.

Particles which stop in a substance can be recognised to a certain extent by their behaviour in that substance. Particles produced by a reaction between the 350 M.e.v. beam and a target in that beam are protons and  $\pi$  mesons. If they stop in a hydrocarbon-filled bubble chamber then they can be identified as follows.

Protons which are stopped in propane have a very low cross-section for reaction with carbon or hydrogen at these energies and since the proton is a stable particle and shows no decay process, no event will be seen at the end of the track.

The cross-section for angle scattering, however, indicates that there is a probability that two large angle scattering events could be expected in 100 proton tracks.

The  $\pi^+$  meson is prevented from inter-reaction with the nuclei in the propane medium by coulomb repulsion forces and therefore when it stops, it lies quiescent until it decays by the now familiar

$$\pi^+ \rightarrow \mu^+ \rightarrow e^+$$

decay scheme. Since the  $\pi^+ \rightarrow \mu^+$  decay is a two body process, the other particle being a neutrino, the  $\mu^+$  meson will always have the same kinetic energy when decaying from a  $\pi^+$  at rest. This is 4.12 M.e.v. with associated track length of 0.30 cm. in propane. Although the positron will not always have the same kinetic energy since there are two neutrinos associated with the  $\mu^+$  decay, it will always be  $\sim 50$  M.e.v.

The half life of the  $\pi^+$  is  $2.54 \times 10^{-8}$  sec. (Ref. 12) and by calculating the time which a  $\pi$  meson takes to leave the target and stop in the propane, the probability that it will decay in flight can be estimated.

The time which it takes to stop is given by the formula (Ref. 13)

$$t = \frac{mu (V_i^3 - V_f^3)}{12 e^4 N Z \left[ \ln \left( \frac{2mv^2}{I} \right) \right]}$$

$m$  = electron mass

$u$  = meson mass

$V_i$  = initial velocity

$V_f$  = final velocity

$e$  = electronic charge

$N$  = No. of atoms/cm.<sup>3</sup>

$Z$  = atomic number

$I$  = Ionization potential

The decay process is governed by the <sup>0.693</sup>equation

$$N = N_0 e^{-\lambda t} \quad \text{where } \lambda = \frac{0.693}{\tau}$$

$\tau$  = half life

Table 9 shows the probability, for  $\mu$  mesons and 2 energies of  $\pi$  mesons, that a decay will take place before the particle has stopped.

$E_{\text{particle}}$	$\tau$	$t$	% decay in flight
35 M.e.v	$2.54 \times 10^{-8}$	$7.5 \times 10^{-10}$	1.5%
45 M.e.v.	$2.54 \times 10^{-8}$	$10 \times 10^{-10}$	2%
4.12 M.e.v.	$2.1 \times 10^{-6}$	$1 \times 10^{-11}$	.01%

As the  $\pi^-$  meson is slowed down to a few K.e.v. it is most likely to be captured by a hydrogen or carbon nucleus. In the case of hydrogen, when the  $\pi^-$  is inside the electronic K shell it can only go to the mesic K shell by optical transition, a rare process in hydrogen. A neutral mesic hydrogen atom then exists, and eventually the meson is most likely to be captured by carbon, that is, the absorptions are nearly all in carbon.

A study of  $\pi^-$  absorption in nuclear plates has shown that for light elements such as carbon,  $\alpha$  particles that are emitted have  $< 30$  M.e.v. kinetic energy. However, a 30 M.e.v.  $\alpha$  particle will not give a track of visible length in propane. Other particles which may be emitted in the subsequent disintegration are protons which will

be seen if they have more than 8 M.e.v. kinetic energy, and neutrons which will not be seen. A precise analysis of the relative numbers of disintegrations involving high energy protons has not been made, but it is clear that a  $\pi^-$  will show either 0, 1, 2 or 3-pronged stars.

Since the capture process is very fast  $\sim 10^{-13}$  sec., the probability that a  $\pi^-$  will decay in flight or before capture is the same as  $\pi^+$  <sup>decay</sup> in flight.

#### Doubtful Cases.

Thus while  $\pi^+$  mesons can be distinguished uniquely provided the positron is seen, there might be confusion between apparently zero-pronged  $\pi^-$  stars and protons, and single-pronged  $\pi^-$  stars and single scattered protons. This can be overcome in some instances by inspection of the multiple coulomb scattering on the track - the meson undergoes more than the proton, but there are instances where this is not conclusive. Further, tracks in bubble chambers are not as fine as tracks in emulsions, therefore accurate measurements of multiple scattering are not possible.

It would be most useful if bubble counting could be used to distinguish between these particles.

#### Experiment.

The dirty chamber was set up in the position



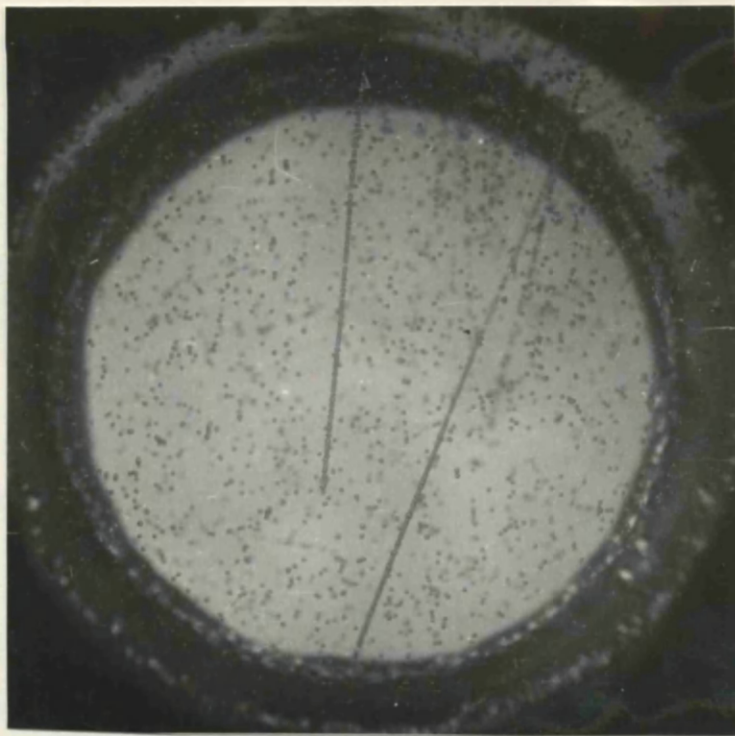
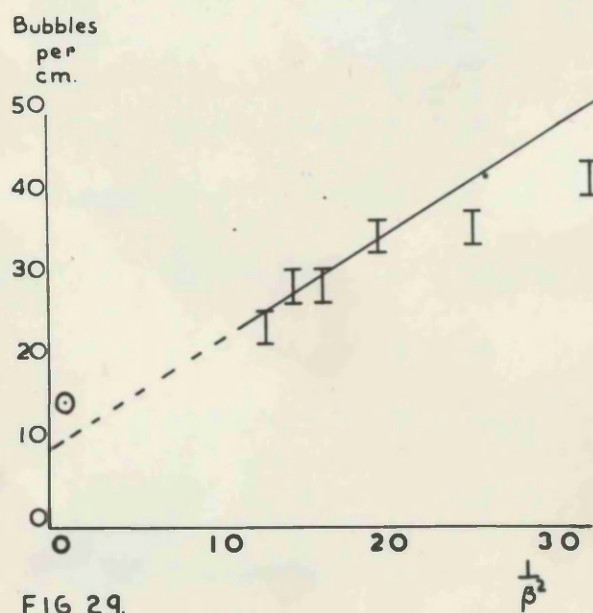


Plate 9.



used with the first chamber, that is, below a target set in the  $\gamma$  beam, and a few photographs taken. Plate 9 is a typical example and shows what was believed to be a proton stopping in the liquid, because of the straightness of the track and no event at the track ending.

The track was divided into equal sections, a bubble count made in each, and converted to bubbles per centimetre, and from the residual range of the mean point of each section, energy and hence  $\frac{1}{\beta^2}$  were obtained from Tables U C R L 2301.

A graph of  $d : \frac{1}{\beta^2}$  however, from this track, did not give a straight line, but fell away at higher values of bubble density. (Fig. 29)

It was possible that the track was of a  $\pi^-$  meson which gave no visible products when captured by a nucleus in the liquid. However, it was clear that this chamber was too small to make a full investigation of the behaviour of particles which, when ejected from a target, stop in the propane medium.

A larger chamber was therefore designed, and the opportunity was taken to investigate a different mode of expansion.

CHAPTER VII.THE NEW CHAMBER.Apparatus.

This new chamber had a capacity of 500 ccs, was 3.25" in diameter and was made of steel with walls 0.25" thick. The cylindrical shape was retained, the windows were 1" thick plate glass, and fluon was again used as gasket material. A 1" diameter pipe 6" long connected the chamber to the expansion mechanism.

To achieve the necessary superheat in the 75 cc chamber, the movement of the piston gave a 2.5% change in the capacity of the system. To repeat this with a chamber of six times the capacity would require a very large piston, and operation by this method would be more difficult and would not be as fast as might be required. Also a problem in piston alignment was becoming serious with the 75 cc chamber.

A system was, therefore, developed which consisted of a diaphragm 5" in diameter of 1/16" thick neoprene sheet rubber separated from the working liquid by a sheet of 0.001" mylar. This diaphragm is supported on a perforated brass plate 1" thick.

To achieve  $2\frac{1}{2}\%$  volume change in this system the centre of the diaphragm would only have to move 0.5".

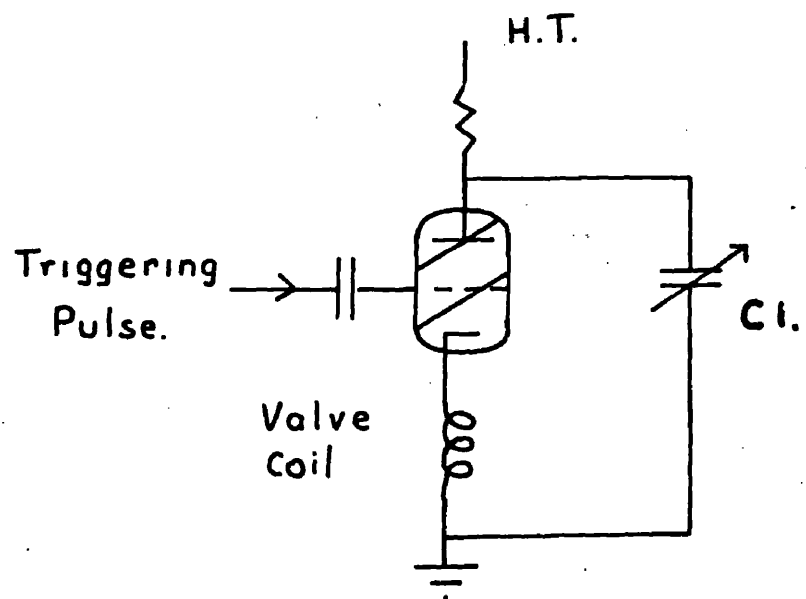


FIG 31

CV 797.

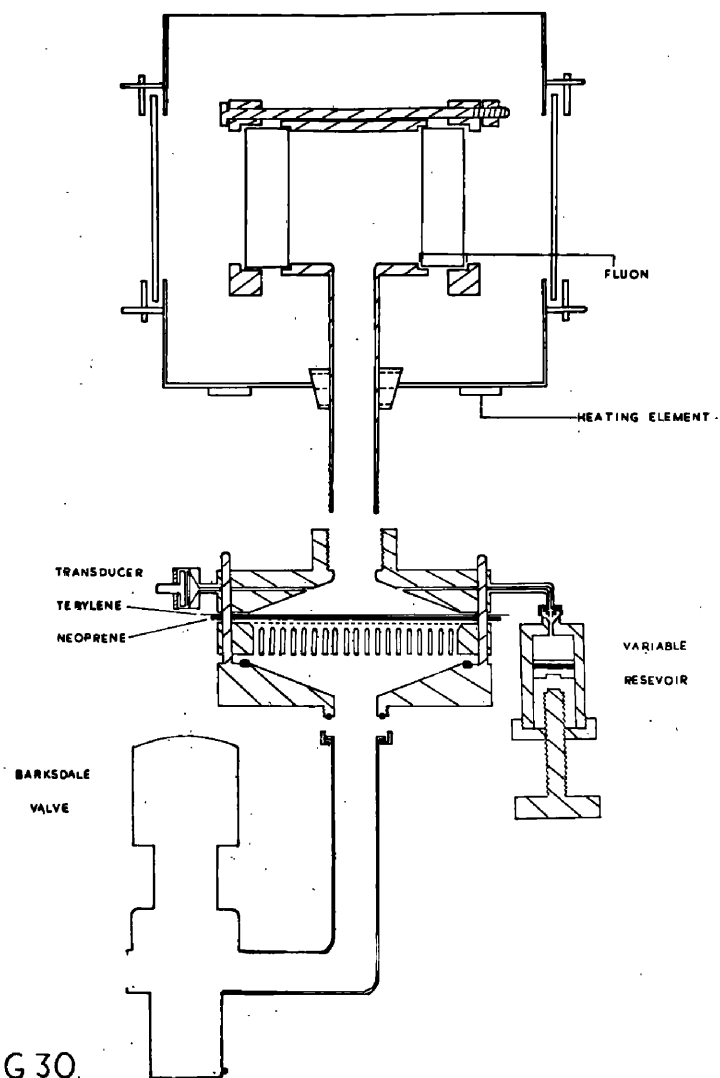


FIG 30.

The apparatus is shown diagrammatically in Fig. 30.

A valve obtained from the Crescent Valve Co., U.S.A., was attached to the base of this unit by a pipe 1" in diameter. This valve is a three-way solenoid type with ports  $\frac{3}{4}$ " in diameter, and could be operated with compressed air up to 35 atmospheres.

Power was obtained from cylinders of nitrogen at a pressure of 70 atmospheres. A suitable regulator valve to give gas at the required pressure was connected to the cylinder.

To expand this system the valve coil was placed in the cathode of a CV797 thyatron. When a +ve pulse was applied to the grid of the thyatron, the condenser C1 discharged through the valve and coil. The time the valve was kept open depended on the capacity of this condenser and could be readily varied. (Fig. 31).

The chamber was again heated by enclosing in a brass bath. Since propane was the operating fluid, water was used as heating fluid. Windows 5" in diameter were placed in opposite faces of the bath, and a 750 watt ring element clamped to the base. The heat was regulated by supplying power to the element through a Variac. Temperature stability was maintained by continuously stirring the water in the bath. The temperature was measured by

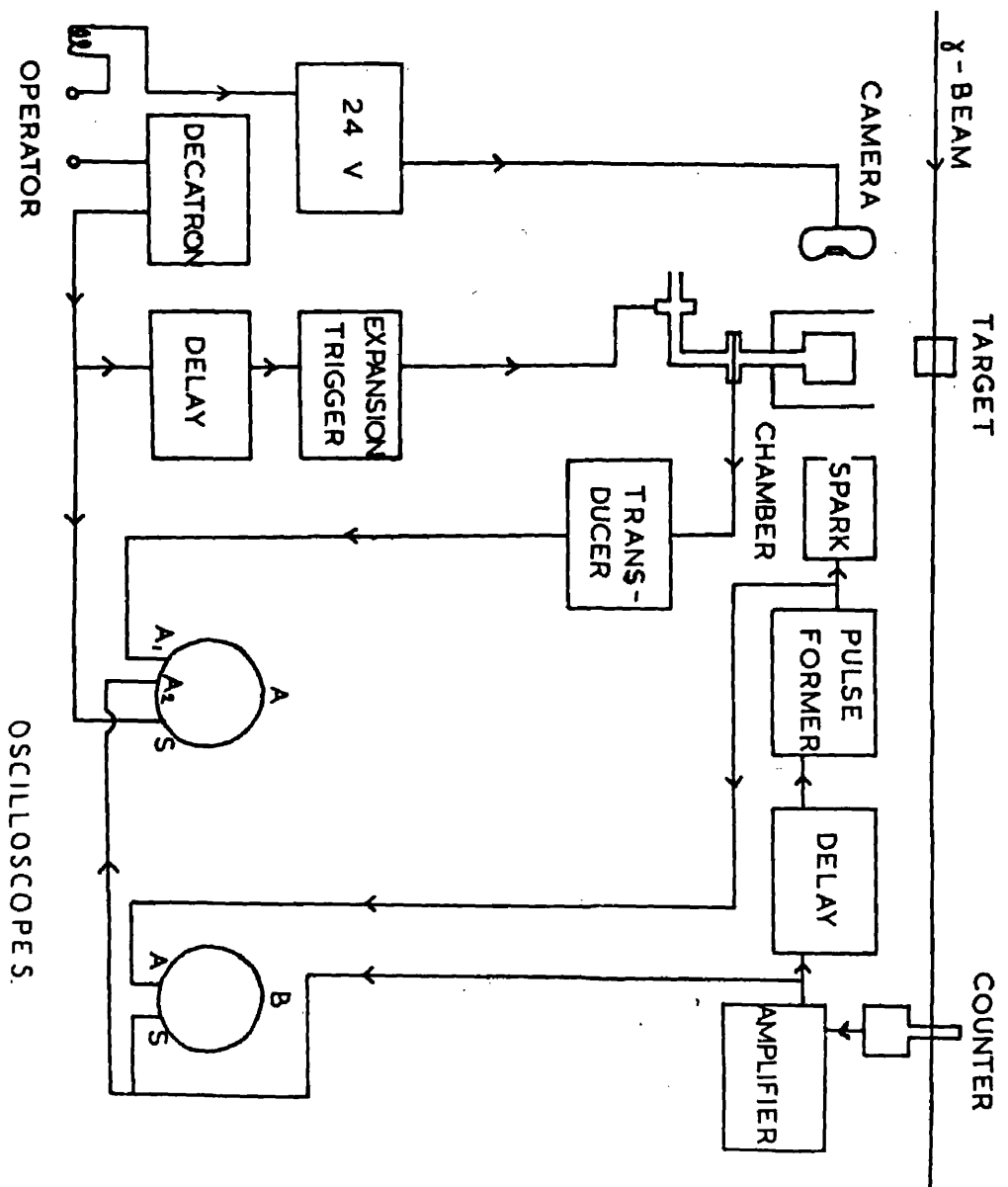


FIG 32.

two mercury thermometers situated 1" and 5" below the surface of the water.

At first it was thought there would be sufficient light from the spark gap if a larger lens was used, and the extension piece of the camera removed. Later a mirror system was set up with the spark gap to increase the quantity of light so that the camera could be stopped down from F3.5 to F8 to give better depth of focus.

Unfortunately, shadows of the electrodes appeared on the film. This spoiled prints but since measurements were to be made directly from the film negative this was not a serious drawback.

The chamber was seen to be radiation-sensitive at about 60°C, by triggering the flash at the minimum point on the transducer trace in the presence of a Co<sup>60</sup> source.

Before taking to the synchrotron, it was decided that the operation of this chamber be made remote from the chamber itself. Most of the cycle of operations was automatic, but the operator, by push button control, started the cycle and watched the oscilloscope trace to ensure that all events occurred at the correct time. The control system is represented on Fig. 32.

It was found that a bubble density of fourteen



bubbles per centimetre was obtained for high energy electrons at  $57^{\circ}\text{C}$ . The chamber was then set below a target in the beam and several photographs taken.

#### Chamber Conditions.

When a count was made of bubble density on tracks of particles which had entered the chamber from the top and gone right through it, it was found that in some cases the bubble density was higher in the top part of the chamber than at the bottom. Since it was known that the particles were entering from the top and hence having lower energy would be expected to give a higher bubble density at the bottom, this effect must be caused by lack of uniformity in chamber conditions.

To explain this apparent decrease in bubble density found on tracks of particles traversing the chamber, if reference is made to the calculation in Chapter III, it can be shown that a gradient of as much as  $4^{\circ}\text{C}$  through the chamber could be set up when 10 ccs. of vapour are recompressed at the top of the chamber. Since on expansion the bottom pressure  $P_0$  in the chamber is the same throughout, the higher temperature will cause a higher bubble density. For particles which only just traverse the chamber, this may cause an apparent uniform bubble density along the track, and for very fast particles

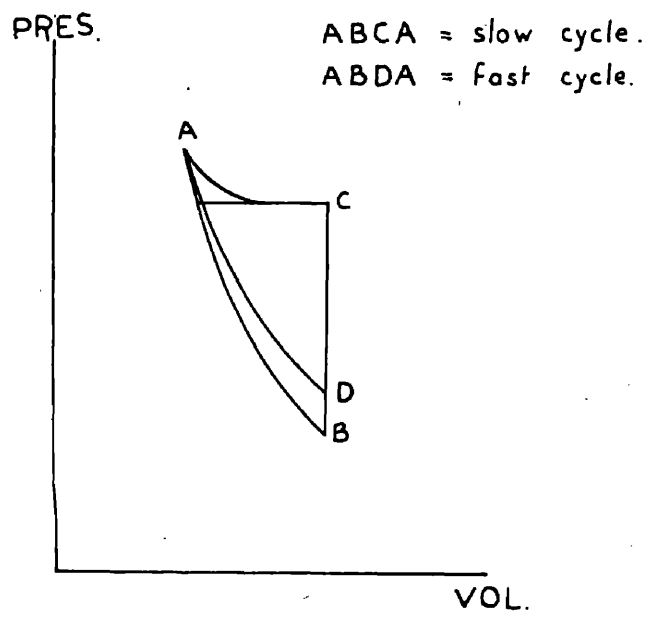


FIG 33.

this would cause a higher bubble density at the top than at the bottom.

This effect could be overcome by recompressing the chamber immediately after expansion, so that the bubbles formed at the wall and by ionizing particles are recondensed where they form and there is an even distribution of exhaled latent heat throughout the chamber.

It was noted earlier that the rate of dissipation of energy from the particles is so rapid that triggered expansion was impossible. However, as soon as all the accumulated vapour has been recompressed, the chamber is ready for the next expansion.

It seemed likely, therefore, that a fast recompression system would serve the dual purpose of removing temperature gradients and speeding up the cycle of operations, which had been about once per minute.

Further, if the P-V diagram is again considered, (Fig. 33) fast recompression implies that much less work is done on the liquid and hence the temperature rise is not so great. This is very important if the chamber is to be cycled fast.

#### Fast Cycling.

To achieve fast recompression, a cylinder of capacity 1.5 litres was placed between the regulator

valve and the expansion valve, being connected to the latter by a pipe of 1" diameter. The electronics were arranged so that the expansion valve was open for 25 m.s. The pressure in the reservoir was raised to saturated vapour pressure plus three atmospheres, such that even after expansion there was sufficient air to raise the pressure in the system to higher than saturated vapour pressure. The main supply took about 0.5 seconds to replenish the lost air.

It could be seen with this system that the bubbles were recompressed where they formed and the chamber was ready for the next expansion in about 0.25 seconds.

It was also seen when further tracks of particles traversing the chamber were examined that in all cases bubble density on such tracks was either uniform or increased down the track.

Although the chamber itself could have been cycled twice per second, the cycling rate was limited by the rate at which the spark unit could recharge. This was not altered in favour of a fast cycling bubble chamber with counter controlled flash when an interesting particle has entered the chamber. Photographs were, in fact taken six times per minute.

It will be shown later that from the point of view of number of particles seen, photographing every shot was an economical proposition for the type of experiments which were performed.

#### Experiments on Chamber Sensitivity.

The mode of operation of this new system was then investigated in more detail. Sensitivity was varied first by varying the temperature. It was thought that by running at as low a temperature as possible, background would be reduced to a minimum, and further, since the corresponding saturated vapour pressure would be reduced, the quantity of compressed nitrogen required for cycling would be reduced. At  $60^{\circ}\text{C}$  it was found possible to cycle two hundred times from one cylinder.

However, as the temperature was reduced, the length of time during the expansion pulse which the chamber was sensitive became shorter. At  $52^{\circ}\text{C}$  this was only about 0.5 m.s. It was not possible to hold the relative positions of expansion pulse and beam pulse within such narrow limits.

It was also noted that background was not reduced by as much as might be expected. This is probably due to some of the background being caused by low energy photons which produce very short range electrons in the  $\text{CH}_2$  medium

and will therefore form a bubble under extremely insensitive conditions.

Sensitivity was also varied by altering the size of the vapour bubble when in the expanded state, and thus the expansion ratio. This was done by altering the capacity of a small 50 cc. cylinder connected to the chamber.

It was found, however, that the same bubble density was obtained when the expansion ratios were respectively 1.5% and 2.5%. This result implies that for this system the growth of vapour bubbles at the walls was causing pressure to increase at the same rate as the system was expanding after the pressure had dropped to a certain level.

It can be shown by calculations on liquid compressibility similar to those in Chapter III that the minimum ratio required - allowing for stretching of the apparatus - is only about 0.2%. Further, on referring to the graph (Fig. 17) on the rate of increase of vapour volume the slope of this curve is very steep when the hydrostatic pressure on the liquid is very low, and the growth of vapour decreases as this pressure rises. It would appear, therefore, that there is an optimum expansion ratio for a particular chamber, which must be found by experiment.

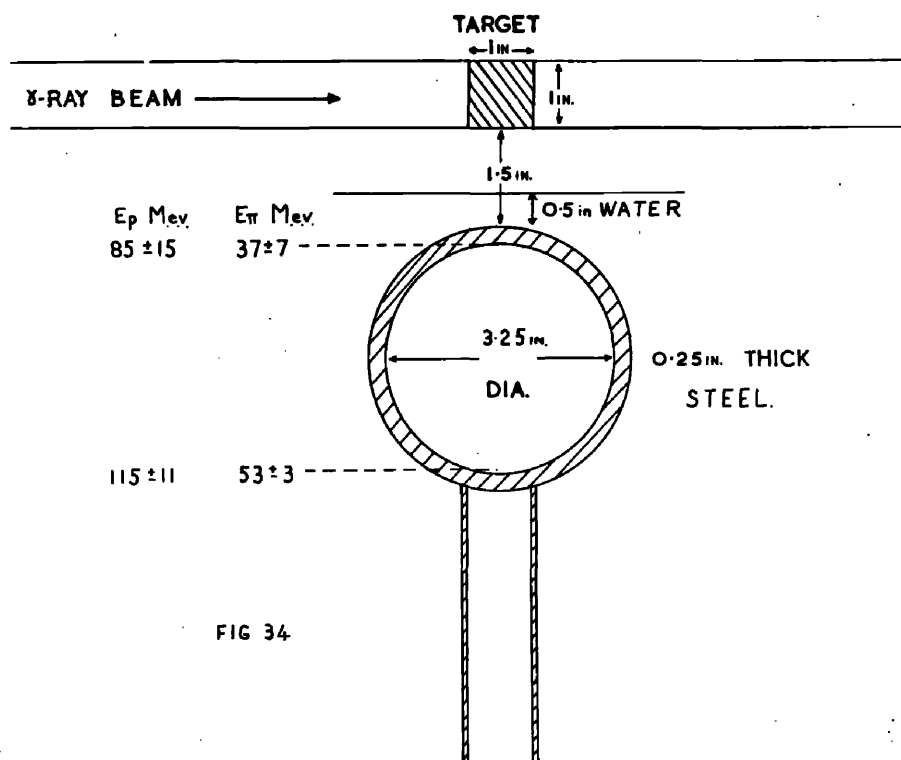


FIG 34

## Chapter VIII. Bubble Counting and Particle Identification.

### Counting Rate.

This chamber was built because the 75 cc dirty chamber was too small to investigate fully events of the type just described. The following calculation shows how many protons and mesons might be expected to stop in the chamber, if a carbon target is used. The experimental set up is shown in Fig. 34.

To calculate the number of particles expected the following formula was used

$$n = C \sigma S p. \quad \text{particles per shot.}$$

where

$C$  = number of carbon atoms presented to the photon beam/cm<sup>2</sup>.

$\sigma$  = cross section for the particular reaction.

$S$  = solid angle subtended by chamber to target.

$p$  = number of photons in beam.

#### 1. Parameters depending on experimental set up.

$$\begin{array}{lcl} \text{Number of carbon atoms} & & \\ \text{presented to beam} & = & \frac{Np}{A} \quad \frac{V}{a} \end{array}$$

$N$  = Avogadro's Number.

$P$  = density of carbon.



V = target volume.

A = Atomic Weight.

a = area presented to target.

$$C = \frac{6.03 \times 10^{23} \times 2.2 \times \pi r^2}{12 \times \pi r^2} \quad \text{per cm}^2$$

Solid angle = 0.4 steradians.

## 2. Beam characteristics.

It was not possible to measure beam strength when operating the synchrotron 6 times per minute from the deatron unit. However, a value of  $10^9$  equivalent quanta per minute was used in the calculation as this had been found in experiments when the synchrotron was running 5 times per second.

## 3. Cross sections.

### (a) Mesons.

The differential cross section for meson production in carbon is given as

$$\left( \frac{\partial \sigma}{\partial \Omega} \right) = 3.87 \times 10^{-29} \text{ cm}^2/\text{steradian/nucleus/equivalent quantum}$$

at  $90^\circ$  (Laboratory co-ordinates) for a 326 MeV Bremsstrahlung spectrum (Ref. 14).

However, this is for mesons of all energies.

To estimate the energies of mesons which stopped in

$$\frac{\partial^2 \sigma}{\partial \Omega \partial E} \times 10^{-31}$$

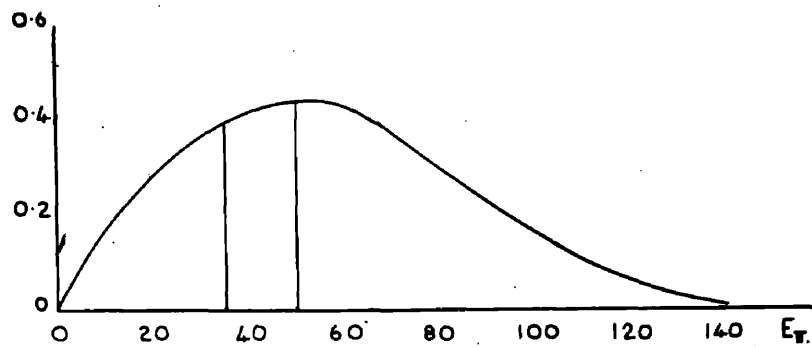


FIG 35

Relative

$\sigma$

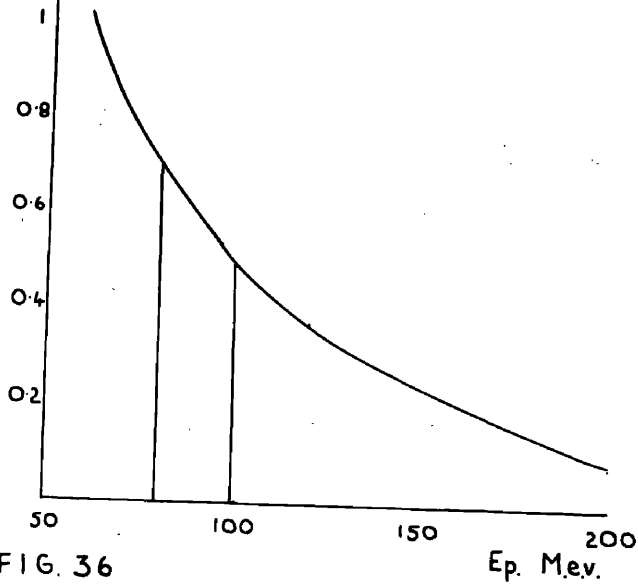


FIG. 36

$E_p$  Mev.

the chamber, the thickness and density of material through which a particle passed, was measured. However, because of the thickness of the target this cannot be done accurately. For mesons it was estimated that particles which stopped in the chamber, left the target with energies in the range 35 - 50 MeV, Fig. 34.

Therefore, from the energy distribution curve in Fig. 35 (Ref. 15) the energy interval for particles stopping in the chamber was about  $\frac{1}{6}$  total area.

Hence,

$$\begin{aligned}\text{Number of mesons} &= 725 \text{ per minute at } 5 \text{ cycles/sec} \\ &= 2 \text{ per shot.}\end{aligned}$$

#### (b) Protons.

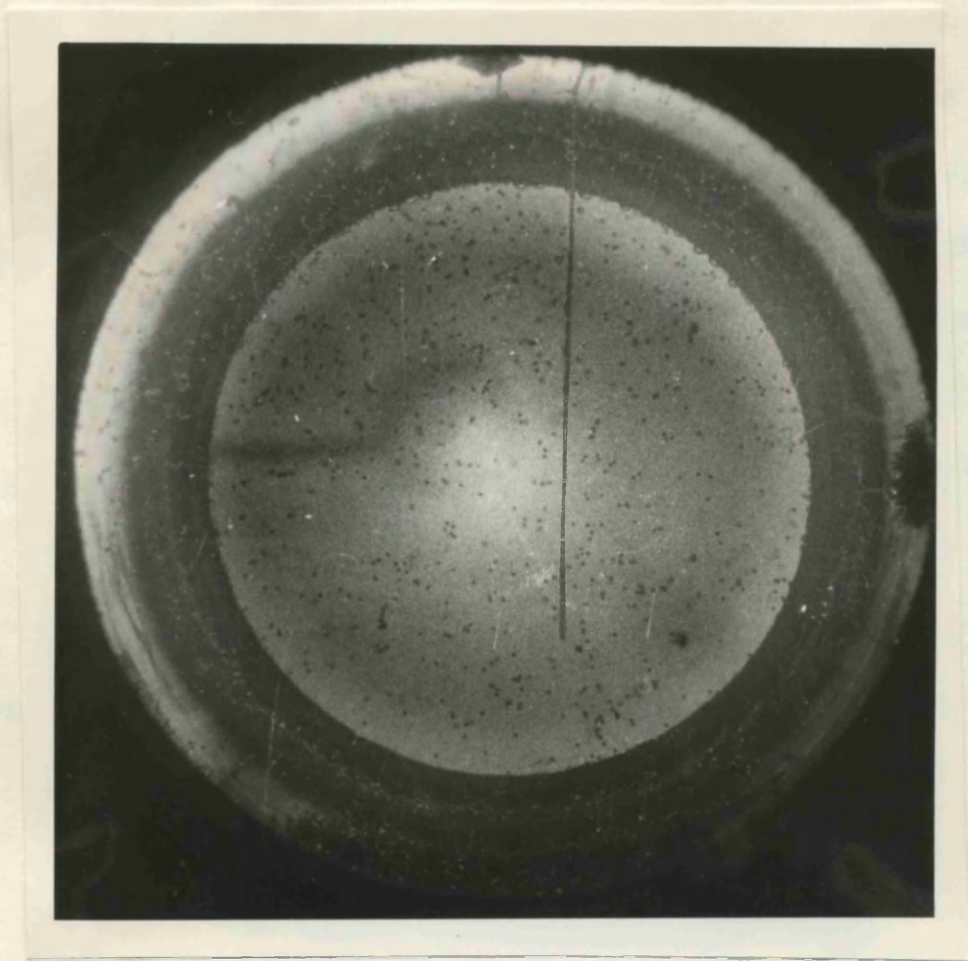
A cross section for production of protons is given by Walker (Ref. 16) as

$$\left( \frac{\delta^2 \sigma}{\delta \Omega \delta \epsilon} \right) = 8.8 \times 10^{-32} \text{ cm}^2/\text{steradian} / \frac{Z}{\text{equivalent quantum/MeV}}$$

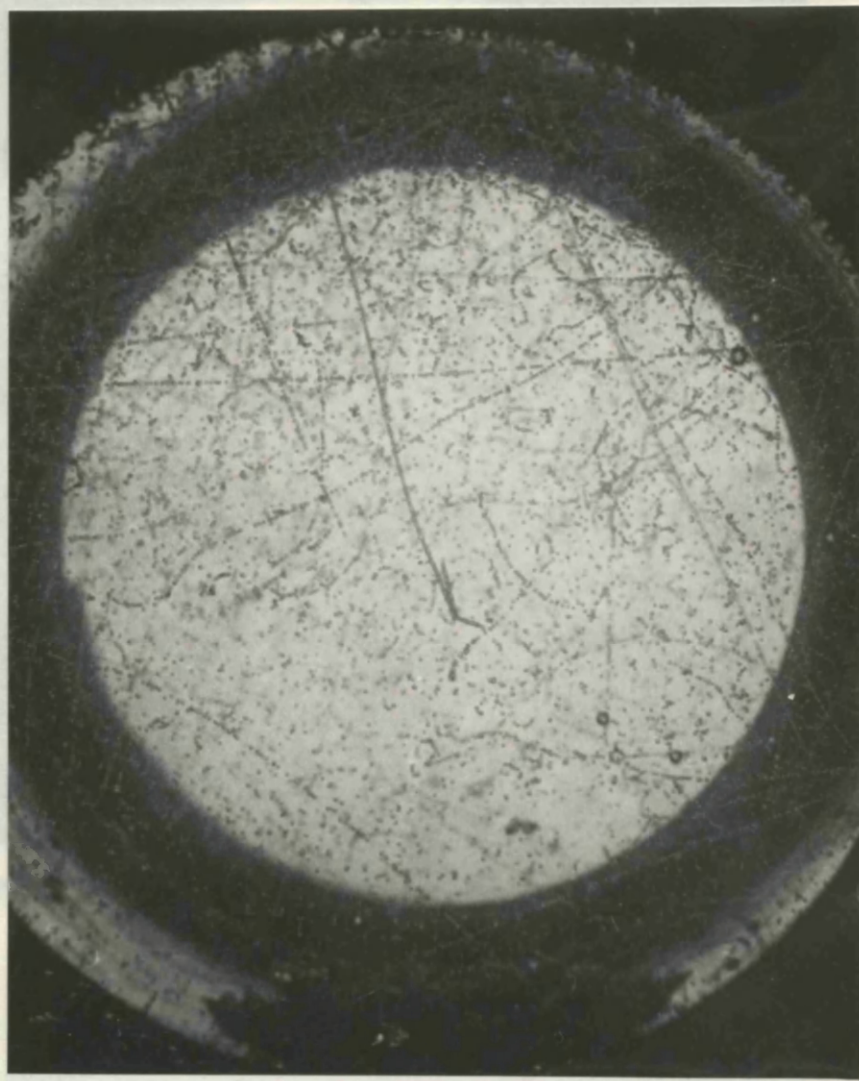
for protons of energy  $80 \pm 4$  MeV at  $90^\circ$  (Laboratory co-ordinates)

to a 300 MeV Bremsstrahlung beam.

An energy distribution is given by Rosengren (Ref. 17) Fig. 37 and from these results a cross section for proton production was deduced for this system.



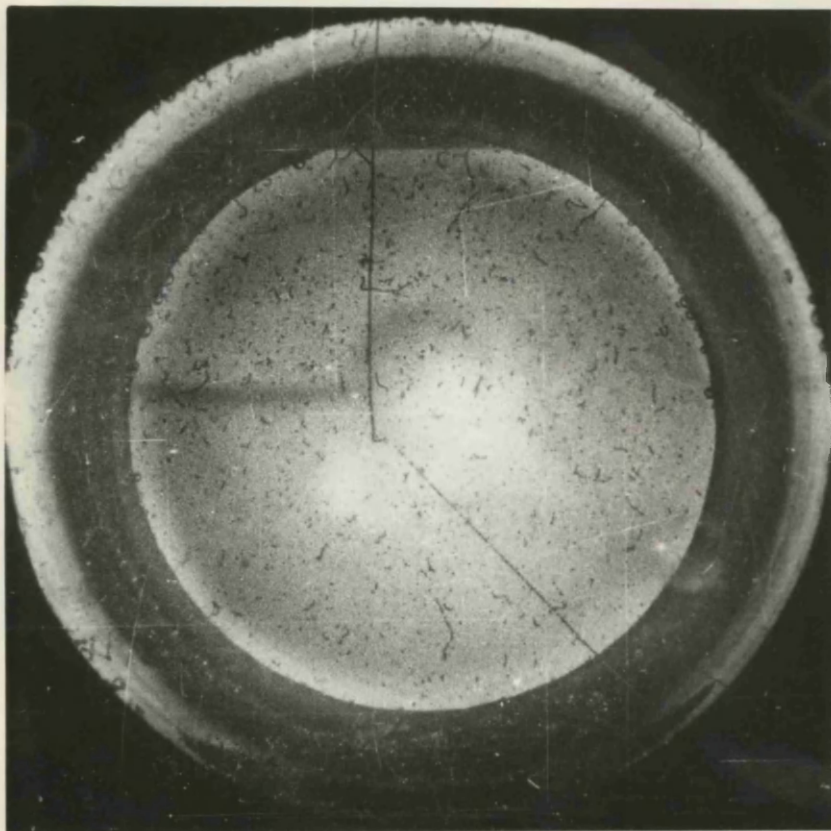
C. proton.



b  $\pi^-$  showing 2 pronged star event



Plate 10.



a.  $\pi^+ \rightarrow \mu^+ \rightarrow e^+$

b.  $\pi^-$  showing 2 pronged star event

The energy with which protons left the target and stopped in the chamber was estimated to be in the range 88 - 112 MeV (Fig. 34).

Hence,

$$\left( \frac{\partial^2 \sigma}{\partial \Omega \partial E} \right) = 6.2 \times 10^{-32} \text{ cm}^2/\text{steradian} / Z \text{ /equivalent quantum/MeV}$$

of energy  $100 \pm 12 \text{ MeV}.$

Number of protons = 806 per minute at 5 cycles/sec  
 $\approx 3$  per shot.

From these calculations it is clear that despite their inaccuracy, about five particles which have stopped in the chamber should be seen on each photograph.

### Experiment.

57

The chamber was maintained at 75<sup>0</sup>C at which temperature ?  
 the bubble density on fast electrons was 14 bubbles/cm  
 and several photographs taken of particles stopping in  
 the chamber.

Several  $\pi^+ \rightarrow \mu^+ \rightarrow e^+$  events were seen in the  
 photographs together with a few  $\pi^-$  stars and tracks which  
 were obviously protons - Plate 10.

There were tracks, however, which could not be  
 identified by their appearance, especially short range  
 tracks where multiple scattering could not be examined.

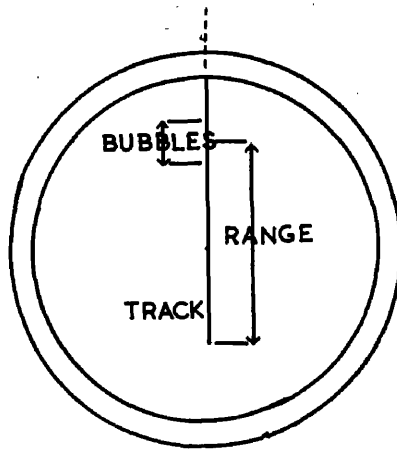
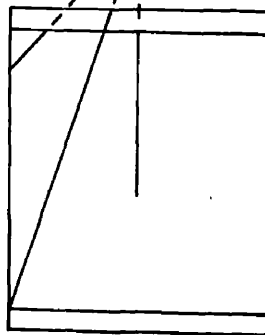
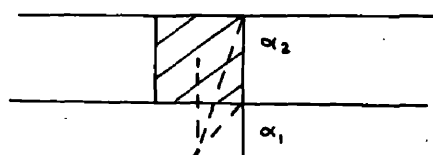


FIG. 37.



$\alpha_1 \approx 35^\circ$   
 $\alpha_2 \approx 15^\circ$   
 Correction  
 $\alpha_1 \rightarrow 18\%$   
 $\alpha_2 \rightarrow 3\%$

FIG 38.



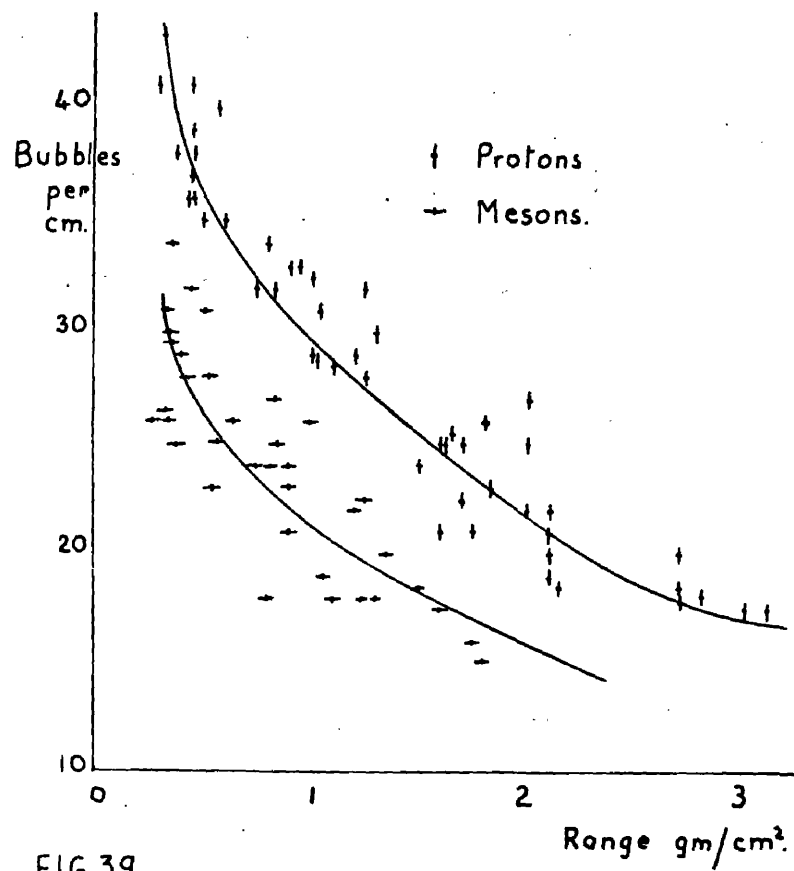


FIG.39.

Further, since a single camera was used there was a finite probability that some of the particles were leaving the chamber by the front or back windows.

An investigation was then made of using bubble counting to identify these particles.

### Bubble Counting.

To do this, tracks of particles whose identity was known without any doubt were selected. The film negative was examined under a microscope and a position a measured distance from the track ending chosen. Bubbles were counted over a range of one unit on the eyepiece scale on either side of this point, Fig. 37. Since a single camera was used an error is introduced by this method because the particle direction in a plane perpendicular to the camera is not known. As can be seen from Fig. 38 in most cases this is not greater than about 3%.

The number of bubbles in the region considered was then converted to bubbles/cm in the chamber and a graph constructed of bubble density against residual range, Fig. 39.

It can be seen that there is a good separation between mesons and protons. The graph was then divided

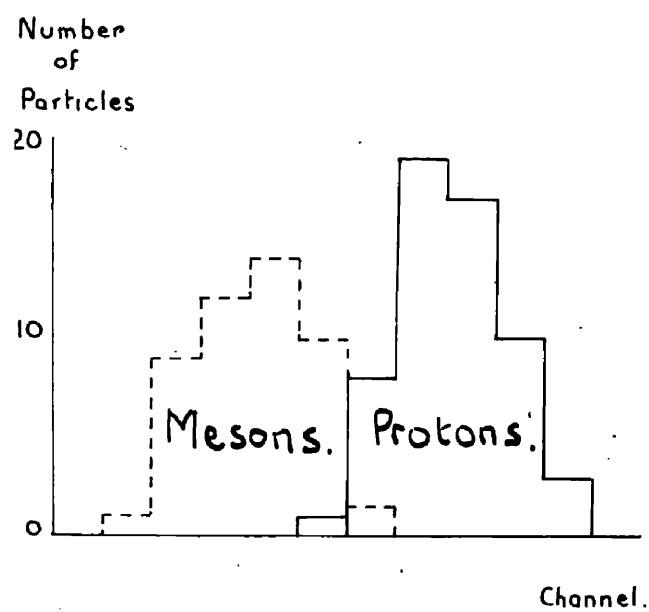


FIG 40.

into channels, a histogram drawn and the separation is again seen to be very marked, Fig. 40.

Bubble counters were then made on unidentifiable tracks, fitted to the curves and the separation into mesons and protons was seen immediately.

Further, tracks which were very straight but exhibited meson type bubble density were rejected as they were probably protons leaving the chamber, and tracks which gave a lower bubble density than expected for either mesons or protons were rejected as they were probably mesons going out. This type of selection is unnecessary if stereo-photography is used.

From this curve it is clear that bubble counting can be a most useful aid to identification of short range particles when there is no field present.

Further, a  $\pi^-$  meson<sup>s</sup> showing no star products, and a proton of range about 1 cm where scattering can not be used at all for identification and which would otherwise be quite indistinguishable, had respectively 30 and 40 bubbles in that distance, under the prevailing chamber conditions. This is the only method of distinguishing between these two cases when no field is present.

TABLE 10.

Particle	Energy range M.e.v.	Number seen	Theoretical ratio	Experimental ratio
proton	90-115	150		
meson	35-50	142	$1.11 \pm 0.1$	$1.06 \pm 0.2$
$\pi^-$ meson	35-50	81		
$\pi^+$ meson	35-50	61	$1.27 \pm 0.07$	$1.33 \pm 0.3$

Comparison of numbers seen and expected.

In order to check the accuracy of the identification of particles a count of the relative numbers of  $\pi$  mesons and protons obtained and expected was made. Also, the ratio of  $\pi^- : \pi^+$  has been measured by many workers since it gives information on nuclear structure.

For  $C(\gamma, \pi^+)$  reactions in the energy range 35 - 50 MeV at  $90^\circ$  in the laboratory this is given as  $1.27 \pm 0.07$  (Ref. 17).

The values of number of particles found by experiment and expected from calculations are shown in Table 10.

It can be seen from these results that the numbers expected and obtained agree within experimental error and therefore the method of identifying particles by bubble counting can be considered reliable.

In practice a lower counting rate than about five particles stopping per shot was recorded. It was nearer one particle stopping per shot. The error in calculation was probably caused by an over optimistic figure being used for the number of equivalent quanta. The fact that the ratio of protons to mesons obtained agrees with the calculated value indicates that the error is some factor common to both.

This illustrates one important feature of a visual detector in general and bubble chamber in particular for this type of measurement. Since more than one type of particle is detected at any one time a relative number is obtained even though outside factors vary or are difficult to measure.

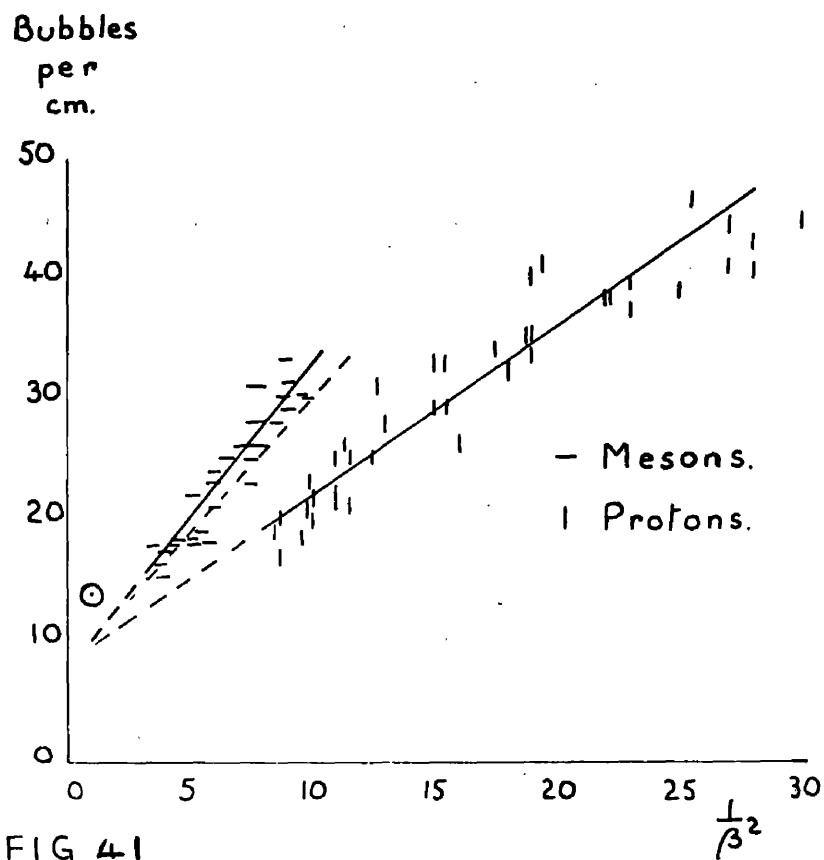


FIG 41



## Chapter IX. Bubble Density and Particle Energy.

### Bubble Density : $\frac{1}{\beta^2}$

The identity of a particle having been established, a new graph of  $d : \frac{1}{\beta^2}$  was constructed and is shown in Fig. 41.

It can be seen at once that while  $d \propto \frac{1}{\beta^2}$ , as Glaser and Blinov had found, there are two distinct curves, one for mesons and one for protons. No other workers have reported a result of this kind.

Because of limited chamber dimensions lower values of  $\frac{1}{\beta^2}$  could not be obtained, but both curves extrapolate to about  $10 \pm 2$  bubbles/cm for  $\beta = 1$  - that is minimum ionizing particles, while bubble density for high energy electrons gave 14 bubbles/cm.

This result agrees with that observed on fast and slow electron tracks in the earlier experiments.

Several errors in measurement and calculation of these  $d : \frac{1}{\beta^2}$  curves will now be considered.

It has already been pointed out that there is a 3% error in bubble counting since only a single camera was used and hence the precise direction of the particle is in some doubt.

A second error is introduced by considering the

TABLE 11.

-----

$$\Delta R = 0.1005 \text{ gms/cm}^2.$$

		Meson	Proton
$\frac{1}{\beta^2}$		11.1	11.1
$\beta$		0.3	0.3
E.M.e.v.		7.3	45.0
Range	gm/cm <sup>2</sup>	0.295	1.68
$\Delta R$	1.	0.395	1.78
	2.	0.195	1.58
$\Delta E$	1.	8.6	46.5
	2.	5.8	43.5
$\Delta \beta$	$\beta_1$	0.33	0.306
	$\beta_2$	0.26	0.295
	$\frac{1}{\beta_1^2}$	9.13	10.7
	$\frac{1}{\beta_2^2}$	14.75	11.5
Mean	$\frac{1}{\beta^2}$	11.94	11.1

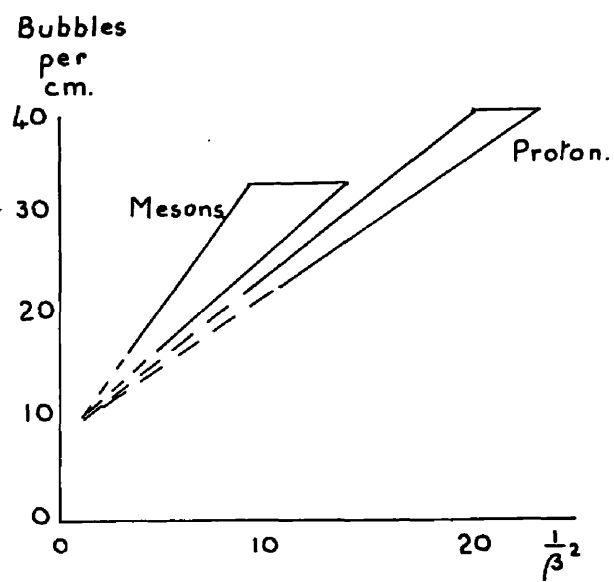


FIG 42

the value of  $\frac{1}{\beta^2}$  can be derived directly from the range and, therefore, energy of the particle at the mid point of the region over which bubbles are counted.

As can be seen in Table 11, while this is true for protons it is not true for mesons.

Instead of choosing a new value of  $\frac{1}{\beta^2}$  for mesons, the error introduced by this is indicated by assuming that when bubble density for mesons is 30 bubbles/cm  $\frac{1}{\beta^2}$  lies in the range 9.13 to 14.75, while a bubble density of 20 bubbles/cm for protons occurs when  $\frac{1}{\beta^2}$  has any value between 10.7 and 11.5. This is shown on Fig. 42, where it can be seen that there is still a mass separation.

An alternative approach to this correction is to decide within what limits of  $\frac{1}{\beta^2}$  a measurement is to be made, calculate the range in centimetres over which bubbles are to be counted and convert to bubbles/cm thus:-

	Range of $\frac{1}{\beta^2}$	$\beta_1$	$\beta_2$	$E_1$ MeV	$E_2$ MeV	$R_1$ gm/cm <sup>2</sup>	$R_2$ gm/cm <sup>2</sup>
Meson	9 - 10	.333	.316	8.6	7.7	.393	.322
Proton	9 - 10	.333	.316	56	50.5	2.5	2.07

A count was then made on several meson and proton

tracks and the result was :-

meson  $29 \pm 2$  bubbles/cm    proton  $21 \pm 1$  bubbles/cm.

Thus, despite these corrections, it can be seen that there is still a mass difference.

Finally, a paper due to Willis (Ref. 18) showed that an underestimate of bubble density was made by counting individual bubbles. He measured bubble spacing on tracks of high energy particles, computed a mean value and this gave a higher ultimate count of bubble density in bubbles/cm.

The cause of the inefficiency in direct bubble counting was attributed to poor bubble resolution and coalescence of individual bubbles.

A measure of mean bubble spacing can not be made on short range tracks since the value of  $\frac{1}{\beta^2}$  is changing so rapidly. However, if bubbles are liable to coalesce, and if resolution is poor on high energy tracks, errors will be even greater on low energy tracks.

It can be seen on the proton curve that there is a falling off at higher values of  $\frac{1}{\beta^2}$ .

Further, this explains the result found when bubble density was measured at various points on a single proton curve, Fig 29.

TABLE 12.

## Meson

Range	Energy M.e.v.	$\frac{dE}{dx}$	Bubbles per cm.	$\frac{dE}{dx/d}$
0.5	9.8	4.85	25	0.19
1.0	14.4	3.5	20	0.18
1.5	18.1	3.1	17.5	0.175
2.0	21.3	2.8	16	0.175

## Proton

0.5	23	11.7	38	0.31
1.0	34	8.3	30	0.28
1.5	42	6.8	25.5	0.27
2.0	49.5	6.0	21.5	0.28

However, this result is a function only of the number of bubbles present, and in no way explains the mass effect.

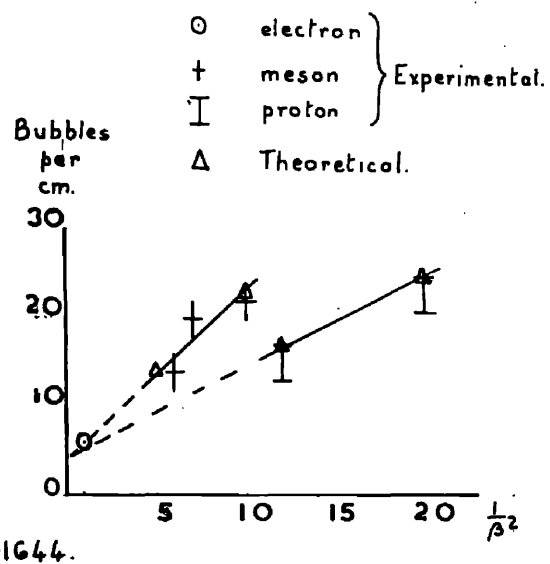
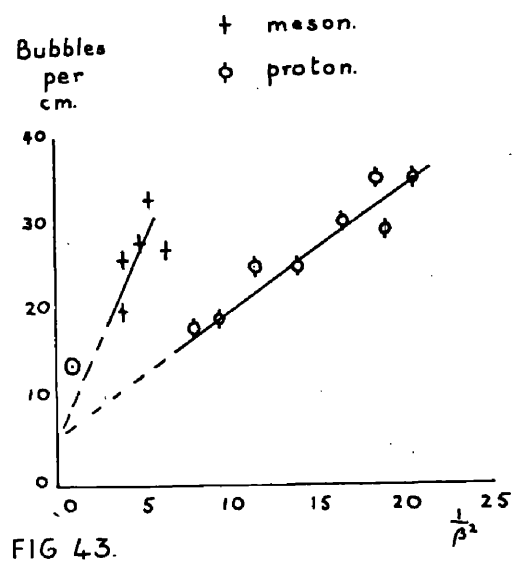
### Bubble Density and $\frac{dE}{dx}$

A comparison was then made between bubble density and rate of energy loss of the particle.  $\frac{dE}{dx}$  was obtained from tables U.C.R.L. 2301 for various values of range of both mesons and protons. As expected a direct correlation was found between  $\frac{dE}{dx}$  and  $d$  of the form  $\frac{dE}{dx} / d = \text{constant}$  (except at high values of bubble density where coalescence effects are more important). Table 12.

The value of this constant, however, was less for mesons than for protons and this is consistent with the previous result.

### Other measurements.

A measure was made of bubble density on the tracks of particles which stopped in the chamber when initial tests were being performed. While these results can not be considered reliable in themselves because of the temperature gradients and the scarcity of the results the mass effect was seen there, and hence, considered





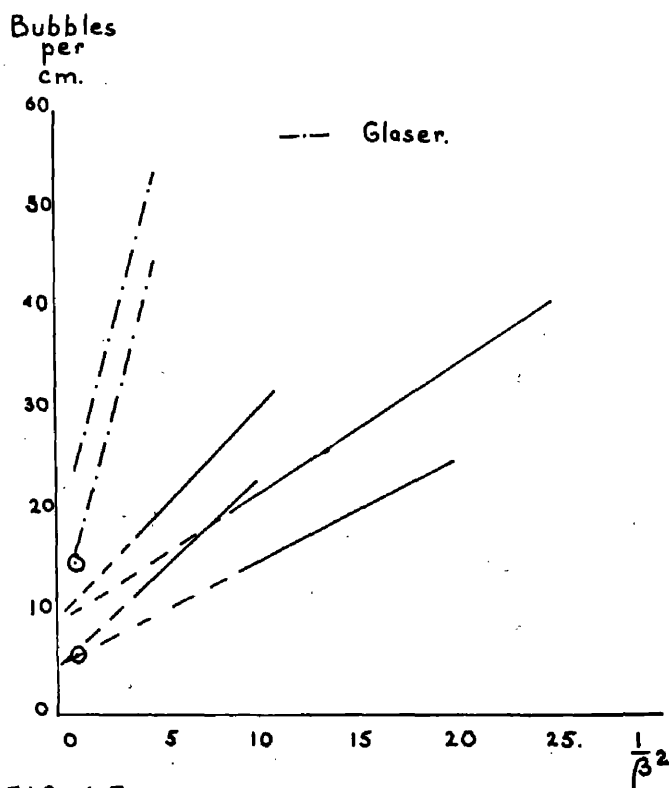


FIG 45a.

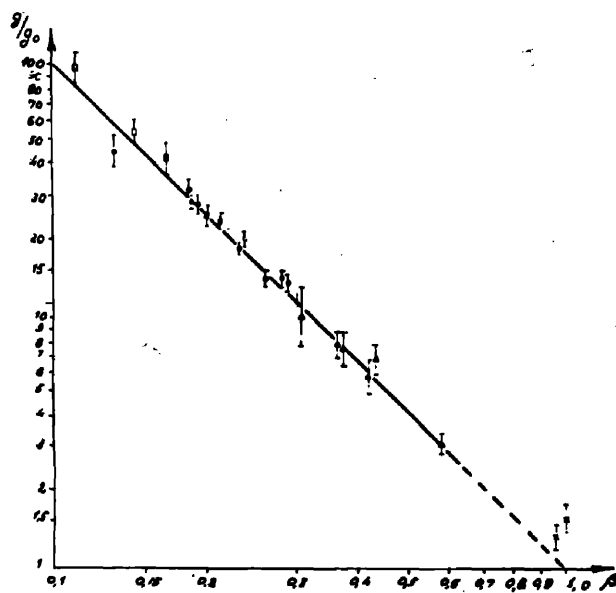


FIG 45b.

with the more refined experiment must be taken as further support of this result, Fig. 43.

A count was also made on tracks of particles which stopped in the chamber when the sensitivity was very low. Again these results taken above are inconclusive since there are so few of them available, but they do support the mass effect, Fig. 44.

### Mass Effect.

From these results, the author feels confident that a mass effect is a true experimental fact. Glaser only measured  $\frac{1}{\beta^2}$  for protons, and besides, in the region where the measured bubble density -  $\frac{1}{\beta^2}$  from 1 to

5 - there is not much separation between mesons and protons.

Blinov claims to have measured bubble density on both mesons and protons but observed no mass separation. He does not indicate which points are from which particles. The results are summarized in Fig. 45a and 45b, Blinov's could not be superimposed on 45a since he gives a relative value for bubble density ( $g_0 = \text{constant}$ ). He used a logarithmic scale rather than bubble density against  $\frac{1}{\beta^2}$ , but obtained a slope = 2 thus agreeing with the relation

$$d \propto \frac{1}{\beta^2}$$

The theory of Seitz proposed that bubbles form by the creation of thermal spikes in the liquid. It is possible that some of these spikes are created by Coulomb collisions between the incident particle and the medium, and if a meson loses more energy by this process than a proton, this might explain the mass effect.

The energy loss by Coulomb collisions was calculated from the formula (Ref. 20)

$$\left(\frac{dE}{dx}\right)_{\text{Coul.}} = 2\pi n_0 \frac{Z_1^2 Z_2^2 e^4}{M_2 v^2} \log \frac{T_{\text{max}}}{T_{\text{min.}}}$$

$$n_0 = \text{density of atoms} = \frac{\rho N}{M} \quad \text{atoms/molecule}$$

$N$  = Avogadro's number.

$M$  = molecular weight

$Z_1 = 1$  for protons and mesons

$Z_2$  = atomic number of absorber

$e$  = electronic charge e.s.u.

$M_2$  = weight of one atom of absorber

$v$  = speed of incident particle

$T_{\text{max}}$  = maximum energy transfer

$$= \frac{4 M_1 M_2}{M_1 + M_2} E$$

TABLE 13.

	Proton.	Meson.
$\beta$	0.255	0.255
Energy M.e.v.	30	5.5
	Hydrogen	Carbon
$T_{\max.}$ M.e.v.	30	8.4
$T_{\min.}$ e.v.	5	20
$\log_e \frac{T_{\max.}}{T_{\min.}}$	15.6	12.9
$n_o$	8x.	3x.
$M_2 v^2$	y	12y
$\frac{dE}{dx}$ e.v.	1600	1500
	1330	1103

$$x = \frac{N}{M} = \frac{0.44 \cdot 6.03 \cdot 10^{23}}{44} \quad y = \frac{2E}{M_1}$$

$\frac{(dE)}{(dx) \text{ Coul.}}$  protons on hydrogen

= 1.2 : 1

$\frac{(dE)}{(dx) \text{ Coul.}}$  mesons on hydrogen

Do. on carbon

= 1.35 : 1

$T_{\min}$  = minimum energy transfer to have significant effect. This was taken as the binding energy of carbon and hydrogen to the molecule.

The calculation, shown in Table 13, was done for a proton and a meson of the same speed, the carbon and hydrogen atoms of the hydrocarbon molecule being considered independently.

It can be seen that the energy lost by proton collisions is greater than that lost by meson collisions, rather than the opposite as required by the experimental result, and therefore, the mass effect is not explained in this way.

#### Empirical Formula for Bubble Density.

An empirical formula for bubble density has been proposed by Glaser of the form

$$d = \frac{A}{\beta^2} + B(T).$$

This result implies that the slope of the curve of  $d : \frac{1}{\beta^2}$  is a constant for all chamber conditions - as in fact Glaser found experimentally. Even excluding the mass effect from this consideration, the results quoted here do not agree with that result - at least not in the region of particle velocity where bubbles were counted, Fig. 45a. Since the extrapolation to  $\beta = 1$  gives a

result consistant with that found for fast electrons when allowance has been made for relativistic effects, the extrapolation can be justified.

From Chapter V a relation between bubble density and Volmer Energy of the form

$$d = \frac{K}{E_V}$$

was found.

It is therefore possible to construct another empirical formula thus:

$$d = c \frac{dE}{dx} \frac{1}{E_V} \frac{1}{m^\alpha} + \frac{b}{E_V}$$

which, in view of the relation between  $d$  and  $\frac{1}{\beta^2}$  in the region  $0.2 < \beta < 0.9$  may be written as

$$d = \frac{a}{\beta^2 E_V m^\alpha} + \frac{b}{E_V}.$$

The values of the constants, calculated from Fig. 41 are:

$$a = 2250$$

$$b = 1200$$

$$\alpha = 0.30$$

$$m_\pi^\alpha = 5.4$$

$$m_p^\alpha = 9.5$$

$$m = \text{electron mass units.}$$

The value of  $E_v$ , since it could not be calculated, was deduced from Fig. 28 taking  $d$  for fast electrons as 14. This gave  $E_v = 160$  e.v.

Since there are so few results available, the formula can not be tested thoroughly. However, the formula was applied to the results given in Fig. 44 where  $d$  for fast electrons was 6. The value of  $E_v$ , deduced again from Fig. 28 was taken as 230 e.v. and it can be seen on Fig. 44 that a remarkably good agreement is found with the experimental results.

For Glaser's chamber where  $E_v = 131$  e.v. at  $55^\circ\text{C}$  the values are:

$d = 14$  from the formula

$d = 18 - 20\% \quad 15$  from  $d : \frac{1}{E_v}$  curve

$d = 15$  by experiment.

However, for protons, where  $\frac{1}{\beta^2} = 3.3$ , the result is very poor:

$d = 30$  by experiment

$d = 19$  from the formula.

The slope of the  $d : \frac{1}{\beta^2}$  curve for protons where  $E_v = 131$ , is only 6 from the formula whereas Glaser got 9.2.

Since, however, Glaser's results do not agree with the results quoted here, this is not surprising. It may

be that the discrepancy can be explained by poorer bubble resolution in the present results.

### Conclusion.

The results shown here tend to confirm the result shown by Glaser, Blinov and those discussed in Chapter V that within certain limits bubble density is proportional to  $\frac{1}{\beta^2}$  and therefore bubbles are probably formed from  $\delta$  -rays.

Since such a good fit was found for the calculated value of bubble density at low sensitivity, it would appear that deducing Volmer Energy  $E_v$  from bubble density was justified. This, however, does not necessarily disagree with the odd shape of the  $d:T$  curves since this shape was not observed in the dirty chamber results.

The poor resolution observed by Willis would tend to emphasise even more the higher bubble density found at high sensitivity.

No reasonable explanation for the mass effect has evolved and it is clear that further experiments are essential to verify or otherwise this most curious result.



Chapter X.General Conclusion.

From this work it is clear that the bubble chamber is a most valuable addition to the detectors available for research into nuclear and particle physics.

The increase in density makes the study of rare events much easier and the high energy products of these events can also be examined in more detail.

The ability of a bubble chamber to be cycled fast is a great advantage when operating with pulsed accelerators since no time is lost waiting for the chamber to recover.

Because of this it might also be possible to perform a cosmic ray experiment reasonably economically. If a bubble chamber was cycled at about 10 cycles/sec and had a sensitive time of  $\sim 10$  ms, it would be sensitive for 10% of the time.

It has been shown that the operation can be controlled so that uniform sensitivity is achieved throughout the chamber. Chamber sensitivity can also be varied depending on the energy of particle which is being observed.

Because of this it has been possible to fire the

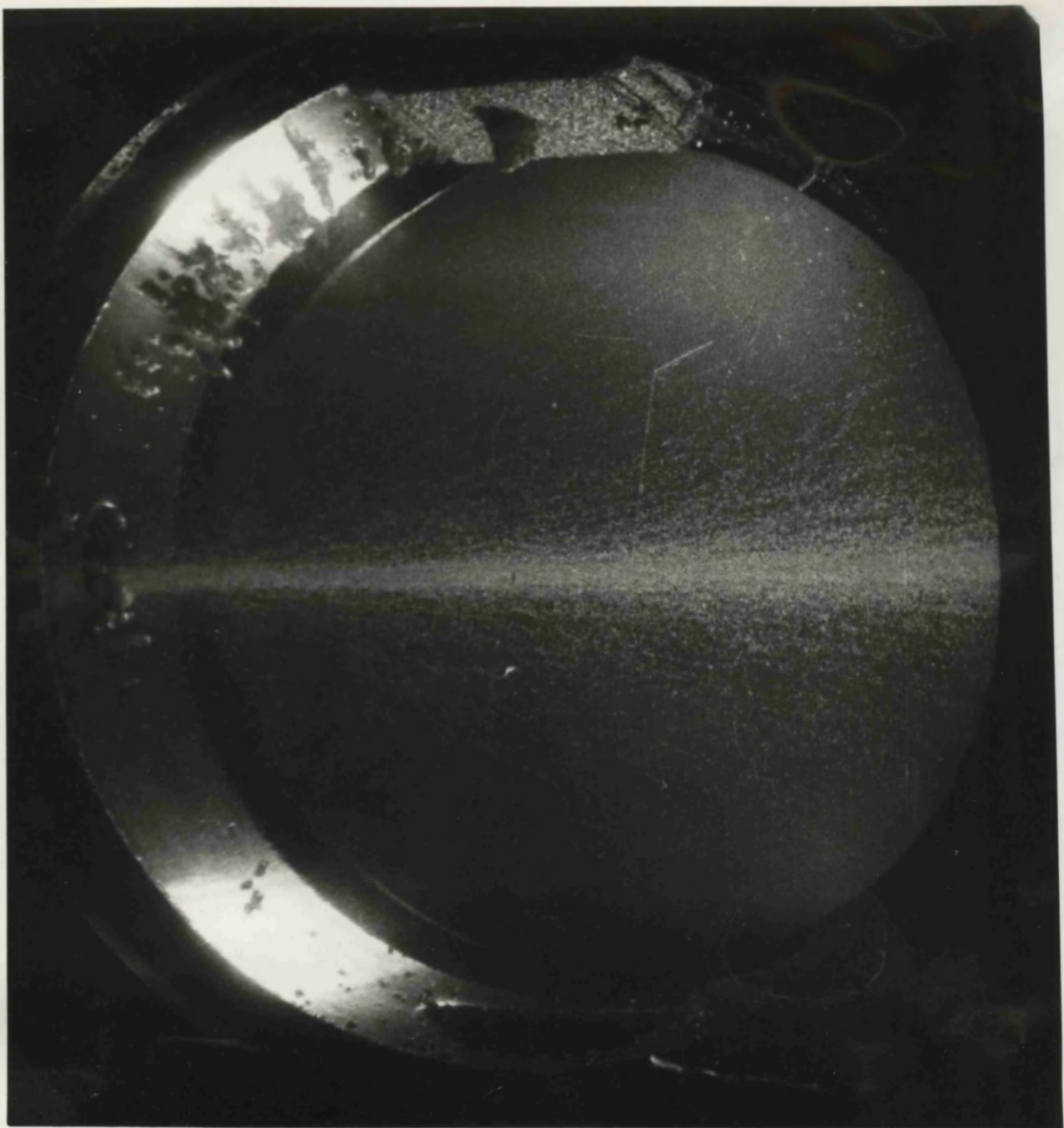


Plate II.

$\gamma$ -beam of the synchrotron through a propane bubble chamber. A chamber has been built in this laboratory, 10" inside diameter and by operating at very low sensitivity, although the beam had to be collimated down from 1" diameter to 0.25" diameter, tracks of particles created by a reaction between a photon and a nucleus could be seen despite the electron core. Plate II. is a typical example, showing a  $\pi^-$  meson with single pronged star event at the end of its track.

Since the bubbles grow so rapidly, distortions on tracks are reduced to a minimum, and resolution of associated events should be possible, within limits, by measuring bubble diameters.

Finally, it has been shown that bubble counting can be most valuable in aiding the identification of particles which stop in the chamber, when no magnetic field is available. Even with a field, it may still be necessary to use bubble counting methods for very short range particles.

It is unfortunate, however, that so few workers have shown an interest in theories of bubble formation. Many more results are necessary in order that the various possibilities can be resolved. In particular, it would be most valuable to measure bubble density in chambers filled with the new liquids such as hydrogen, helium, Xenon,  $\text{CF}_3$  Br etc., with quite different physical properties.

The use of a high energy electron beam for this type of work is ideal since any change in bubble density is caused by a change in chamber conditions. It would be of interest, in addition, to investigate further the region between values of  $\beta = 0.96$  and  $\beta = 0.99$ , since a difference has been observed. This may lead to a better analysis of the bubble forming process.

Clearly a dirty chamber with a system by means of which the bottom pressure  $P_0$  can be measured is essential for work of this kind in such chambers.

As has already been stated, it is clear that the

mass effect must be studied further, and more measurements made of variation of bubble density with all values of particle velocity. Performed in a much bigger chamber, a continuous set of results could be obtained, covering a wider range of particle velocity.

### References.

1. Glaser, D.A., Physical Review, 87 (1952) 665.  
   "  "  91 (1953) 762.
2. Bertanza, L., IL Nuovo Cimento, 10 No.2 (1955) 487.
3. McFarlane, W., Nature, 176 (1955) 666.
4. Atkinson, J.R., Nuclear Instruments, 1 (1957) 152.
5. Plesset, M.S., Journal of Applied Physics, 25 (1954) 493.
6. Bertanza, L., IL Nuovo Cimento, 5 No.4 (1957) 940.
7. Glaser, D.A., Handbuch der Physik XLV.  
   Nuclear Instrumentation II, p.329.
8. Glaser, D.A., Proceedings C.E.R.N. Conference 1956.
9. Blinov, , Proceedings C.E.R.N. Conference 1956.
10. Volmer, , Kinetic der Phasenbildung.  
                   Pless, I.A., Review of Scientific Instruments, 27  
   No.11 (1956) 935.
11. Seitz, F., Physics of Fluids, 1, 1 (1958) 2.
12. Marshak, , Meson Physics, p.135.
13. Marshak , Meson Physics, p.168.
14. Luckey, D., Physical Review, 97 (1955) 469.

15. Physical Review, 86 (1952) 171.  
    "          "          81 (1951) 1003.  
    "          "          91 (1953) 468.  
    "          "          97 (1955) 469.  
    "          "          93 (1954) 900.
16. Walker, D., Physical Review, 81 (1951) 634.
17. Rosengren, , Physical Review, 85 (1952) 766.
18. Peterson, J.M., Physical Review, 81 (1951) 1003.
19. Willis, W.J., Private Communication.
20. Seitz, F., Solid State Physics, Vol. 2 (1953) 327.

Appendix.

-----

Photographs of Apparatus.

- Plate    A.    First chamber set up.
- B.    Heater, showing thin window for entry  
              of particles.
- C.    20cc. clean chamber.
- D.    Clean chamber opposite electron beam.  
              (  $\gamma$ -beam emitted through centre port.)
- E.    First dirty chamber.
- F.    500cc. chamber.
- G.    500cc. chamber set up, showing camera,  
              Barksdale valve, reservoir, and position  
              of carbon target.
- H.    Control equipment when operating the  
              500cc. chamber with the synchrotron.



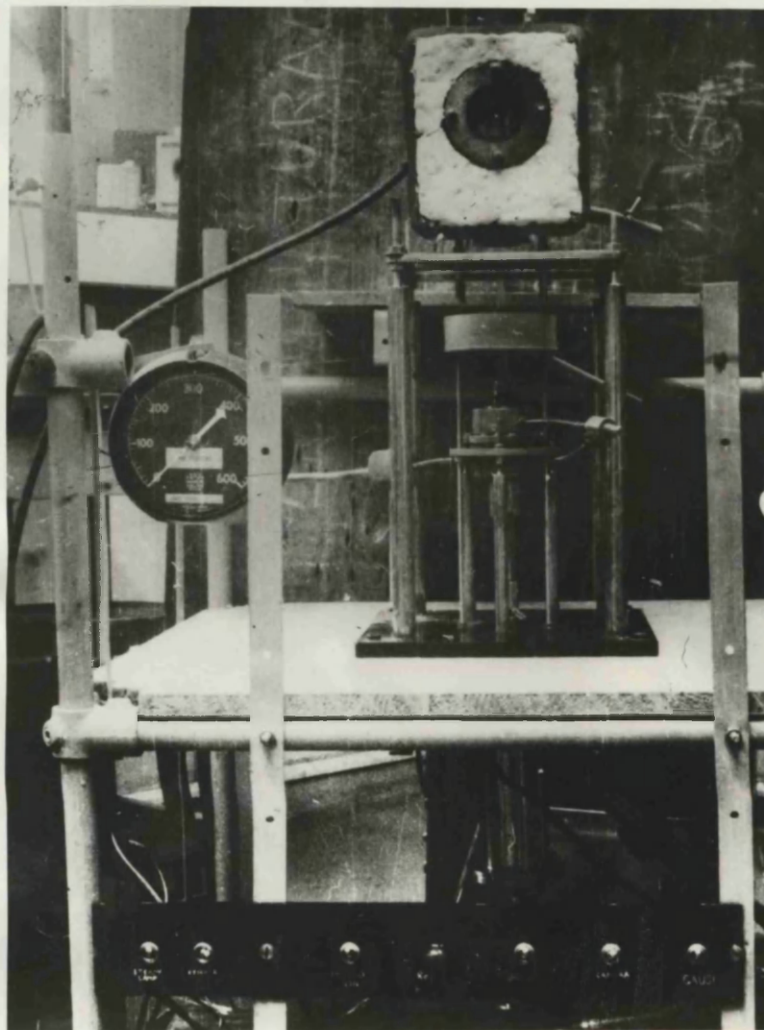


Plate A.

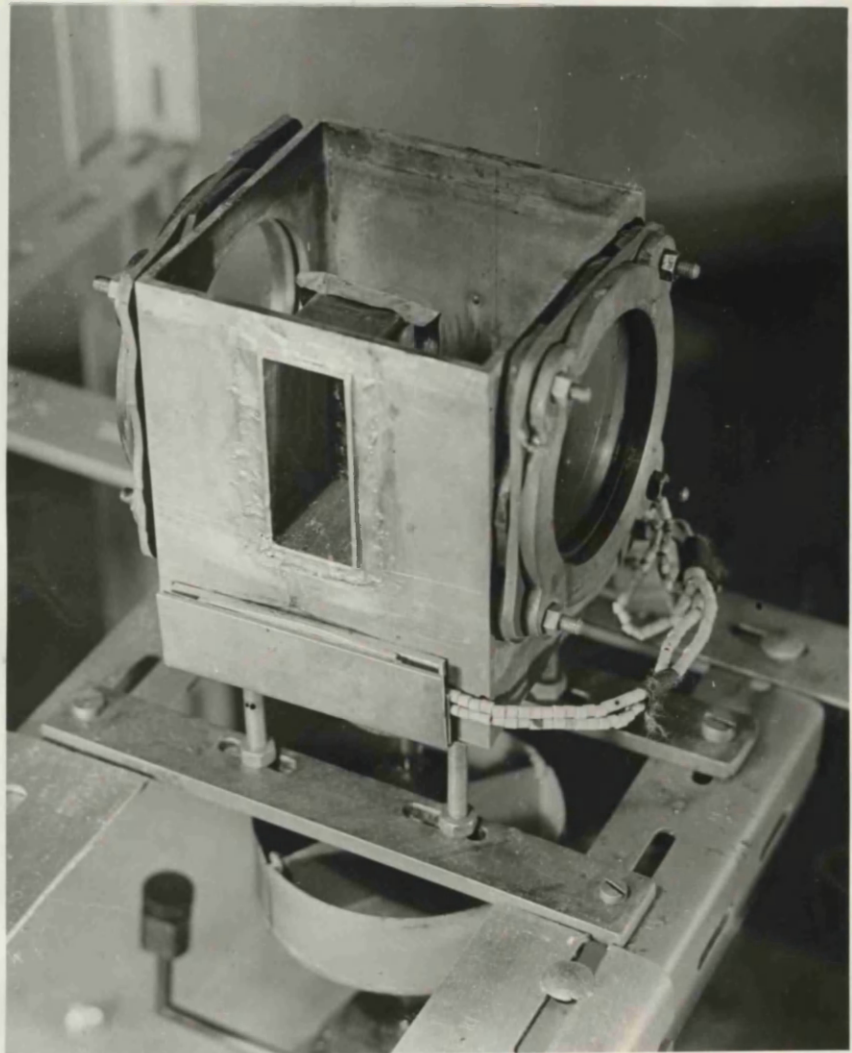


Plate B.



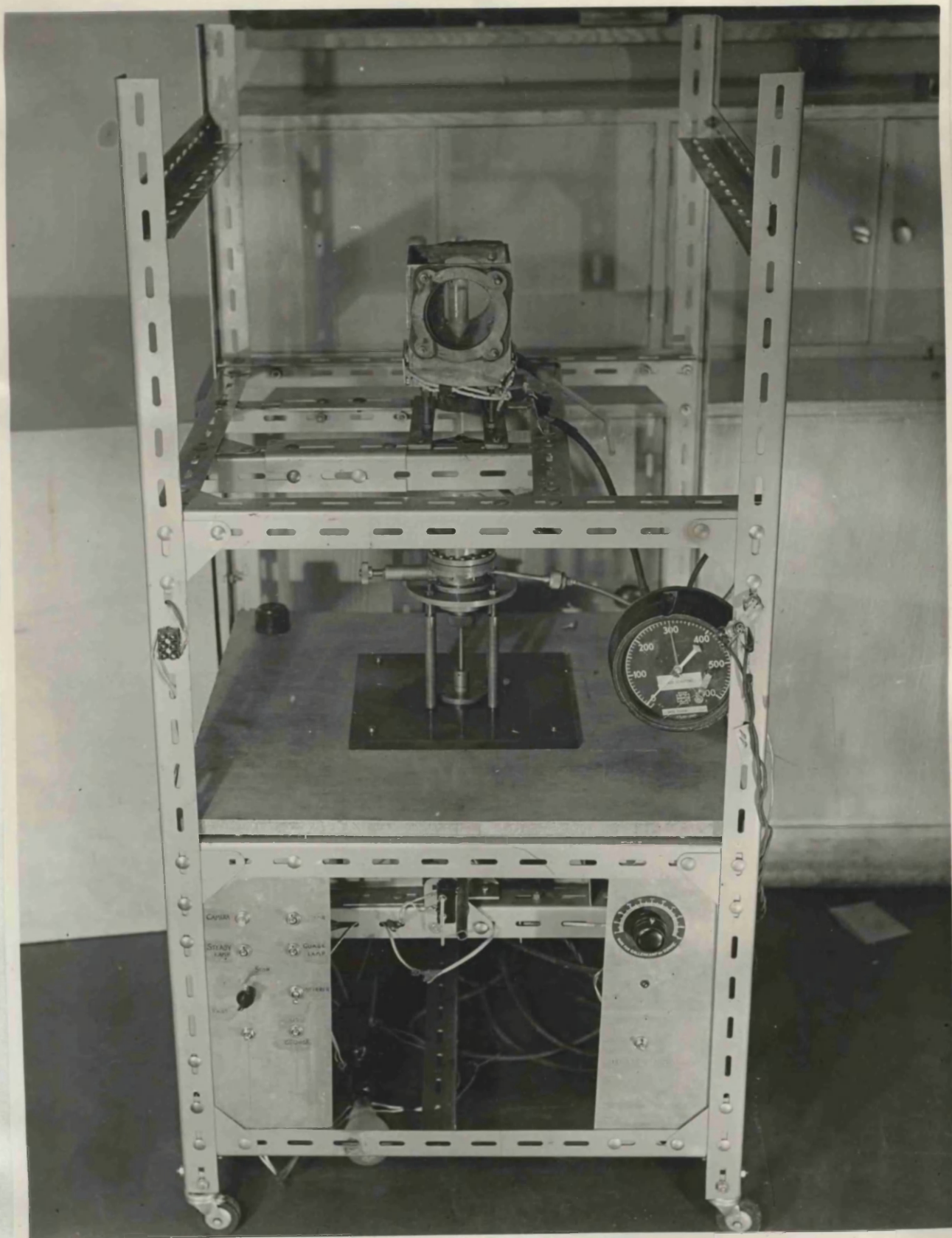


Plate C

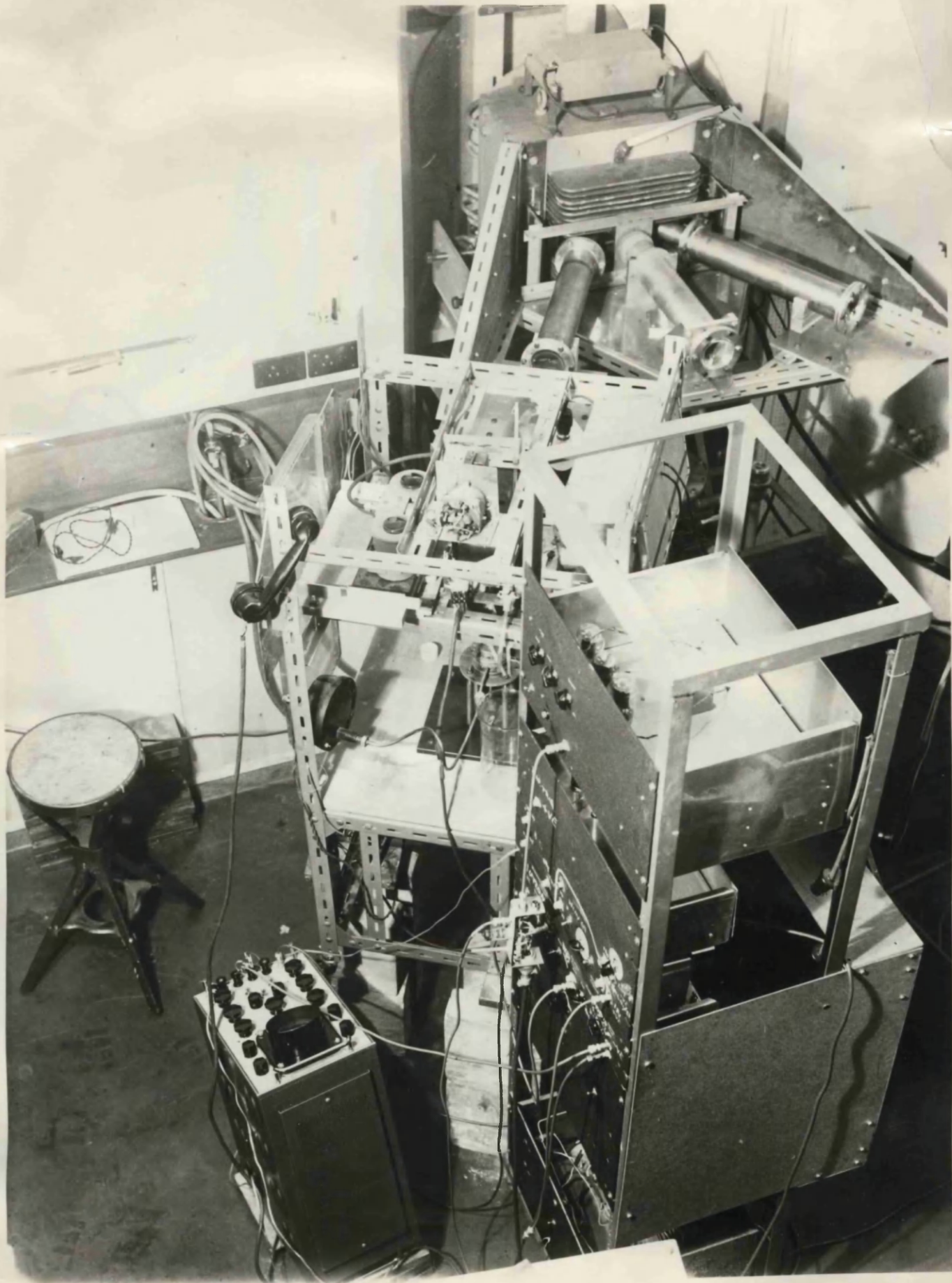


Plate D.



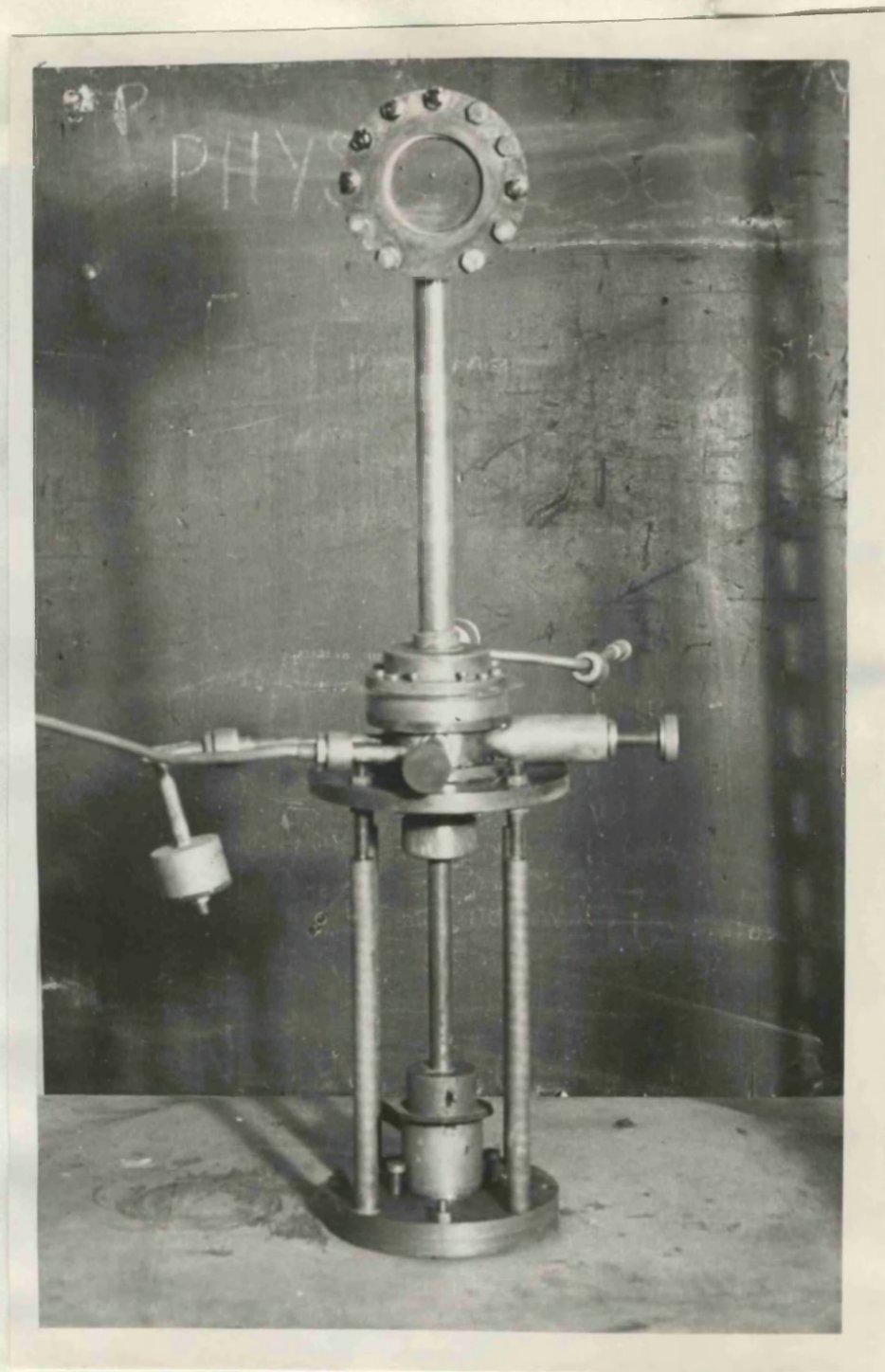


Plate E.

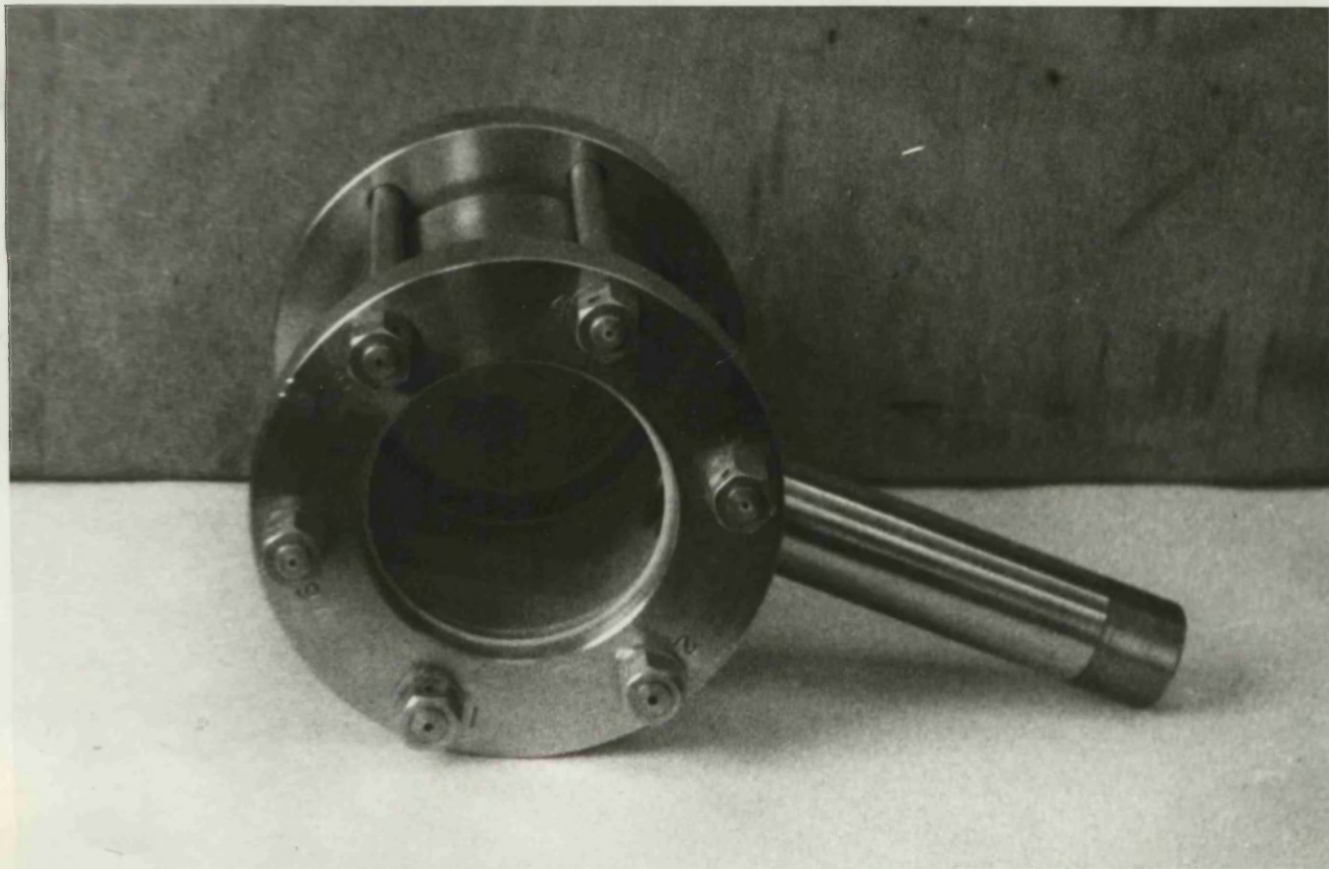


Plate F.

Plate G.



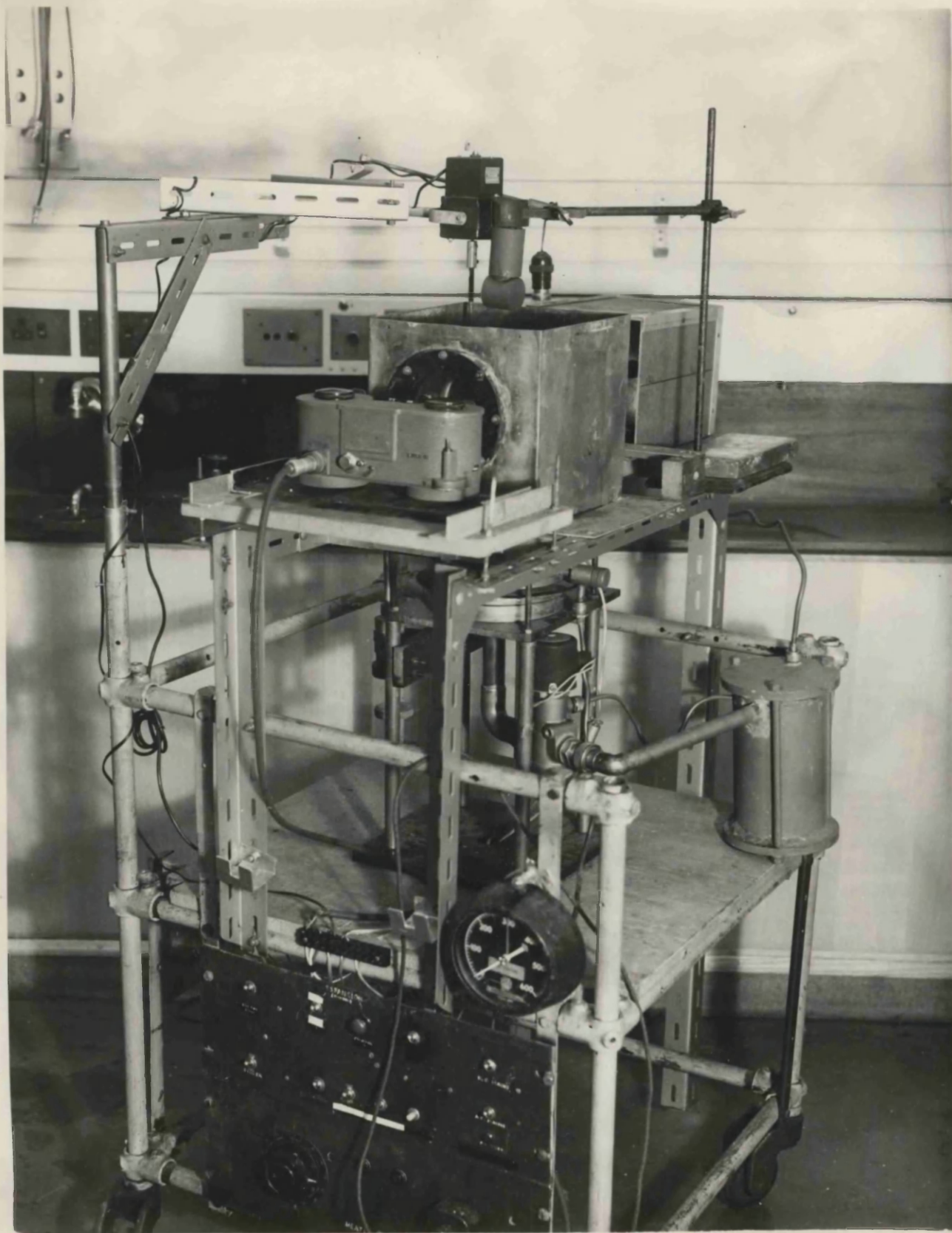


Plate G.

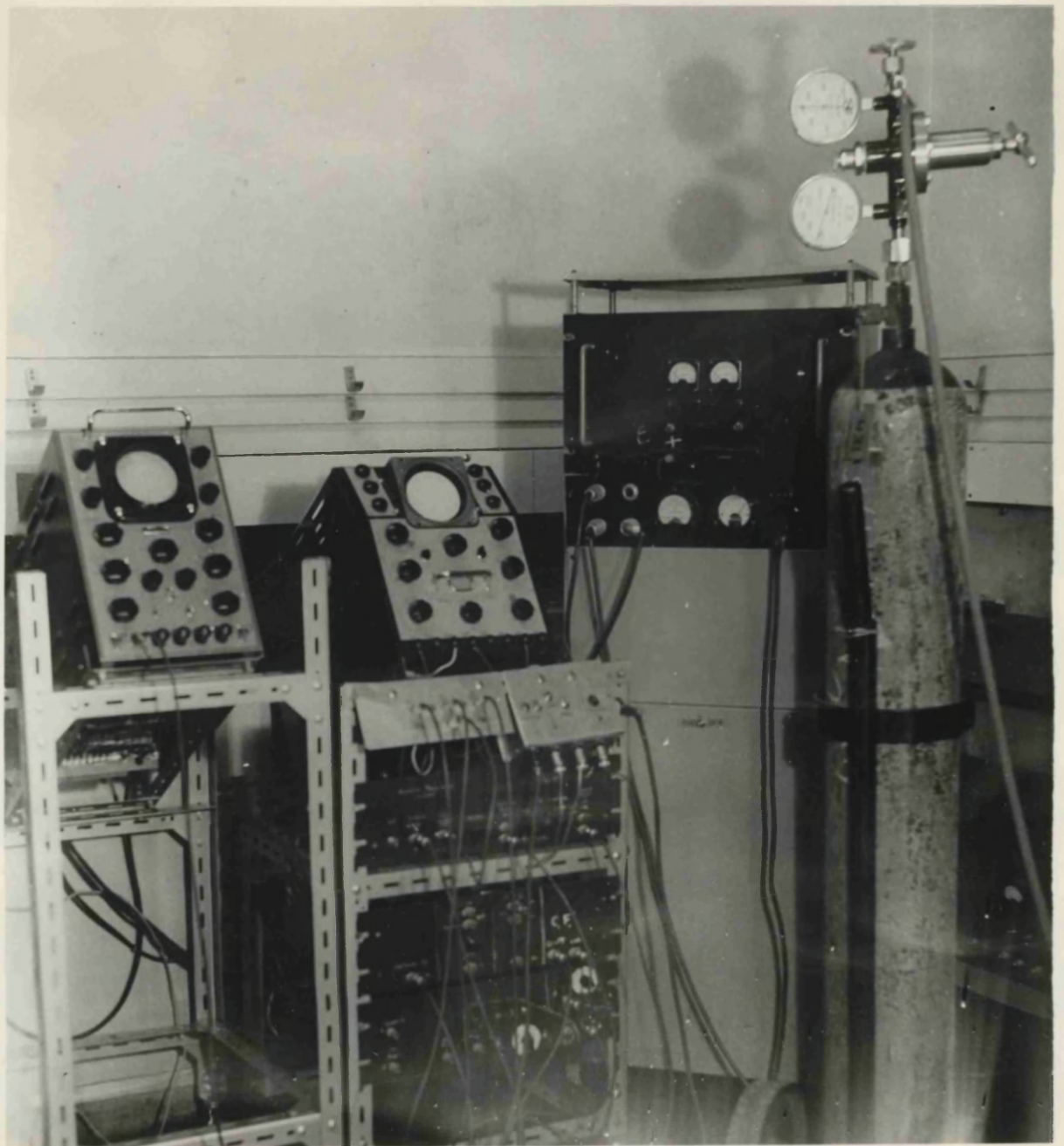


Plate H.